AETHER

Advanced Executive Transport for High-Efficiency and Range

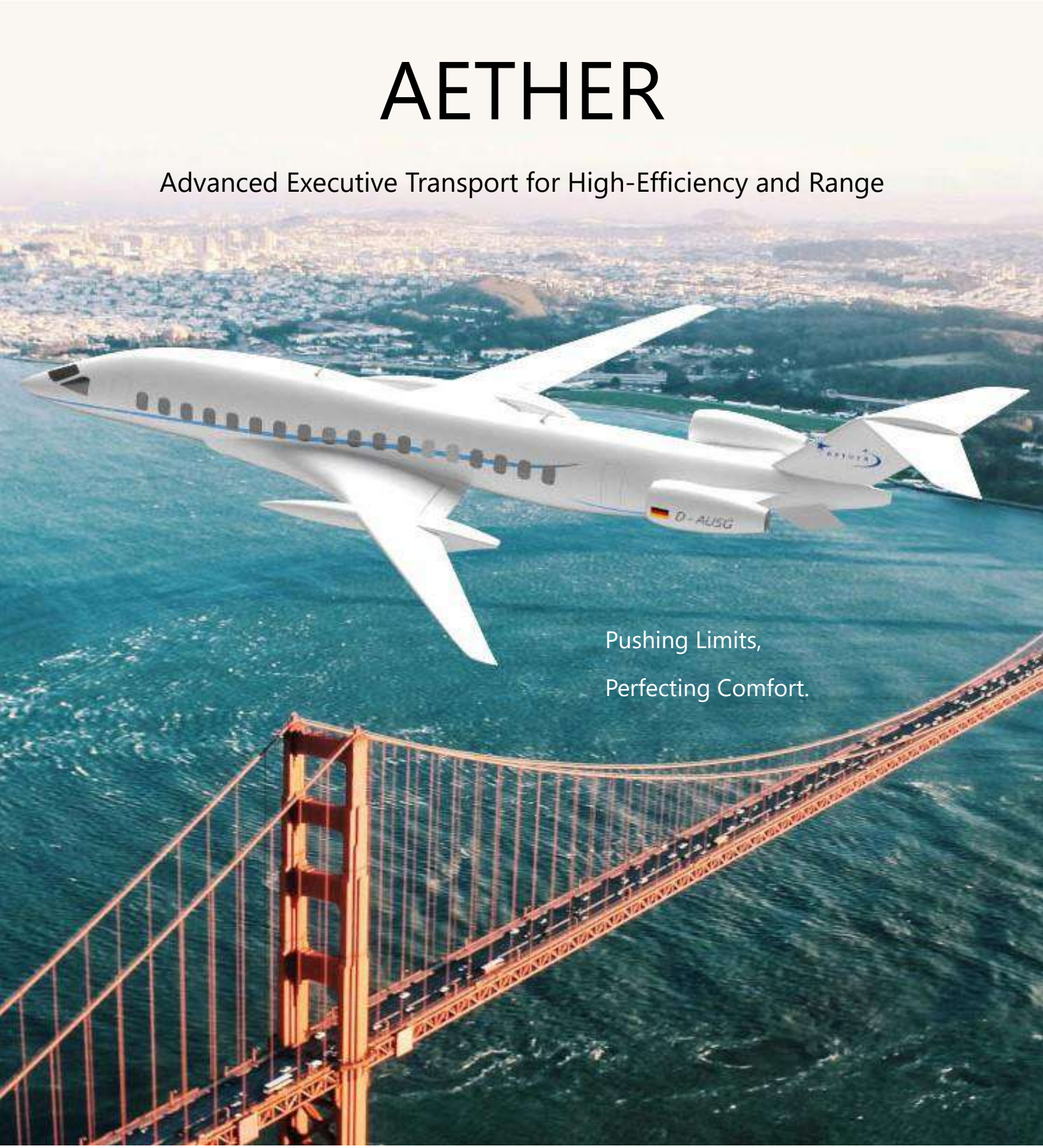

Pushing Limits,

Perfecting Comfort.

University of Stuttgart
Germany

KU THE UNIVERSITY OF KANSAS

AIAA

Team Members

Olivia Caudillo

AIAA 1422281

Gail Ghettalae

AIAA 1810479

Callahan Elo

AIAA 1811189

Simon Köhler

AIAA 1810030

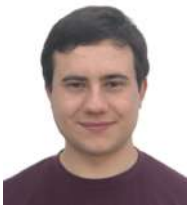

Jakob Staudt

AIAA 1811134

Ainsley Marshall

AIAA 1404953

Steven Meis

AIAA 985214

Reanne Reida

AIAA 1326154

Jennifer Relan

AIAA 1811167

Joshua Poznański

AIAA 1601832

Instructor: Dr. Ron Barrett, AIAA 022393

Department of Aerospace Engineering, University of Kansas

Compliance Matrix

Table 0.0.1 Compliance Matrix [1]

General Requirement	Compliance	Page #
Standard Airport Runway TO and Landing Capabilities	Airport Constraints	8
Minimum Cruise M = 0.85	Mach 0.85	57
Target Cruise M = 0.92	Mach 0.92	57
IFR and VFR Capabilities	Honeywell Anthem and Synthetic Vision	50, 25
Capable of Flight in Known Icing Conditions	Graphene-based thermal systems	30
FAA 14 CFR Part 25 Certifiable	V-N and Fault Tree	21, 55-56
Reserves and Equip. for Missions Meet FAA 14 CFR Part 25	Cockpit, Survivability	24, 52
Document Engine Energy Efficiency, Thrust, Power, and Weight	Met	26-28
Interior Requirements	**Interior Compliance**	**Page #**
Seating for 8, 60" pitch, 22" wide	10 Passenger for TO and Landing (13 for during flight)	26
Lay Flat Reclinable	Flat Reclinable	26
Seating for Flight Attendant in Pax Cabin	1 seat	26
Private Room with Queen Bed (60"x 80")	1 Queen Size Bed	26
2 Lavatories (1 standard and 1 Handicap Accessible Lavatory)	1 standard and 1 handicap accessible lavatory	51
Shower In Handicap Accessible Lavatory	Met	51
30 minute shower Capability	Met	51
Galley Sized for Long Range Mission	Met	51
Modern Flight Deck with at least 1 jump seat	2 Jumpseats	24, 26
Wifi and Satellite TV	Met	55
Crew Rest Area	Met	26
Business Provisions (Conference table and Televisions that display laptop connection)	6 Televisions	26

Table 0.0.1 – continued from previous page

Cabin Pressurization of 6000’ Equivalent Cabin Altitude at maximum service Ceiling	4000’	48
Air Condition to keep 30% of Baggage Area at 45F on 100F Day at Sea Level	Climate Controlled	52-53
PAX Requirements	**PAX Compliance**	**Page #**
3 crew: 2 Pilots, 1 Flight Attendant	2-4 Pilots, 1 Attendant	
Passenger Capacity of 8	Capacity of 10	26
Per Passenger Weight of 215 lbs	Met	1-3, 11
Baggage Weight per passenger: 50 lbs and 8 ft^3	Met	1-3, 11
8000 nmi Range	8000 nmi	3,11
TO from 6000’ Runway at Standard Sea Level Conditions on Grooved Land on 6000’ Runway at Standard Sea Level Conditions on Grooved Concrete, Dry Runway	4,590 ft and 3,010 ft	62-63
Aspen Requirements	**Aspen Compliance**	**Page #**
4 Pax, 215 lbs per Pax Weight, 100 lbs per Pax Baggage Weight, 20 ft^3 of Baggage per Pax	Met	1-3, 11
Takeoff from KVNY, Optimal RW, 59 F, Standard Pressure	Airport Constraints, Weights	8, 11
KVNY - KASE + Great Circle Distance +5%	Airport Constraints, Weights	8, 11
Landing at KASE, Optimal RW, 75 F, Standard Pressure, Medium Braking Action	Airport Constraints, Weights	8, 11
Napa Requirements	**Napa Compliance**	**Page #**
8 Pax, 215 lbs per Pax Weight, 40 lbs per Pax Baggage Weight, 5 ft^3	Met	1-3, 11
Wine Storage (12 Cases), 40 lbs per Case, 1 ft^3 per Case, 4 Cases Stored in Climate Controlled Space at 45 F	Climate Controlled	52-53
Takeoff from KAPC, Optimal RW, 75 F, Standard Pressure, Dry RW	Airport Constraints, Weights	8, 11
KAPC - MEX + Great Circle Distance + 5%	Airport Constraints, Weights	8, 11

Table 0.0.1 – continued from previous page

Landing at MEX, Optimal RW, 85 F, Standard Pressure, Dry RW	Airport Constraints, Weights	8, 11
Other Design Requirements	**Other Compliance**	**Page #**
Flying Qualities Meet 14 CFR Part 25	AAA Analysis	59-60
ID Systems and Components Required to Operate in Controlled and Uncontrolled Airspace	Cockpit Instrument and Safety and Survivability	50, 52
Design with Minimum Production Cost	Met	67-71
Justify Trade Between Min. Production Cost and Appeal	Met	67-71
Assume EIS of 2031	2031	10, 26-28, 39-42, 75-80

Acknowledgements

The SkyBridge team would like to thank Ms. Mieke Dichter-van Hamburg, Dr. Roland Wilhelm, and Mr. Frank Köpf from Rolls-Royce Germany for their support with questions regarding engines and engine integration. The team also thanks Dr. Barrett from the University of Kansas and Prof. Stephan Staudacher from the University of Stuttgart for their guidance throughout this project. The team thanks Hetrick Air Services and Dream Aviation for access to their aircraft and guidance throughout the design process. Additional thanks to Erik Dallman, Nicholas Yeary, and Duncan Marshall for their help in ground operations and market analysis. Lastly, the teams would like to thank Niels Braaten for their contributions in the discussion for the 200 variant.

Table of Contents

List of Symbols

Symbol	Definition	Units
C_D	Drag Coefficient	—
C_L	Lift Coefficient	—
d_f	Max hydraulic diameter of fuselage	ft
e	Oswald factor	—
F/F_{cr}	Thrust reduction	—
k	Feedback gain	deg/deg
L/D	Lift-to-drag ratio	—
l_f	Fuselage length	ft
l_n	Nose section length	ft
M	Mach number	—
m	Mass	—
n	Load factor	—
n_e	Number of engines	—
P	Perimeter	ft
q	Dynamic pressure	lbf/ft^2
R	Requirements	—
S	Wing area	ft^2
S_{TOG}	Takeoff ground distance	ft
S_{TOL}	Takeoff field length	ft
T	Thrust	lbf
t_R	Time to double amplitude	s

List of Symbols – *Continued from previous page*

V_A	Maneuvering speed	—
V_B	Gust speed	—
V_C	Cruise speed	—
V_D	Dive speed	—
V_S	Stall speed	ft/s
W	Weight	lbf
W_E	Empty weight	lbf
W_L	Landing weight	lbf
W_{OE}	Operating empty weight	lbf
W_{TO}	Initial weight	lbf
X_{CG}	Center of gravity position	in

Greek Symbol	**Definition**	**Units**
α	Angle of attack	deg
$\dot{\alpha}$	Angle of attack rate	deg/s
β	Sideslip	deg
$\dot{\beta}$	Sideslip rate	deg/s
δ_a	Aileron deflection	deg
δ_e	Elevator deflection	deg
δ_r	Rudder deflection	deg
η	Incidence angle	deg
γ	Climb gradient	
Λ	Aspect Ratio	
ζ	Damping coefficient	
ρ	Density	slug/ft^3
ω	Frequency	rad/s
ϕ_T	Thrust Inclination	deg

Subscript	**Definition**
dr	Dutch roll
fus	Fuselage
m	Moment

List of Symbols – *Continued from previous page*

ndr	Natural Dutch roll
nph	Natural Phugoid
nsp	Natural Short Period
p	Roll rate
ph	Phugoid
q	Pitch rate
r	Yaw rate
sp	Short period
TO	Take-Off
u	Forward velocity
S	Stall
SL	Sea Level
wet	Wetted

Acronyms	**Definition**	
6-DOF	Six Degree of Freedom	—
AAA	Advanced Aircraft Analysis	—
ACJ	Airbus Corporate Jets	—
AEI	All Engine Inoperative	—
AETHER	Advanced Executive Transport for High-Efficiency and Range	—
AL	Aircraft Lifetime	—
AO	Ancillary Objectives	—
AoA	Angle of Attack	—
BBJ	Boeing Business Jet	—
CAGR	Compound Annual Growth Rate	—
CFM	Cubic Feet per Minute	—
CFRP	Carbon Fiber Reinforced Polymer Composites	—
CG	Center of Gravity	—
CO	Carbon Monoxide	—
CO2	Carbon Dioxide	—
CPU	Central Proccessing Unit	—

List of Symbols – *Continued from previous page*

DAC	Dynamically Aerocompliant	—
EASA	EU Aviation Safety Agency	—
ECS	Environmental Control System	—
EGLC	London City	—
EI	Emission Index	—
EIO-LCA	Economic Input-Output Lifecycle Assessment	—
EIS	Entry Into Service	—
ELT	Emergency Locator Transmitter	—
FAA	Federal Aviation Administration	—
FAR	Federal Aviation Regulations	—
FS	Fuselage Station	—
GLARE	Glass Laminate Aluminum Reinforced Epoxy	—
GPU	Ground Power Unit	—
HC	(Unburned) Hydro Carbons	—
HNWI	High Net Worth Individuals	—
ICAO	International Civil Aviation Organization	—
IFR	Instrument Flight Rules	—
KAPC	Napa County Airport	—
KASE	Aspen-Pitkin County Airport	—
KLWC	Lawrence Regional Airport	—
KTEB	Teterboro	—
KVNY	Van Nuys	—
LCA	Lifecycle Emissions Analysis	—
LFPB	Paris Le-Bourget	—
LSZS	Samedan	—
LTO	Landing-Takeoff	—
MEX	Mexico City/Lic Benito Juarez International	—
NOX	Nitrous Oxide	—
OEI	One Engine Inoperative	—
PCR	Pavement Classification Rating	—

List of Symbols – *Continued from previous page*

PEEK	Polyether Ether Ketone	—
PKT	Passenger Kilometers Traveled	—
PSD	Power Spectral Density	—
PW	Pratt & Whitney	—
RDTE	Research Development Test and Evaluation	—
RFP	Request for Proposal	—
RVI	Relative Value Index	—
RW	Runway	—
SAF	Sustainable Aviation Fuel	—
SEP	Specific Excess Power	—
STAMPED	Statistical Time and Market Predictive Engineering Design	—
TBW	Truss-Braced Wing	—
TCAS	Traffic Alert and Collision Avoidance System	—
TSFC	Thrust Specific Fuel Consumption	—
UHNWI	Ultra High Net Worth Individuals	—
ULR	Ultra-Long Range	—
UV-C	Ultraviolet-C	—
VDV	Vibration Dose Value	—
VFR	Visual Flight Rules	—
VFW	Vereinigte Flugtechnische Werke	—
VKT	Vehicle Kilometers Traveled	—
VTOL	Vertical Takeoff Landing	—
WME	Wing Mounted Engines	—

List of Figures

List of Tables

page #

1 Introduction, Mission Specification and Profile

The objective of the report is to design a high-end business jet, with a focus on meeting demanding performance requirements while incorporating creative and luxurious interiors. The motivation for the design is to redefine the flying experience by blending innovation with personalized comfort, ensuring that every passenger enjoys a journey that goes beyond expectations and boundaries.

Table 1.0.1 summarizes the mission specifications for a long-range luxury business jet, as outlined in the Request for Proposal (RFP). The specifications include passenger capacity, interior and lavatory specifications, and details for the three missions: the design mission, the Aspen economic mission, and the Napa economic mission.

Table 1.0.1 Mission Specifications [1]

Requirement ID	Description
General Specifications	
G-01	Standard Airport Runway Takeoff and Landing Capabilities
G-02	Minimum Cruise Mach Number of 0.85
G-03	Target Cruise Mach Number of 0.92
G-04	Capable of Flight in Known Icing Conditions
G-05	Meets all applicable certification rules in FAA 14 CFR Part 25
G-06	Engine and Propulsion Assumptions Documented
G-07	Engine Used in Service by 2035
Interior Specifications	
I-01	Seating Capability for 8 Passengers
I-02	Seating Capability of 60 Inch Pitch and 22 Inch Width
I-03	Seating Capability of Lay Flat Reclinable
I-04	Seating for 1 Flight Attendant in Passenger Compartment
I-05	One Queen Size Bed in Private Room
I-06	One Galley, Accessible by Flight Attendant and Sized for the Design Range
I-07	Modern Flight Deck for Two Pilots
I-08	One Jump Seat Accessible by Passenger While in Flight
I-09	Provisions for Satellite TV and Wifi
I-10	Crew Rest Area for Design Range
I-11	Provisions for Business Productivity

Requirement ID	Description
I-12	Pressurization Capability for 6,000 ft Equivalent Cabin Altitude at Max Service Ceiling
I-13	AC Capability to Keep 30% of Baggage Area at 45°F on a 100°F Day at SL
Lavatory Specifications	
L-01	Two Lavatories (one standard for passengers and flight crew and one handicap accessible)
L-02	One Hot Water Shower in Handicap Accessible Lavatory
L-03	Provisions for 30 Minutes of Shower Total Water Capability
Design Passenger Mission Specifications	
D-01	3 Person Flight Crew (2 Pilots, 1 Attendant)
D-02	Passenger Capacity: 8 Passengers
D-03	Passenger Weight Assumption: 215 lbs
D-04	Baggage Weight Per Passenger: 50 lbs
D-05	Baggage Space Per Passenger: 8 cubic feet
D-06	8,000 Nautical Mile Range
D-07	6,000 ft Takeoff Capability from SL Standard Conditions and Grooved Dry Runway
D-08	6,000 ft Landing Capability from SL Standard Conditions and Grooved Dry Runway
Aspen Economic Mission Specifications	
A-01	4 Passengers, 215 lbs per passenger
A-02	100 lbs and 20 ft^3 per passenger for baggage
A-03	Takeoff from KVNY: Optimal runway, 59°F, standard pressure
A-04	Range from KVNY to KASE: Great circle +5% (wind and airways)
A-05	Landing at KASE: Optimal runway, 20°F, standard pressure, $\mu = 0.16$
Napa Economic Mission Specifications	
N-01	8 Passengers, 215 lbs per passenger
N-02	40 lbs and 5 ft^3 per passenger for baggage
N-03	Storage for 12 cases of wine: 40 lbs/case, 1 ft^3/case, 4 climate-controlled at 45°F
N-04	Takeoff from KAPC: Optimal dry runway, 75°F, standard pressure
N-05	Range from KAPC to MEX: Great circle +5% for wind and airways
N-06	Landing at MEX: Optimal dry runway, 85°F, standard pressure

Table 1.0.2 Additional Objectives

Other Features and Considerations
Flying qualities should meet 14 CFR Part 25
Identify all systems needed for operation in controlled and uncontrolled airspaces.
Assume an entry into service of 2031 when making technology decisions.
Design Objectives
Design an aircraft with the minimum production cost, with assumptions on market size documented.
Trade-off production cost for features that differentiate or enhance the aircraft, with documentation and justification.

1.1 Mission Profile

Due to the RFP specifying a Long Range Business Jet with a range of 8,000 nmi, a typical long range mission was taken into account for the mission profile. It meets industry standards and can reach altitudes up to 46,000 ft. The mission profile takes into account the 100 nmi cruise to an alternate airport and the 45 min loiter at the final destination. Although the RFP states two extra missions, none reaches the required mandatory range of 8,000 nmi, leading the team to focus on the long-range mission profile shown in Figure 1.1.1.

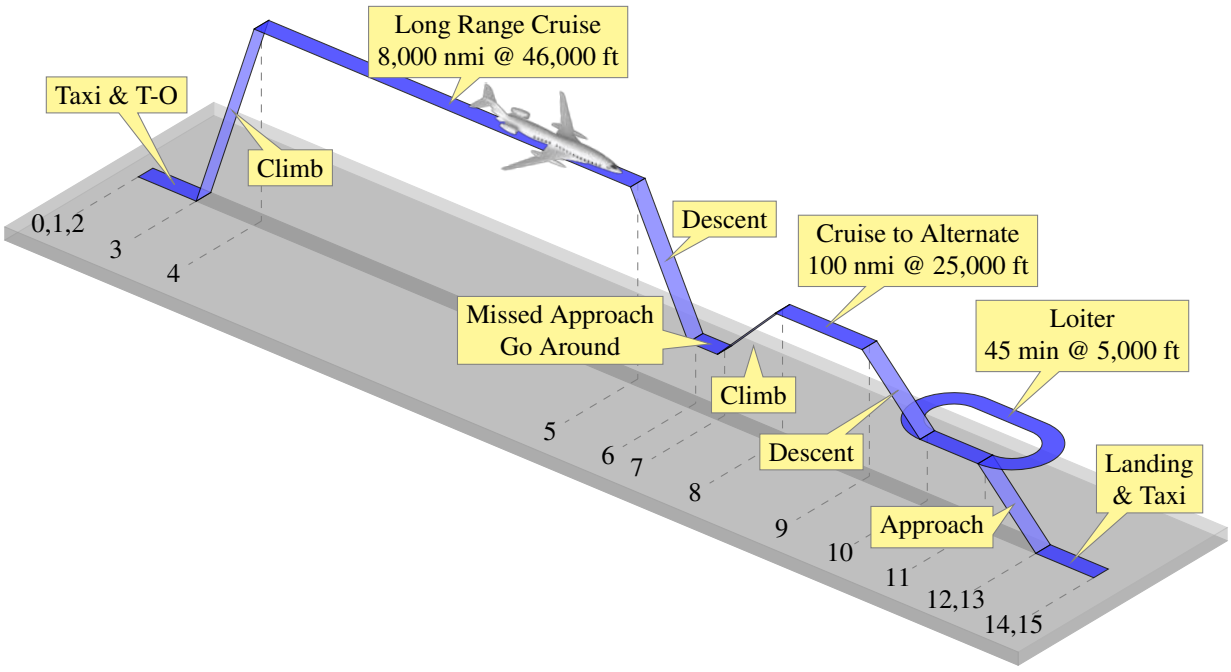

Figure 1.1.1 Mission Profile

2 Historical Review, Competition in the Market

The evolution of the business jet industry has been shaped by decades of advancements in technology, shifting market demands, and the continuous desire for high performance, luxury and efficiency. In this section, a historical review of long-range

business jets is provided to understand trends and developments in the past, as well as to find the major competitors of the requested jet. This historical review serves to highlight major milestones and trends that have influences industry. Furthermore, a market analysis is conducted to understand the needs of customers. This market review examines current demand drivers and the competitive landscape of the industry, offering insight to the evolving preferences of business aviation customers.

2.1 Historical Review

The long-range business jet market is very competitive with currently three major manufacturers competing against each other. Since the first long-range business jet with a large cabin, the Grumman Gulfstream II, entered service in 1967, its design has been continuously developed and improved [2]. Although it is a configuration from the 1960s, dedicated modern long-range business jets still use the configuration of the Grumman Gulfstream II. Only business jets derived from commercial aircraft such as the Airbus Corporate Jet, ACJ 320, or Boeing Business Jet, BBJ 737, use a different configuration on long ranges. The trend is moving ever further in the direction of greater ranges and flight Mach numbers in order to reach any point in the world ever faster. With range as the strongest driver for new business jets and a forecast annual growth of 2% in deliveries, large long-haul jets will account for the largest share of new business jets over the next 10 years, according to 2024 Global Business Aviation Outlook by Honeywell Aerospace [40].

2.1.1 Dedicated Long-Range Business Jets

Figure 2.1.1 Gulfstream II [2]

The Grumman Gulfstream II was the first business jet with a large cabin for up to 19 passengers and the ability to fly long distances such as transatlantic routes. It was derived from the Gulfstream I, a turboprop powered business plane. Powered by Rolls-Royce engines, the Gulfstream II had its first flight in 1966 and entered service in 1967. With 11 400 lb of thrust, it could fly up to Mach 0.85 [2].

Figure 2.1.2 Gulfstream G800 [3]

The Gulfstream G800 is the latest aircraft of the very traditional Gulfstream series. It features the shorter fuselage of the older Gulfstream G650 combined with the new wing of its longer predecessor, the Gulfstream G700. It achieves the longest range in the market with up to 8000 nmi. It is powered by Rolls-Royce Pearl 700 engines and can accommodate up to 17 passengers or 10 with sleeping configuration. Its maximum flight speed is up to Mach 0.925. The Gulfstream G800 features the lowest cabin altitude with 2916 ft at flight level 410 [3].

Figure 2.1.3 Bombardier Global 8000 [4]

The Bombardier Global 7500 is the latest family member of the Global series with the Global 8000 currently in development. Both planes feature the highest speeds of all long-range business jets with Mach 0.925 and Mach 0.94 respectively. The Global 7500 entered service in 2018 and the Global 8000 is predicted to be certified in 2025, then being the fastest civilian airplane since the

Concorde. They feature a new transonic wing optimized for Mach 0.85. In terms of luxury the Global 8000 will be equipped with the Bombardier Nuage seat, offering extraordinary comfort. Both jets are powered by General Electric Passport 20 engines and have a range of 7700 nmi and 8000 nmi respectively [4, 9].

Figure 2.1.4 Dassault Falcon 10X [5]

The Dassault Falcon 10X is the latest long-range business jet of the successful Falcon series made by the French plane maker. With a range of up to 7500 nmi and a speed of up to Mach 0.925 it is one of the most capable long range business jets currently on the market. The Falcon 10X is setting new standards when it comes to luxury with the most spacious cabin on the market for dedicated long-range business jets. With a cabin height of 6 feet 8 inches and a width of 9 feet 1 inch, it will be the tallest purpose-built business jet by 2025. The Falcon 10X is powered by two Rolls-Royce Pearl 10X engines, being 100% compatible with Sustainable Aviation Fuel (SAF). Its EIS is projected in 2025 [5].

2.1.2 Derived Business Jets

The Boeing Business Jet family of aircraft preceded the Airbus Corporate Jets, and today offer BBJ variations of multiple airliners, including the 737 MAX series, 777X, and 787. These aircraft were converted from traditional airliners with maximum space and passenger capacity in mind while maintaining competitive ranges. The BBJ 737-7 has a maximum range of 6500 nmi and can fly up to 19 passengers or more depending on the interior configuration. Powered by two CFM56-7 engines, the BBJ 737-7 has a maximum speed of Mach 0.70 and an operation ceiling of 41 000 ft [6, 12].

Figure 2.1.5 Boeing BBJ Select 737-7 [6]

The Airbus ACJ series of business jets are converted airliners made in response to the Boeing Business Jet program that began in 1998. The ACJ aircraft make use of extra fuel tanks and more spacious cabin interiors to provide range boosts and maximize passenger comfort. Airbus offers several options, which include the ACJ TwoTwenty and ACJ319/320neo. As the newest ACJ aircraft, the ACJ TwoTwenty is the smallest of the ACJ fleet with a wingspan of 115 ft, can seat up to 18 passengers, and reaches a range of 5650 nmi. Powered by two Pratt & Whitney PW1500G engines, it has a maximum flight speed of Mach 0.82 and a maximum cruising altitude of 41 000 ft. The TwoTwenty made its first delivery in 2023 joining the over 200 ACJ aircraft in service today. The ACJ319neo is slightly larger with a wingspan of 117 ft, can fly 19 passengers, and has a maximum range of 6750 nmi. It has a maximum flight speed of Mach 0.82 and is equipped with an additional fuel tank compared to the standard A319neo [7, 41].

Figure 2.1.6 ACJ TwoTwenty [7]

Figure 2.1.7 Embraer Lineage 1000e [8]

The Lineage 1000e is Embraer's offer of an airliner turned business jet. Derived from the Embraer 190 regional jet, the

Lineage 1000e has a range of 4600 nmi and can seat up to 19 passengers. The 1000e utilizes extra fuel tanks stored in the cargo hold to extend its range farther than what the E190 would typically offer. The 1000e is smaller and less expensive than Airbus and Boeing's converted planes, which both can cost more than $100 million. Yet it still outsizes similarly priced business jets in the $50 million price range. The Lineage 1000e's two CF34-10E7 engines bring the aircraft to a maximum speed of Mach 0.82 and a maximum operating altitude of 41 000 ft [8, 11].

2.1.3 Comparison of Concept of Operations

Tables 2.1.1 and 2.1.2 compare the latest long-range business jets in terms of their concept of operations and the requirements of the RFP. It can be seen that the latest long-range business jets already meet the requirements of the RFP only being limited in terms of wingspan. Aspen (KASE) is a challenging airport with wingspans limited to 95 ft. The Falcon 10X does not reach 8000 nmi.

Table 2.1.1 Comparison of Dedicated Long-Range Businessjets

Aircraft	 **Dassault Falcon 10X [5]**	 **Bombardier Global 8000 [4]**	 **Gulfstream G800 [3]**	**RFP Requirement**
Max Service Ceiling (ft)	51,000	51,000	51,000	-
Max Speed (Mach)	0.925	0.94	0.925	0.85 (0.92 Target)
Max Range (nmi)	7,500	8,000	8,000	8,000
Baggage Capacity (ft^3)	198	195	195	80
Max Passengers	19	19	17	8
Takeoff Distance (ft)	6,000	5,760	6,000	< 6,000
Landing Distance (ft)	2,500	2,220	2,500	< 6,000
Wingspan (ft)	111	104	103	≤ 95 (KASE)
Cabin Length (ft)	54'	54'5"	46'10"	-
Pressurization Capability (Altitude, ft)	3,000	2,900	2,916	6,000 @ Max Service Ceiling

Table 2.1.2 compares business jets derived from commercial aircraft. Those jets feature lower ranges and lower flight Mach numbers. They do not meet the requirements in many respects and tend to be too large, as can be seen from the high baggage capacity.

Table 2.1.2 Comparison of Derived Long-Range Businessjets

Aircraft	 Airbus ACJ220 [7]	 Boeing BBJ 737-700 [6]	 Embraer Lineage 1000 [11]	RFP Requirement
Max Service Ceiling (ft)	41,000	41,000	41,000	-
Max Speed (Mach)	0.82	0.7	0.82	0.85 (0.92 Target)
Max Range (nmi)	5,650	6,500	4,600	8,000
Baggage Capacity (ft^3)	944	1,125	443	80
Max Passengers	18	19+	19	8
Takeoff Distance (ft)	5,478	6,085	6,076	< 6,000
Landing Distance (ft)	2,300	2,360	2,450	< 6,000
Wingspan (ft)	115	118	94	≤ 95 (KASE)
Cabin Length (ft)	78'1"	85'8"	84'4"	-
Pressurization Capability (Altitude, ft)	5,850	6,500	7,000	6,000 @ Max Service Ceiling

3 Configuration Constraint Establishment

In order to determine the configuration constraints, the four airports named in the RFP and four additional airports were examined with regard to restrictions. Each airport presents unique constraints for which the team must take into account.

Aspen-Pitkin County Airport/Sardy Field (KASE) is particularly challenging as the airport is located at an altitude of 7680 ft and has a very narrow runway of only 98 ft wide and 8006 ft long which is rather short considering the altitude. Due to the narrow runway and its proximity to a parallel taxiway, the wingspan of the aircraft allowed to land at Aspen is limited to 95 ft. However, it should be noted that the airport will be modernized so that the runway will be widened to 150 ft and the distance to the taxiway will increase to 400 ft [42, 43].

Napa County Airport (KAPC) is a challenge due to its short runway and weight restrictions. The length of the shorter runway is only 5008 ft and the maximum weight bearing capacity is 76 000 lb for aircraft with double wheels [44].

Van Nuys Airport (KVNY) has particularly strict noise protection regulations. Aircraft taking off or landing here may not be louder than 77 db according to AC36-3. In addition, there are restrictions for aircraft with a wingspan greater than 100 ft [45].

Mexico City/Lic Benito Juarez International is an international airport at high altitude. It places special demands on the approach, such as long holding patterns, but has very long runways and can handle wide body aircraft such as the Boeing 747-8, which is why no special requirements can be derived for the design [46].

In addition to the four mentioned airports, other important airports for business travel were also considered. The airports of

Teterboro (KTEB), Paris Le-Bourget (LFPB), London City (EGLC) and Samedan (LSZS) were also examined for special requirements. Teterboro is one of the busiest airports for business travel in the United States. It has strict noise regulations similar to those of the Van Nuys Airport with a maximum of 90 db. In addition, the approach to runway 24 is quite steep with an approach ratio of 19:1. Paris Le-Bourget does not have any special requirements. London City is known for its steep approach with an approach angle of 5.5°, which corresponds to an approach ratio of 10:1. Aircraft must be certified separately for this approach. Samedan (St. Moritz) is the highest airport in Europe. Its short runway with a length of 6037 ft combined with its altitude of 5600 ft should be emphasized here [16–19]. Table 3.0.1 summarizes the airport constraints.

Table 3.0.1 Airport Constraints [16–19]

	Value	Airport
Shortest Runway @ Elevation	8006 ft x 98 ft @ 7838 ft	KASE*
	5008 ft x 150 ft @ 35 ft	KAPC
	6037 ft x 131 ft @ 5600 ft	LSZS**
ICAO Aerodrome Reference Code	4C	KASE*
	3D	KAPC
Max. Wingspan	95 ft	KASE*
	100 ft	KVNY
Weight Bearing Capacity	76 000 lbf double wheel***	KAPC
	100 000 lbf double wheel	KASE
Max. Noise	77 db AC 36-3	KVNY
Approach Ratio**	19:1	KTEB**
	10:1	EGLC**
* KASE is about to be modernized, wingspan restriction may fall ** not requested by the RFP *** restriction only applies to shorter runway		

4 Design Optimization Function

To design a business jet, an outline of requirements (R), objectives (O), and ancillary objectives (AO) is necessary to meet all items. All three of these components are needed for the development of the design optimization function (OF). The requirements presented in Table 4.0.1 were extracted directly from the RFP. Each of these designs are required to be met in order to have a competitive design. Thus, utilizing Equation (1), a binary method was used to.

$$R_i = \begin{cases} 0 \text{ if objective not met} \\ 1 \text{ if objective is met} \end{cases} \quad (1)$$

Table 4.0.1 Requirements

Variable	Requirement	Variable	Requirement
$\mathbf{R}_1$	Take off/land from standard airport runways	$\mathbf{R}_2$	Cruise Mach M 0.85
$\mathbf{R}_3$	Capable of VFR/IFR flight	$\mathbf{R}_4$	Capable in known icing conditions
$\mathbf{R}_5$	Meets FAA 14 CFR Part 25 rules	$\mathbf{R}_6$	Engine for service by 2035
$\mathbf{R}_7$	Seats 8 passengers, 60" pitch, 22" wide	$\mathbf{R}_8$	One queen-size bed (60"x80") in private room
$\mathbf{R}_9$	Two lavatories (1 accessible for crew and passengers and 1 handicap accessible)	$\mathbf{R}_{10}$	Shower in handicap lavatory
$\mathbf{R}_{11}$	30 minutes of shower water capacity	$\mathbf{R}_{12}$	One galley, accessible by flight attendant
$\mathbf{R}_{13}$	Modern flight deck, jump seat accessible to passengers	$\mathbf{R}_{14}$	Provisions for Wi-Fi, satellite TV
$\mathbf{R}_{15}$	Business productivity provisions	$\mathbf{R}_{16}$	Cabin pressurization to 6000 ft at max service ceiling
$\mathbf{R}_{17}$	Air conditioning to maintain 30% of baggage area at 45°F on 100°F day at sea level		
Design Passenger Mission			
$\mathbf{R}_{18}$	Crew: 3 (2 pilots, 1 flight attendant)	$\mathbf{R}_{19}$	Passenger capacity: 8
$\mathbf{R}_{21}$	215 lbs/passenger, 50 lbs baggage/passenger	$\mathbf{R}_{22}$	8000 nmi range
$\mathbf{R}_{23}$	Take off/land from 6000 ft dry runway		
Aspen Economic Mission			
$\mathbf{R}_{24}$	4 passengers, 215 lbs/passenger, 100 lbs baggage, 20 cubic ft baggage/passenger	$\mathbf{R}_{25}$	Take off/land from KVNY
$\mathbf{R}_{26}$	Range from KVNY to KASE		
Napa Economic Mission			
$\mathbf{R}_{27}$	8 passengers, 215 lbs/passenger, 40 lbs baggage, 5 cubic ft baggage/passenger	$\mathbf{R}_{28}$	Take off/land from KAPC
$\mathbf{R}_{29}$	Range from KAPC to MEX		

The objectives and ancillary objectives presented in Table 4.0.2 and Table 4.0.3 are designs that do not need to be met to be considered a competitive design. The objectives are tradable designs listed in the RFP. The ancillary objectives are additional objectives that were considered to allow the design to be more competitive, typically determined by the designers. Equation (2) and Equation (3) utilizes a linear method for ranking.

$$O_j = \begin{cases} 0 \text{ if objective not met} \\ \text{Linearly Weighted if partial} \\ 1 \text{ if objective is met} \end{cases} \quad (2)$$

$$AO_k = \begin{cases} 0 \text{ if objective not met} \\ \text{Linearly Weighted if partial} \\ 1 \text{ if objective is met} \end{cases} \quad (3)$$

Table 4.0.2 Objectives

Variable	Objective
$\mathbf{O}_1$	Minimize production cost
$\mathbf{O}_2$	Target cruise Mach: M 0.92
$\mathbf{O}_3$	Seating: lay flat reclinable
$\mathbf{O}_4$	Crew rest area

Table 4.0.3 Ancillary Objectives

Variable	Objective
$\mathbf{AO}_1$	Hot Turn Capability
$\mathbf{AO}_2$	Meet Latest ICAO Noise Standards
$\mathbf{AO}_3$	Optimal Mission & Airport Compatibility
$\mathbf{AO}_4$	Steep Approach Capabilities
$\mathbf{AO}_5$	Appealing Aesthetics
$\mathbf{AO}_6$	Handicap Accessibility
$\mathbf{AO}_7$	Ride Quality

$$OF = \prod_{i=1}^{29} R_i \cdot \left(\sum_{j=1}^{4} O_j + \sum_{k=1}^{7} AO_k \right) \quad (4)$$

Equation (4) shows the design optimization function in terms of the requirements, objectives, and ancillary objectives. The equation is applied to each design configuration to ensure standardized evaluation.

5 STAMPED Analysis

To forecast market trends and predict business jet designs for 2031, the Statistical Time and Market Predictive Engineering Design (STAMPED) techniques were applied. It offers insight into the current landscape of large business jets and projects future market developments. Figure 5.0.1 shows the empty weight-to-takeoff weight ratio. Figure 5.0.2 shows the aspect ratio.

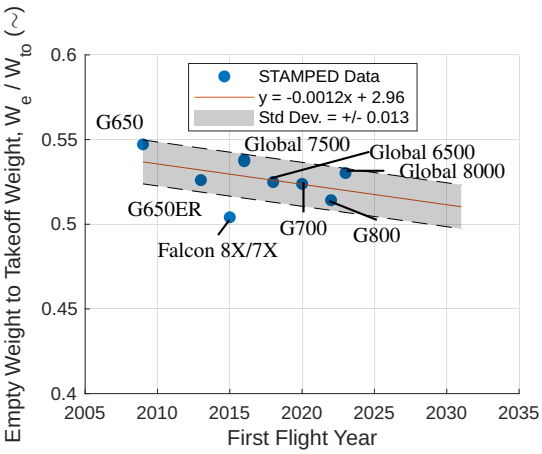

Figure 5.0.1 Empty Weight to Takeoff Weight Ratio Market Trend Through Time [3–5, 9–12]

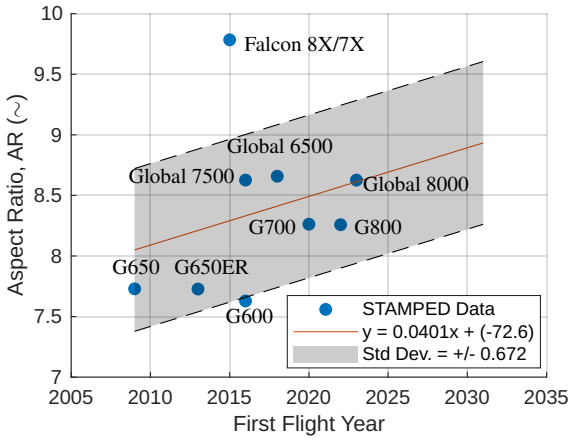

Figure 5.0.2 Aspect Ratio Market Trend Through Time [3–5, 9–12]

6 Class I Weight Sizing

To size the aircraft, several design parameters were determined using methods outlined by Jan Roskam in *Aircraft Design Part I* [47]. Table 6.0.1 presents the breakdown of the fuel fraction in the various phases of flight. It is important to note that the team set the aircraft to be constructed primarily of carbon fiber reinforced polymer composites (CFRP). Based on the material choice and supporting references, a 20% reduction in the empty weight-to-takeoff weight ratio was applied. The empty weight-to-takeoff ratio were used from the STAMPED trends of long-range business jets.

Table 6.0.1 Aircraft Fuel Fraction

Weight Ratio	Flight Segment	Fuel Fraction [R] Roskam [C] Calculated
W_1/W_{to}	Engine Start, Warm up	0.99 [R]
W_2/W_1	Taxi	0.995 [R]
W_3/W_2	Takeoff	0.995 [R]
W_4/W_3	Climb	0.98 [R]
W_5/W_4	Cruise	0.638 [C]
W_6/W_5	Climb to Alternate	0.98 [R]
W_7/W_6	Divert to Alternate	0.98 [R]
W_8/W_7	Loiter	0.985 [C]
W_9/W_8	Descent	0.99 [R]
W_{10}/W_9	Landing	0.992 [R]

Table 6.0.2 presents the Class I weight sizing for the design passenger mission. The mission is examined in detail due to it serving as the governing design case. In other words, if the aircraft can successfully meet the requirements of the design passenger mission with the maximum passenger weight and baggage, it will be capable of fulfilling the other two missions as well.

Table 6.0.2 Design Mission Class I Weight Sizing

W_{pl} (lbf)	2,600	W_f (lbf)	39,600
W_e (lbf)	30,500	W_{to} (lbf)	73,700

7 Wing and Powerplant Sizing

Aircraft parameters were determined to obtain the design point and thus the wing and engine sizing. These parameters include wing area, take-off thrust and lift coefficients for take-off, landing, climb and cruise. These parameters were determined based on the preceding STAMPED analysis and adjusted to meet the requirements of all airports and missions considered.

The sizing chart was used to determine the design point. The aim is to maximize the load on the wings while keeping the thrust requirement as low as possible. Translated for the sizing chart, this means that the design point should be as far to the bottom right as possible. In addition, design points from existing long-haul business jets were used to validate the result.

7.1 Takeoff and Landing Sizing

For take-off the thrust-to-weight ratio T/W is a function of the wing loading W/S. It is dependent on the take-off field length s_{TOL}, the lift coefficient $C_{L,TO}$ and the density at take-off conditions ρ, as shown in Equation (5).

$$\frac{T}{W} = \frac{37.5\, W/S}{s_{TOL}\, \frac{\rho}{\rho_0}\, C_{L,TO}} \quad (5)$$

To calculate the take-off, the conditions defined in the RFP [1] in Aspen and Napa were compared and Napa was used as the dominant case for the sizing chart. Three $C_{L,max,TO}$ values were plotted to determine the optimum design point and to have some leeway in its selection.

$$\frac{W}{S} = \frac{\frac{1}{2}\rho V_{SL}^2 C_{L_{\max}}}{S\frac{W_L}{W_{TO}}} \quad (6)$$

The landing distance is affected by landing weight, deceleration methods, flying qualities and approach speed. Equation (6) was used to determine the wing loading for three different $C_{L,max,L}$ values. Again, the landing field lengths of all airports mentioned in the RFP [1] were compared and Napa was chosen to size the landing.

7.2 Climb and Ceiling Sizing

FAR 25 guidelines were used to calculate the climb. The climb was evaluated accordingly for various scenarios with One Engine Inoperative (OEI) and All Engine Inoperative (AEI). It is mainly influenced by the mass ratio $\frac{m_{climb}}{m_0}$ at the start of climb, the number of engines n_e and the ratio of drag to lift $\frac{c_D}{c_L}$ as well as the required climb gradient γ_{min} according to FAR 25. The lift-to-drag ratio is dependent on the drag polar equations.

Seven main configurations are considered for the drag polar chart. Each configuration is characterized by a different flap and landing gear position and thus different drag. The drag equation is given for each configuration. The drag polars are based on wind tunnel data for area ruled aircraft [48]. These drag polars can be found in Figure 7.2.1.

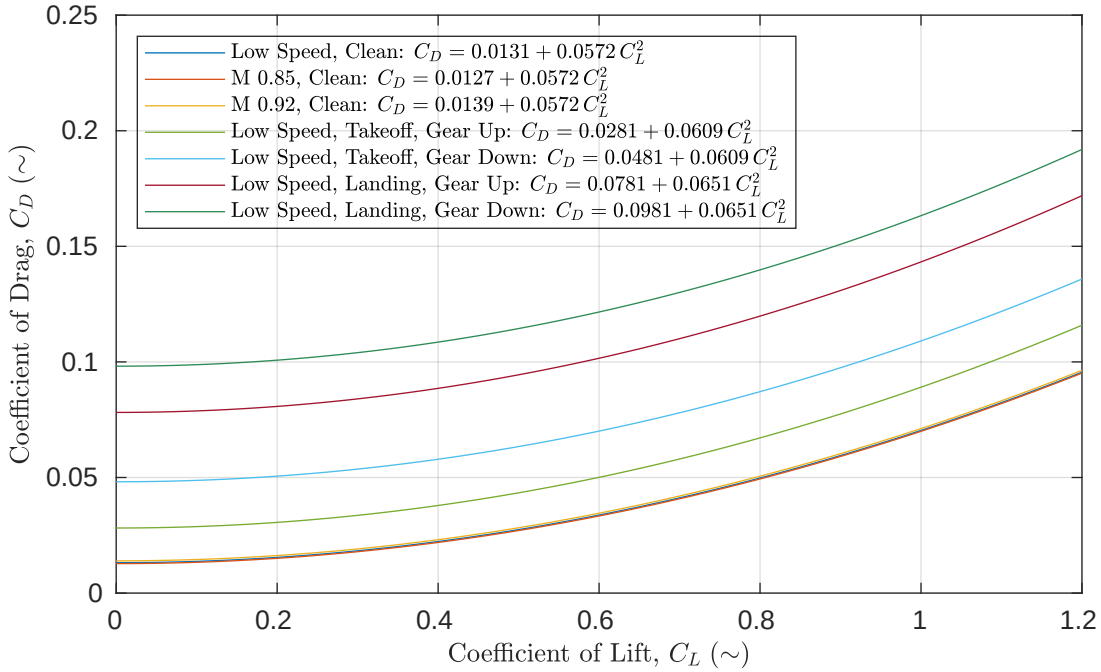

Figure 7.2.1 AETHER Drag Polars

Equation (7) shows the governing equation for the climb phases.

$$\frac{T}{W} = \left(\frac{m_{climb}}{m_0}\right) \frac{n_e}{n_e - 1} \left(\gamma_{min} + \frac{c_D}{c_L}\right) \tag{7}$$

7.3 Cruise Sizing

For cruise the thrust-to-weight ratio T/W is a function of wing loading W/S. It is influenced by the thrust reduction $\frac{F}{F_{cr}}$, the drag coefficient C_{D0} (both functions of altitude and Mach number), the cruise mass ratio $\frac{m_{cr}}{m_0}$, the aspect ratio Λ, the dynamic pressure q and the Oswald factor e. Raymer [49] provides a method to derive the thrust reduction, as shown in Equation 8

$$\frac{T}{W} = \left(\frac{F}{F_{cr}}\right) \cdot \left[\frac{C_{D0}\, 0.5\, \rho\, v^2}{(W/S)\, g} + \frac{(W/S)\, g}{0.5\, \rho\, v^2\, \pi\, \Lambda\, e} \cdot \left(\frac{m_{cr}}{m_0}\right)^2\right] \tag{8}$$

7.4 Sizing Chart

The sizing chart in Figure 7.4.1 shows very well that the assumptions made are reasonable, as it converges very closely with existing aircraft families from Bombardier, Dassault and Gulfstream. The fact that Gulfstream aircraft were taken as the starting point for the Class I weight sizing can be seen from the optimal match. All of the requirements are shown to be met. To choose the design point, the previous mentioned method was applied by minimizing the thrust-to-weight ratio and maximizing wing loading.

The design point is characterized by a thrust-to-weight ratio T/W of 0.325 and a wing loading W/S of 83.5 $\mathrm{lbf/ft^2}$. Based on these values, the wing area, the required fuel volume and the required thrust were determined. There were a number of challenges, particularly for the engines. This is discussed in more detail in Chapter 11.

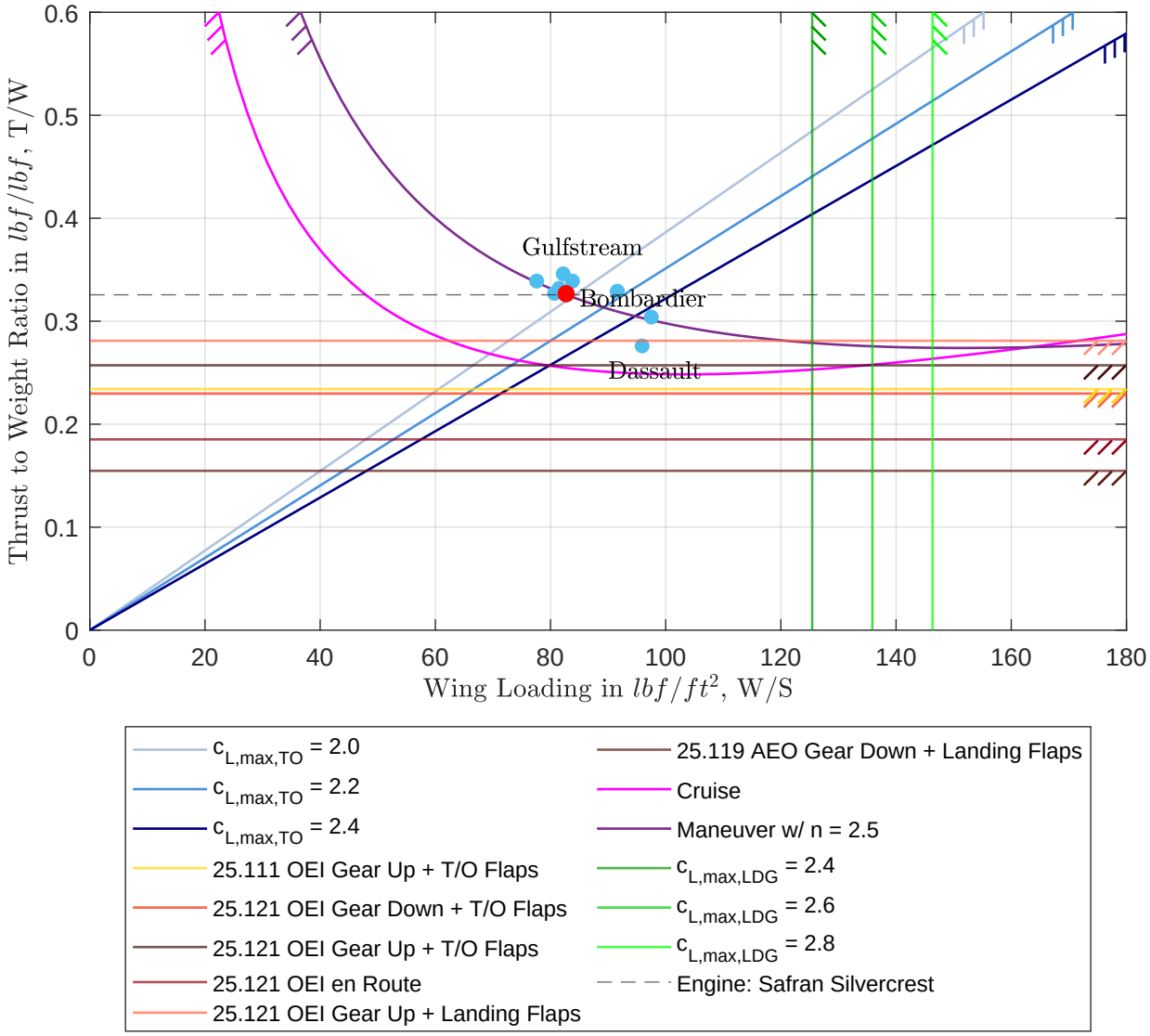

Figure 7.4.1 Sizing Chart - 2 engines

8 Candidate Configuration Matrix

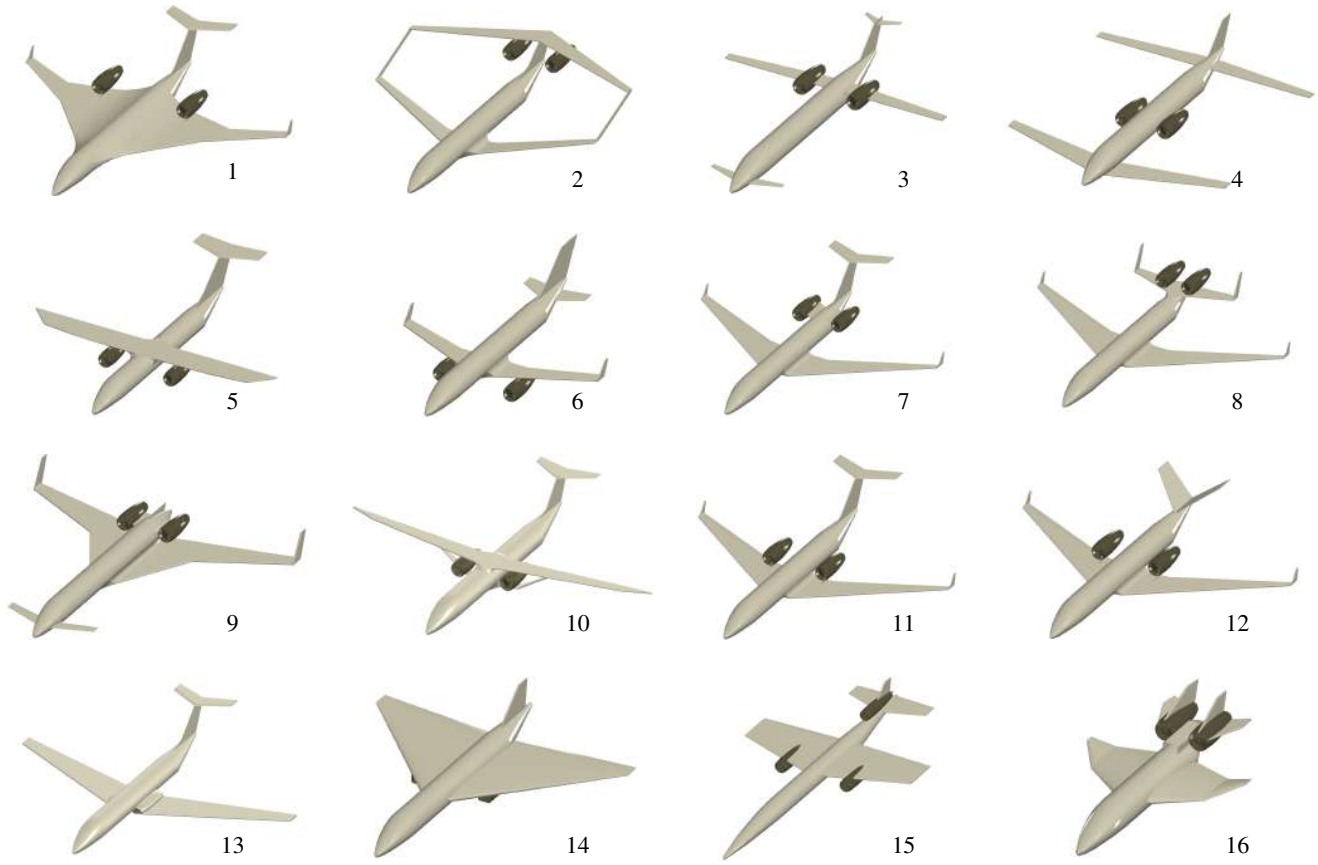

Figure 8.0.1 Configurations Considered for Class I Design

8.1 Rejected Configurations

Some configurations, especially new ones, assessed by the SkyBridge team were determined to not be feasible or practical. A key argument is certification by the FAA, as innovative configurations recivieing certification is shown to be time consuming and uncommon. With an EIS targeted for 2031 and certification processes that have recently become more prolonged (compare Airbus A321 XLR or Boeing 777X) and due to the Covid pandemic, only configurations based on currently certified aircraft or whose development is well advanced will be considered. Nevertheless, the following section is intended to provide an overview of why certain configurations were considered by analyzing the advantages, disadvantages, and other parameters.

Blended Wing Body	
+ low wetted area	- pressurization
+ low mass	- evacuation
+ payload distribution	- certification cost
+ high L/D	- passenger comfort
	- high lift aids limited

Figure 8.1.1 Blended Wing Body

Joined Wing	
+ reduced induced drag	- high interference drag
+ high aspect ratio	- ground operation
+ less trim drag	- landing gear integration
	- certification costs
	- EIS

Figure 8.1.2 Joined Wing

Three Surface	
+ smaller wing or reduced wing load	- interference canard with main wing
+ better lift distribution	- small lever of the stabilizer
+ high L/D	- split spar → increased weight
+ low trim drag	- aesthetics/acceptance
	- landing gear integration

Figure 8.1.3 Three Surface

Tandem Wing	
+ less mass	- interference of wings
+ high aspect ratio	- engine placement
+ low trim drag	- uneven lift distribution
	- ground handling
	- pitch break characteristics

Figure 8.1.4 Tandem Wing

Low Wing Canard	
+ canard & wing before/after cabin	- interference canard with main wing
+ no stall	- engine placement
+ combined winglets & vert. stabs	- yaw stability
	- high wetted area
	- aestethics

Figure 8.1.5 Low Wing Canard

Low Wing L-Tail	
+ approved design	- fuselage high above ground
+ use as airliner	- ground ops at remote airports
+ use of high bypass ratio engines	- noise on ground
	- usually lower Mach numbers
	- no dedicated business jets with that configuration

Figure 8.1.6 Low Wing L-Tail

Wing Mounted Engines - V-Tail	
+ less wetted area	- interference exhaust jet with tail
+ less CG excursion	- engine replacement/maintenance
	- roll-yaw coupling
	- interference drag
	- engine placement with respect to uncontained engine failure & noise

Figure 8.1.7 V-Tail

Supersonic	
+ reduced travel times	- development cost
	- efficiency
	- noise constraints over land
	- limited range
	- limited cabin cross section

Figure 8.1.8 Supersonic

Delta Wing	
+ delayed stall	- high landing AoA
+ transonic performance	- higher approach/landing speed, longer runway needed
	- low L/D

Figure 8.1.9 Delta Wing

Wing Root Engines	
+ reduced drag	- maintenance engine access
	- cabin noise
	- limited engine bypass ratio
	- wing spar conflict

Figure 8.1.10 Wing Root Engines

Twin V-Tail	
+ increased fuel efficiency	- complex VTOL mechanisms
+ VTOL capabilities	- increased weight
	- high development cost
	- limited market demand

Figure 8.1.11 Twin V-Tail

8.2 Accepted Configurations

The advantages and disadvantages of the accepted configurations are presented in the following section. They are then examined in the next chapter with regard to their suitability for the requirements of the RFP in order to select one to three configurations, which are then further developed in a Class II design process.

High Wing	
+ easy engine access	- landing gear integration
+ fuselage low on ground	- interference drag
+ handicap accessibility	- noise radiation downwards
+ use as regional jet possible	- customer acceptance

Figure 8.2.1 High Wing

The high-wing configuration has proved particularly successful in the regional aircraft sector. It enables good operability even from remote or poorly equipped airports thanks to the low-wing fuselage. The main disadvantage is that this configuration is associated more with regional aircraft than with business jets.

T-Tail	
+ customer acceptance	- engine accessibility
+ fuselage low on ground	- CG excursion
+ established design	- no unique design
+ noise in cabin	
+ low certification cost	

Figure 8.2.2 T-Tail

The T-tail configuration is the classic configuration for business jets. All dedicated ultra long range business jets use this configuration.

U-Tail	
+ fuselage low on ground	- engine accessibility
+ distinctive design	- CG excursion
+ noise in cabin	- jet blast of tail
+ noise on ground	- customer acceptance
	- engine replacement with special equipment

Figure 8.2.3 U-Tail

The U-tail is a modification of the T-tail configuration. Both designs have many advantages and disadvantages in common. The U-tail configuration promises less noise that is radiated downwards, but is more complicated in terms of engine maintenance and has disadvantages with the elevator.

Truss-Braced Wing (TBW)	
+ fuselage low on ground	- interference drag
+ innovative design	- limited engine bypass ratio
+ high aspect ratio wing	- noise in cabin
+ lower structural weight	- stiffness of wing
+ lower wing loading	- certification cost/EIS
	- bad ride quality

Figure 8.2.4 Truss-Braced Wing

The truss-braced wing concept is a new design from Boeing for regional aircraft and is being traded in specialist circles as the future 797. It has numerous advantages, but the lack of experience and therefore high development costs, a long development period and high resistance at high Mach numbers speak against the concept.

Wing Mounted Engines - T-Tail (WME)	
+ low CG excursion	- market acceptance
+ distinctive design	- noise in cabin
+ structural benefits	- certification
+ reduced drag	
+ noise on ground	
+ engine maintenance	

Figure 8.2.5 Wing Mounted Engines

The idea of wing-mounted engines was first implemented with the VFW Fokker 614. The Hondajet uses this configuration for business jets and is considered to be very successful. The placement of the engines close to the center of gravity promises advantages such as low ground clearance and less trim drag, but also disadvantages in the event of uncontained engine failure or noise emissions into the cabin.

All configurations have advantages and disadvantages. The following chapter evaluates the configurations based on the previously defined requirements for the design.

8.3 Final Configuration Selection

The final configuration selection is based on the design optimization function Equation 4. Every design was assessed and weights for objectives by the RFP and ancillary objectives were created. The evaluation can be found in Table 8.3.1.

Table 8.3.1 Objectives Evaluation

Configuration	 High Wing	 T-Tail	 U-Tail	 TBW	 WME
O_1: Minimize Production Cost	0.7	1	0.8	0	0.3
O_2: Target Cruise Mach: M 0.92	1	1	0.8	0.2	1
O_3: Flat Reclinable Seating	1	1	1	1	1
O_4: Sized Crew Rest Area	1	1	1	1	1
WEIGHTED SUM	0.93	1	0.9	0.55	0.83
AO_1: Hot Turn Capability	0	1	1	0	0
AO_2: Meet Latest ICAO Noise Standards	1	1	1	1	1
AO_3: Optimal Mission & Airport Compatibility	1	1	1	0	1
AO_4: Steep Approach Capabilities	1	1	1	0	1
AO_5: Appealing Aesthetics	0.5	1	0.8	0.6	0.6
AO_6: Handicap Accessibility	1	1	1	1	1
AO_7: Modular Section Compatibility	1	1	1	1	1
AO_8: Ride Quality	0.8	1	1	0.2	0.8
WEIGHTED SUM	0.79	1.00	0.98	0.48	0.80
COMPLETE WEIGHTED TOTAL	1.72	2	1.88	1.03	1.63

The T-Tail configuration shown in Figure 8.2.2 is the most suitable design based on the weighted evaluation since it balances aerodynamic efficiency, operational feasibility, production cost, and passenger comfort better than other configurations. Its strong performance in both primary and additional objectives makes it the optimal choice for implementation. Furthermore, the design is well known in the industry. It can be assumed that the T-tail design will be best received by customers and operators of business jets. It also poses fewer challenges for certification and pilot and technician training.

9 V-n Gust and Maneuver Diagram

Table 9.0.1 V-n Speeds for Clean Climb Condition

	Clean Climb True Air Speeds
V_{S1} (ft/s)	269
V_A (ft/s)	484
V_B (ft/s)	428
V_C (ft/s)	512
V_D (ft/s)	639

Loads the airframe may experience during flight are calculated using equations specified by 14 Code of Federal Regulations (CFR) Part 25 Subsection C section CFR25.333 - CFR25.341 [50]. It should be noted that the equations used are consistent with those found in Dr. Roskam's Aircraft Design Part V [47] which uses the former gust equations as specified by CFR25 prior to 1996. This was used as these calculated that the aircraft may experience higher gust loads and is therefore more conservative than the current standards.

From analyzing different phases of flight, takeoff, takeoff with flaps, climb, climb with flaps, and cruise. It was found that the climb conditions showed that the aircraft may experience the highest loads in that phase with a peak load of 3.24 g's as seen in Figure 9.0.1 - 9.0.3. The calculated stall, maneuver, gust, cruise, and dive speeds are found in Table 9.0.1.

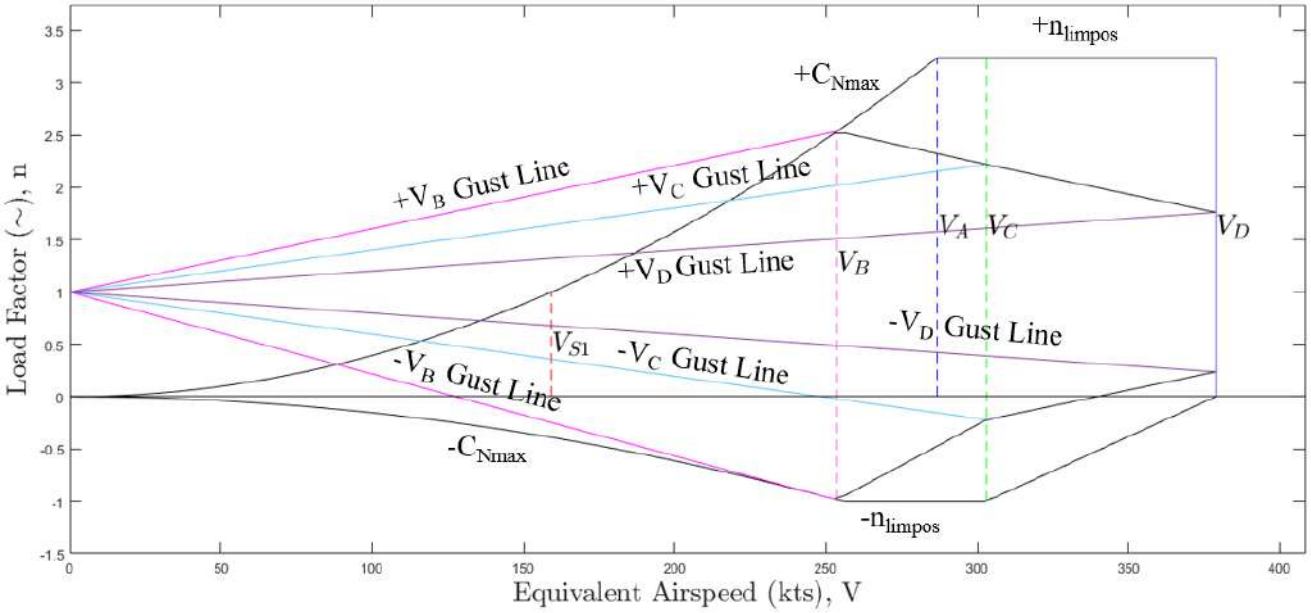

Figure 9.0.1 Superimposed V-n Diagram

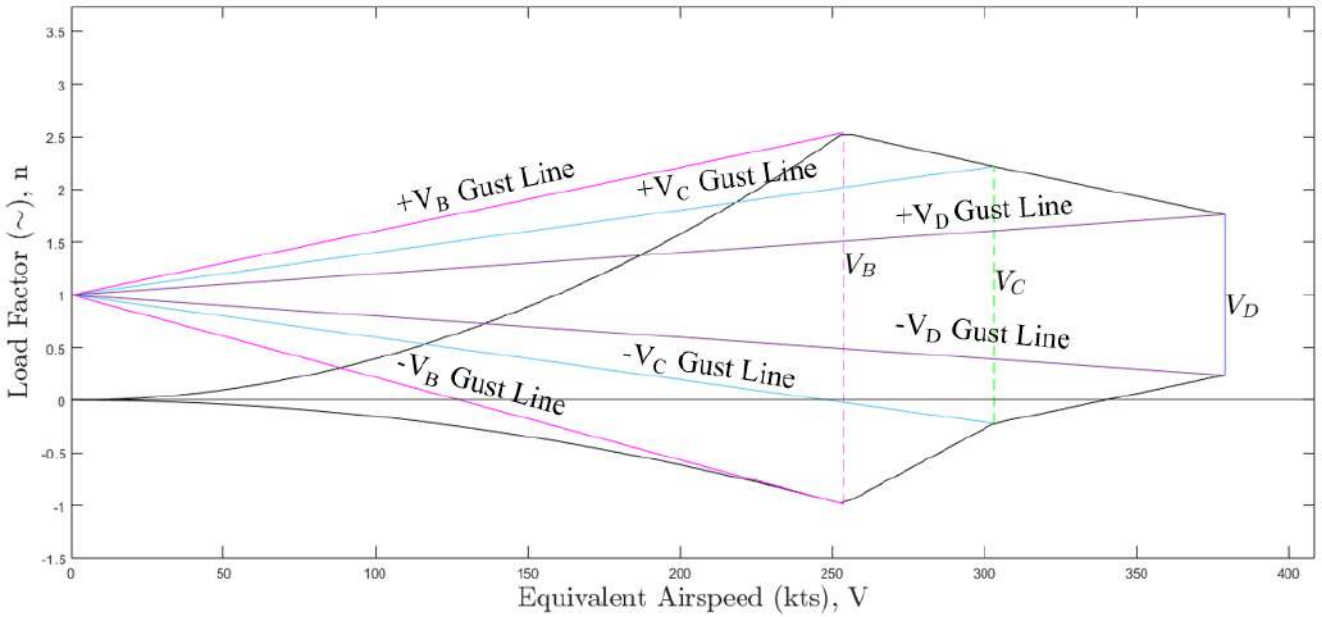

Figure 9.0.2 Gust Diagram

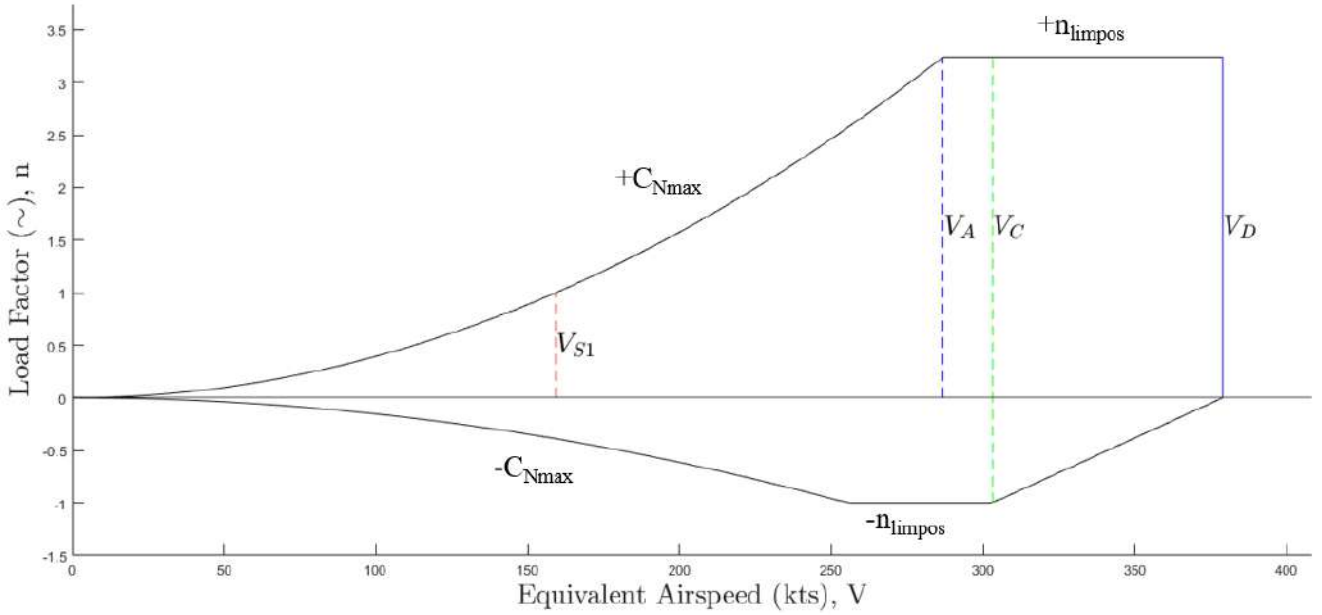

Figure 9.0.3 Maneuvering Diagram

10 Payload Range Diagram

The payload-range diagram uses a variety of parameters that affect aircraft efficiency to calculate the range of different payloads. The Breguet Range equation is used to generate Figure 10.0.1, and is shown in Equation (9). The weight fraction is altered through out the diagram due to the differing payload cases. The differing payload cases can be seen in Table 10.0.1. The weight fraction at each point was calculated by calculating the weight of the fuel used, and the mass fraction at that point. The values for W_5/W_4 are listen in Table 10.0.2.

$$R\,(\text{nmi}) = \left(\frac{V\,(\text{kts})}{c_j\left(\frac{\text{lbf}}{\text{lbf}\cdot\text{hr}}\right)}\right)\left(\frac{L}{D}\right)\ln\left(\frac{W_i}{W_{i+1}}\right) \qquad (9)$$

Table 10.0.1 Payload weights for each case

A	B	C	D
2600 lbf	2600 lbf	2120 lbf	0 lbf

Table 10.0.2 Fuel weight fractions for each case

	A	B	C	D
$\frac{W_5}{W_4}$	—	0.633	0.627	0.601

It can be seen that the lower Mach number of 0.85 allows the aircraft to extend its range. This is due to the lower fuel consumption rate of the engine and the higher lift-to-drag ratios achieved during a lower speed cruise. It should be noted that the aircraft operates at max. fuel and max. payload at the same time.

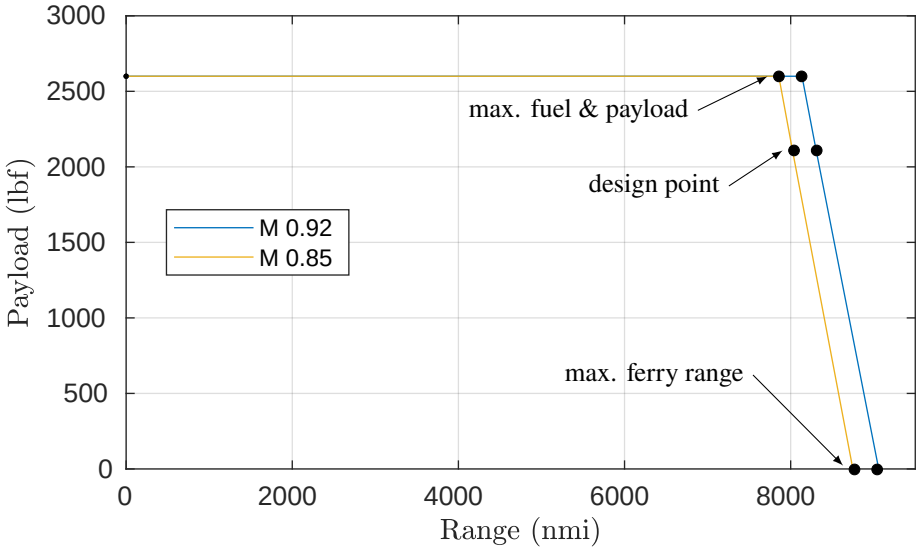

Figure 10.0.1 Payload-Range

The payload-range diagram uses a variety of parameters that affect aircraft efficiency to calculate the range of different payloads. The Breguet Range equation is used to generate Figure 10.0.1, and is shown in Equation (9). The weight fraction is altered through out the diagram due to the differing payload cases. The differing payload cases can be seen in Table 10.0.1. The weight fraction at each point was calculated by calculating the weight of the fuel used, and the mass fraction at that point. The values for W_5/W_4 are listed in Table 10.0.2.

11 Aircraft Design and Sizing

The aircraft characteristics sized for the design is shown in Figure 11.0.1 and Figure 11.0.2. The characteristics include fuselage and cabin sizing as well as the wing and empennage characteristics.

Table 11.0.1 Fuselage and Cabin Characteristics

Characteristic	Fuselage	Cabin
Length, l (ft)	101	54
Maximum Diameter, d_{max} (ft)	10.8	10.3

Table 11.0.2 Wing and Tail Characteristics

Characteristic	Wing	Horizontal Tail	Vertical Tail
Airfoil	Root: NASA SC(2)-0516 Tip: NASA SC(2)-0410	NACA/Langley n0011 sc-il	NACA/Langley Symmetrical n0011 sc-il
Area, S (ft^2)	875	158	67.3
Span, b (ft)	76.8	22.5	9.6
Mean Geometric Chord (ft)	17.3	8.01	11.5
Aspect Ratio, AR	6.7	3.21	1.36
Taper Ratio, λ	–	0.323	1
Thickness-to-Chord Ratio, t/c	Root: 16% Tip: 10%	11%	11%
Incidence Angle (deg)	0	3	0
Sweep Angle (deg)	42	41.4	50
Dihedral Angle (deg)	5	0	0

Table 11.0.3 Control Surface Sizes

Control Surface	Spanwise Ratio	Chordwise Ratio
Inboard Flap	10% – 22.9%	9%
Outboard Flap	23.5%	20%
Aileron	21%	8.3%
Slat	10.6% - 8.1%	29%
Elevator	21%	42%
Rudder	23%	73%

11.1 Cockpit Layout and Design

The cockpit was designed with two main criteria in mind: 1) Pilot compatibility and 2) visibility requirements. The AETHER cockpit features a glass cockpit. It should be noted that the outer mold line of the cockpit is similar to the Piaggio P-180 for styling purposes. The overall layout of the cockpit, shown in Figure 11.1.1, remains similar to that of current market leaders to increase pilot comfort in the AETHER aircraft.

Figure 11.1.1 Cockpit Layout

Figure 11.1.2 95th Percentile and 20th Percentile Female in Cockpit

To account for pilots of various sizes, the cockpit was sized to accommodate both a 95th percentile male, and 20th percentile female, in accordance with methods in Roskam's Airplane Design Part III. Figure 11.1.2 depicts both the 20th percentile female and 95th percentile male operating the aircraft. The maximum viewing angles of the aircraft are direct line of sight, with an upper viewing angle of 48.5°and lower viewing angle of 15.6°. However, it should be noted that the pilot does not experience complete visibility at 30°and -135°azimuth. Additionally, due to the large structural component separating the forward and side windows, pilot visibility is also limited. Pilot visibility restrictions can be seen in Figure 11.1.3. Due to this, synthetic vision will be used by AETHER pilots. Synthetic vision will allow the pilot a full range of vision, and eradicates the issues of the blind spots.

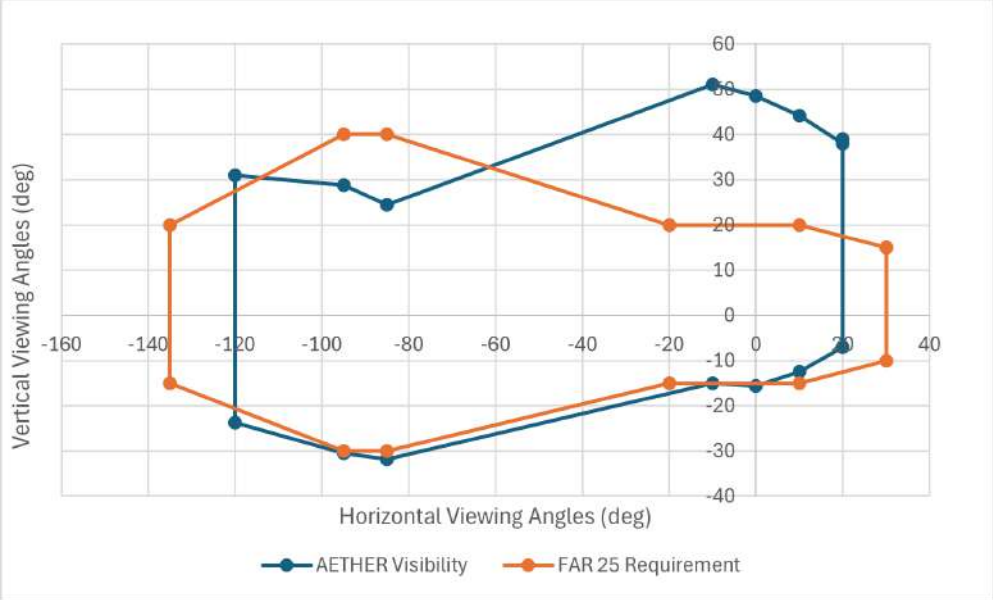

Figure 11.1.3 Pilot Visibility Chart

11.2 Fuselage Layout

The fuselage design of AETHER was driven by a dual objective: to maximize volumetric efficiency for cabin comfort and systems integration, while minimizing wave drag through aerodynamic refinement. The initial layout process began was an internal component analysis to determine the minimum envelope dimensions, ensuring proper accommodation of the cockpit, avionics, galley, lavatories, pressurized cabin, and baggage hold. Following the initial layout of the internal volume, area ruling was applied to the fuselage based on the area ruled Boeing 747 [51]. This smooths the longitudinal distribution of the cross-sectional area, reducing transonic in the cruise regime.

Figure 11.2.1 depicts a cross section of the widest point of the aircraft. This cross section in 10.8 feet in diameter, demonstrating the superior cabin volume of the fuselage. This enhances the passenger experience, allowing maximum cabin comfort. The seating configuration was based on the passenger capacity requirements and the comfort of the passenger. The

cabin is easily able to accommodate a 95% male and a 20% female with space for amenities. The internals of the fuselage contain a queen bed, two lavatories, storage where 30% is climate controlled, ten passenger seats, one flight attendant seat, an additional bunk above the flight attendant seat for crew, a couch with seating for three, and two additional jump seats in the cockpit. Additionally, the seats are lay flat reclinable. The internal layout of the fuselage is shown in Figure 11.2.2.

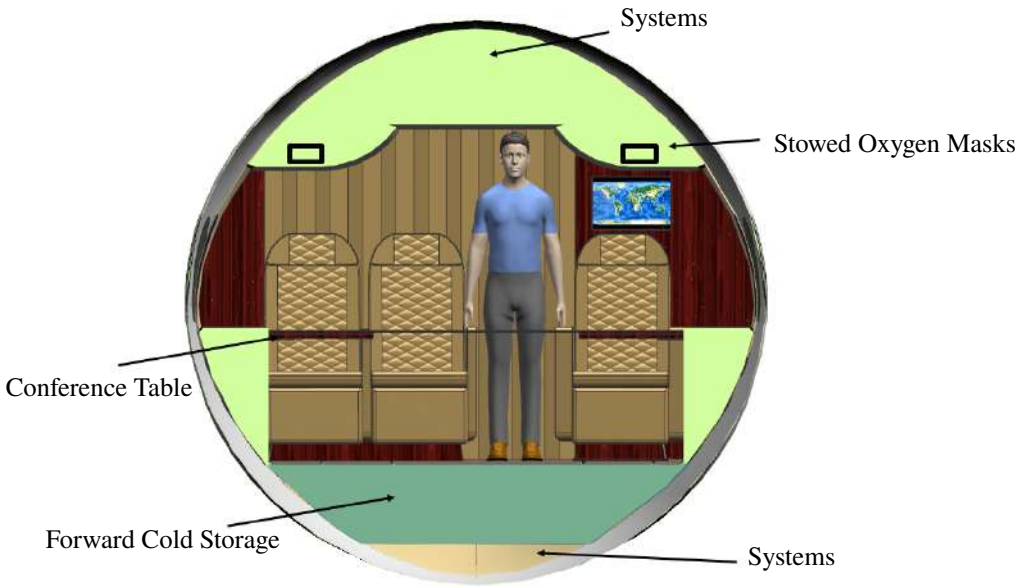

Figure 11.2.1 Fuselage Cross Section

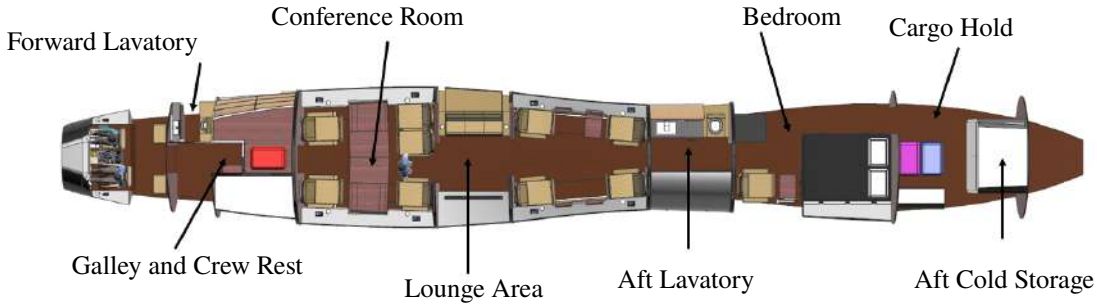

Figure 11.2.2 Fuselage Internal Layout

11.3 Engine Selection and Installation

Long-haul business jets are typically powered by two or three engines. Based on the thrust requirements, the engine selection poses a challenge since there are no certified engines matching the required thrust of 12000 lbf per engine. The Pratt & Whitney PW800 family is more powerful than required, as is the Rolls Royce BR700 series. A three engine aircraft would only need engines with 8,000 lbf thrust. A trade study was conducted to decide between two or three engines powering AETHER. It compares the Safran Silvercrest, an engine under development with 12,000 lbf thrust, and the Rolls-Royce AE 3007A1P, an engine used in the RQ4 Global Hawk with 8,000 lbf thrust. The results can be found in Table 11.3.1.

Table 11.3.1 Comparison of 2- and 3-engined aircraft

	2 engines (Safran Silvercrest)	3 engines (Rolls-Royce AE 3007A1P)
Commonality of Configuration	Very common	Dassault Falcon 8X last trijet, no new trijets under development
Development Cost Engine	Higher costs; due to no certified engine in this thrust class	Lower costs; engines exist but still adaptions necessary
Initial Cost Engine	Higher costs	Lower costs
Operating Cost	Lower costs	Higher costs
Risk in Development	Slightly higher risk	Average risk
Engine Total Mass	4580 lb	4932 lb
Effort for Engine Integration	Low effort	Very high effort: structural mass increment, inlet development, space, maintenance
Engine Technology	Higher level	Lower level
Accordance with Design Philosophy	All new long-range business jets have two engines. This design is considered as modern.	Three-engined aircraft might be seen as old and outdated.

The two-engine variant was selected for AETHER as it offers operational advantages and is considered more advanced. However, it should be noted that the engines will be more expensive. In addition, there is a development risk as there are currently no certified engines with 12,000 lbf thrust per engine, which is necessary according to aircraft sizing. The development of the Safran Silvercrest faced several drawbacks, but the PW800 family can serve as a backup.

The engine chosen for installation is the Safran Silvercrest. The dimensions of the engine and the mounting hard-points - highlighted with red circles - are depicted in Figure 11.3.1. As a two-spooled engine, the Silvercrest will be used as an APU on the ground by running the inner spool. The Silvercrest will be 15.5% more fuel efficient regarding Thrust Specific Fuel Consumption (TSFC) as compared to first generation BR700 engines powering the Gulfstream G650.

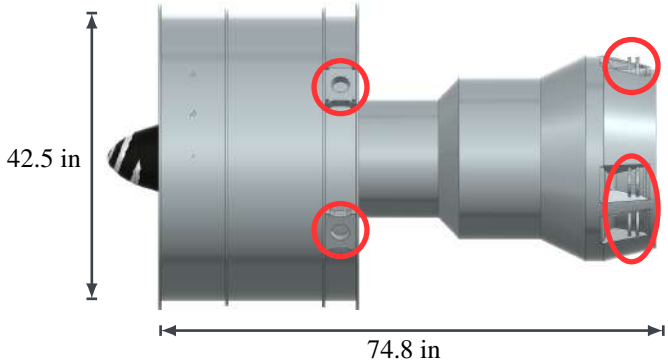

Figure 11.3.1 Side View, Engine Dimensions and Mounting Hard-points

Table 11.3.2 Safran Silvercrest Engine Statistics

Thrust [lbf]	12,000
Length/Diameter [in]	74.8 / 42.5
Dry Weight [lb]	2,290
Overall Pressure Ratio	39.5
Bypass Ratio	5.9:1
TSFC in cruise/loiter [lb/lbf h]	0.53 / 0.38

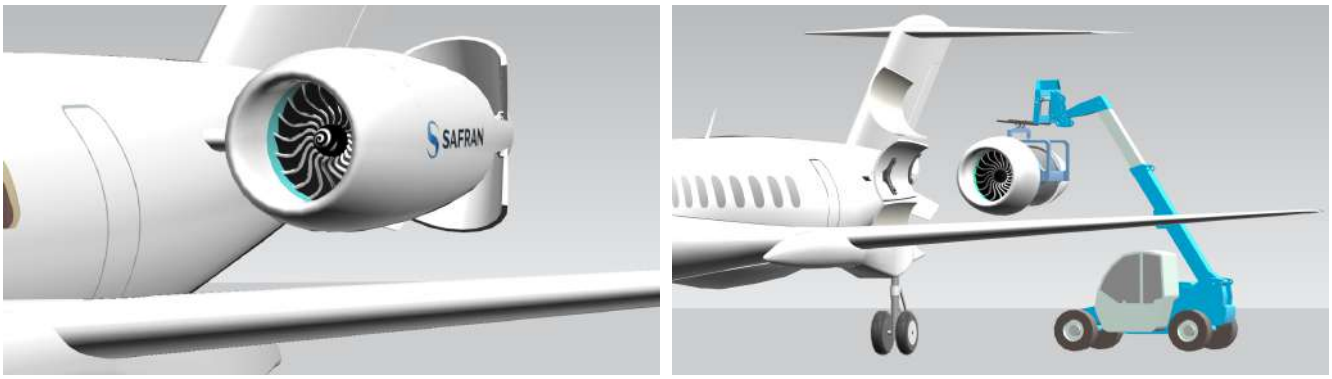

Figure 11.3.2 Thrust Reverser, Engine Replacement and Mounting Structure, Safran Logo from [13]

Figure 11.3.2 shows the engine mount in the nacelle which is located on the tail according to the T-Tail configuration. The nacelle contains two Y-struts, which hold the engine and transfer the thrust to the fuselage and is equipped with a clamp-shell thrust reverser. The Y-struts are arranged according to the hard points shown in Figure 11.3.1. To remove the engine, a crane or telehandler is required, as shown in Figure 11.3.2. After the engine has been removed from the fuselage, the inlet and thrust reverser can be dismantled to access the core engine. As is usual with business jets, the engine manufacturer also supplies the AETHER engine including the bypass casing. Safran is also a manufacturer of thrust reversers, so it is possible to have the entire nacelle manufactured and assembled by Safran.

11.4 Wing Layout

The wing characteristics to develop the wing layout are determined in this section. The wing design for this aircraft is based on the Boeing 747 area ruled concept, and utilizes aero-isoclinic properties to minimize wave drag [51].

The preliminary thickness of the wing was sized using an 18% thick airfoil to meet wing fuel volume requirements. However, this proved to be too robust of an estimate. Thus, a 16% thick airfoil was selected for the root airfoil and 10% thick airfoil was selected for the tip airfoil. The varying airfoil thickness makes the wing loss prone to flutter and leads to a decreased aerodynamic moment.

A wing span of 76.8 ft was determined to be the most optimal wing span to fit the area ruled concept. The wing itself is large in size, with a root chord of approximately 30 ft and a tip chord 3.8 ft. Due to the complex geometry of the wing, trapezoidal integration was used to determine the area of the wing, the mean geometric chord, and the location of the mean geometric chord. Using this methodology, the wing area was determined to be 875 ft^2, and the mean geometric chord to be 17.3 ft in length. The wing area results in an aspect ratio of 6.7.

Table 11.4.1 Wing Geometry

Parameter	Value
Root Chord	NASA SC(2) - 0516, 335 in
Tip Chord	NASA SC(2) - 0410, 45.6 in
Wing Span	902.4 in, 76.8 ft
Wing Area	875 ft^2
Aspect Ratio	6.7
Mean Geometric Chord	17.3 ft

The sweep angle, Λ, for the aircraft was selected to be approximately 42°. A dihedral angle was determined to be 5°. The dihedral angle was selected to match current Boeing 747 aircraft in operation. The incidence angle was based on other

historical data and Boeing 747 aircraft and determined to be 0°. It should be noted that supercritical airfoils were utilized for this aircraft. Super critical airfoils were selected based on the aircraft's high Reynolds number and high cruise Mach number that it will experience in cruise flight. The wing configuration specifications are shown in Table 11.4.1. The final wing layout is shown in Figure 11.4.1.

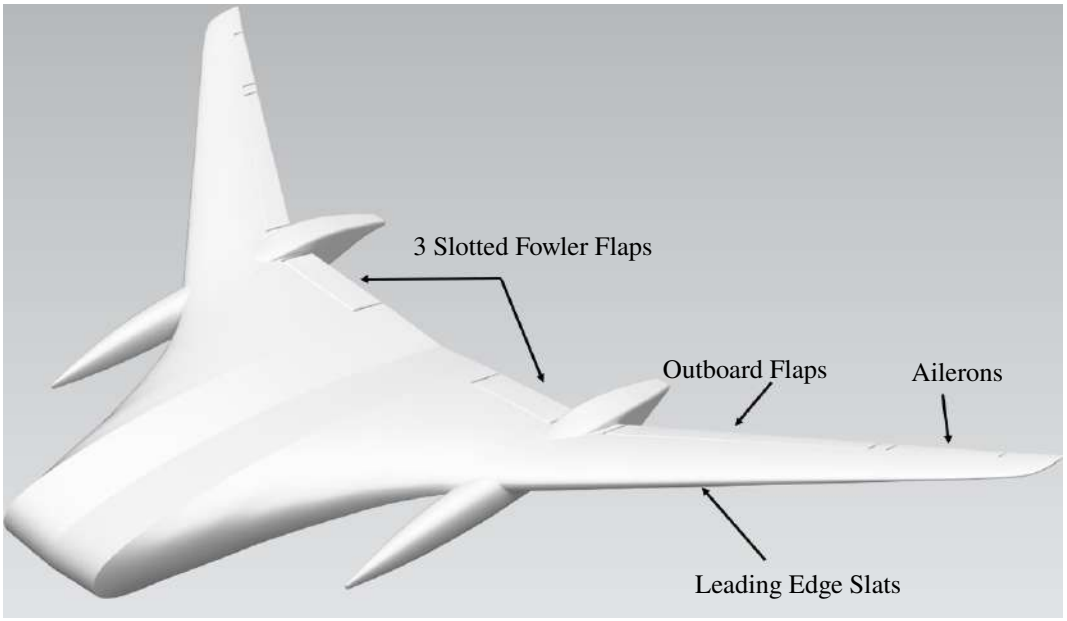

Figure 11.4.1 Proposed Wing Layout

11.5 High Lift Devices

Three-slotted trailing edge flaps and slats on the leading edge of the wing were chosen for the high-lift aids. This combination is necessary to generate sufficient lift for take-off and landing. Due to the special wing geometry resulting from the area rule fuselage design, the flaps cannot cover the entire wingspan. Leading edge flaps are not possible at the wing root and therefore close to the fuselage. This setting of high lift devices will cause higher maintenance costs which are accepted for better performance. Figure 11.5.1 shows the flap setting at the wing root, Figure 11.5.2 at mid wingspan.

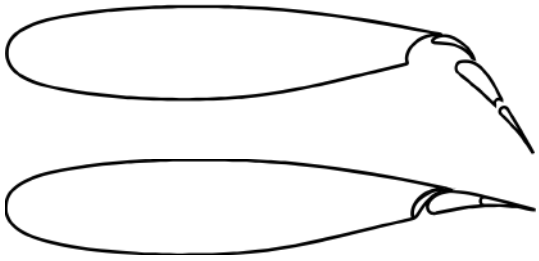

Figure 11.5.1 Flap setting at wing root extended and retracted

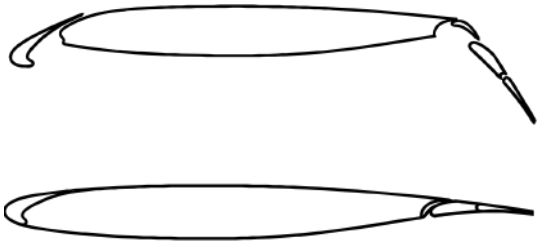

Figure 11.5.2 Flap setting at mid wingspan extended and retracted

A $C_{L,max}$ of 2.06 for Take-Off and 2.58 for Landing are calculated. Those $C_{L,max}$ values are sufficient for the chosen design point in Figure 7.4.1. However, it should be noted that wind tunnel data and flight testing of the complicated wing geometry will be necessary in order to determine the exact $C_{L,max}$ values.

11.6 Empennage Sizing

The design of the empennage of AETHER is derived from a scaled area ruled concept of the Boeing 747 [51]. The 747 empennage features a conventional low tail configuration. However, AETHER was prescribed a T-Tail configuration for the empennage. As such, the horizontal tail size and location relative to the center of gravity is maintained from the from the 747 layout. The vertical tail is altered to support the chosen T-Tail configuration. To begin sizing, the area ruled 747 is scaled relative to the fuselage length of AETHER. With the scaled layout and the horizontal tail location set, the vertical tail is translated aft of the original location such that the quarter chords of both tail surfaces are aligned.

To size the vertical tail in the new location with the T-Tail configuration, the ratio of the lift curve slope between AETHER and the scaled 747 is found. A lift curve slope of 2π per radian was assumed for AETHER due to the T-Tail configuration. The Polhamus equation was used to determine the lift curve slope of the down-scaled 747 as 2.54 per radian. This lift curve slope ratio is used to determine the dimensions of AETHER's vertical tail. The dimensions for both the scaled area ruled 747 and AETHER are shown in Table 11.6.1 and Table 11.6.2. It should be noted that the airfoil chosen is a symmetric super critical airfoil advised in a technical conversation [52]. The final empennage configuration is shown in Figure 11.6.1.

Table 11.6.1 Vertical Tail Sizing

Parameter	Scaled B747 Area Ruled	AETHER
Tail Span	15.0 ft	9.6 ft
Tail Area	165.0 ft^2	67.3 ft^2
Root Chord	13.1 ft	11.5 ft
Tip Chord	3.9 ft	11.5 ft
Volume Ratio	0.070	0.046
Airfoil	NACA/Langley n0011sc-il	Symmetrical

Table 11.6.2 Horizontal Tail Sizing

Parameter	Scaled B747 Area Ruled and AETHER
Tail Span	22.5 ft
Tail Area	158 ft^2
Root Chord	10.6 ft
Tip Chord	3.42 ft
Volume Ratio	0.86
Airfoil	NACA/Langley Symmetrical n0011sc-il

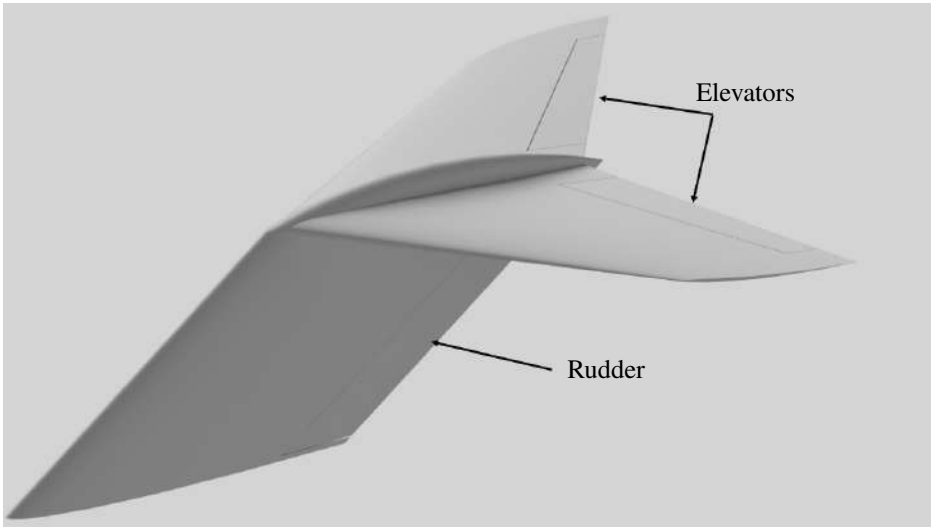

Figure 11.6.1 Proposed Empennage Layout

11.7 Landing Gear Design

The landing gear is laid out in a twin configuration for both the nose gear and the main gear. An actuator will be attached to the landing gear struts, allowing them to retract into the fuselage or wing. The landing gear was laid out according to Roskam Part IV [47]. As such, it maintains a 15 degree clearance of the empennage as to ensure strike upon landing does not occur. To further combat this, strakes are incorporated to the aft end of the fuselage to ensure that if touch down strike occurs, non-essential structures will be hit first. The main gear was additionally placed using a 35 degree half angle, which allows lateral stability. The placement of the landing gear is seen in Figure 11.7.1.

(a) Landing Gear Placement **(b) Landing Gear Side View and Clearance Angle**

Figure 11.7.1 Landing Gear Views

The initial sizing of the tires for both the main gear and nose gear was heavily dependent upon the static loads sustained by the landing gear system. Table 11.7.1 depicts the loads sustained by both the tires and the gear systems. It should be noted that to remain compliant with FAR 25, each static landing gear loads were increased by 7%.

Additionally, the recommended allowable for 25% growth in aircraft weight or tire load was not applied to the main landing gear tires, as doing so would have increased the dimensions of the slipper tanks, which would have impacted the drag polars and the desired lift-to-drag ratio. As a result, the allowable growth was restricted to 4%.

Table 11.7.1 Landing Gear Load Distribution

Parameter	Load (lbf)
Max Static Main Gear Load	37 300
Max Static Nose Gear Load	17 000
Main Max Static Tire Load	18 700
Main Max Dynamic Tire Load	15 800
Nose Max Static Tire Load	8510
Nose Max Dynamic Tire Load	11 200

From the determined loads, the tires could then be selected. Table 11.7.2 shows the selected tires for AETHER. Also, it should be noted that the airports outlined in the RFP has tire pressure restrictions based on their respective Pavement Classification Ratings (PCRs). This was considered when selecting the tires, as several runways are subject to tire pressure code X, which limits the pressure to 254 psi [53].

Table 11.7.2 Tire Specifications [20]

Pos.	Brand	Type	Part No.	Size	Rated Load	Rated Inflation	Rated Speed	Static Load Radius
Nose	Goodyear	Three-Part	258K63-2	H25×8-12	11 300 lb	187 psi	210 MPH	10.5 in
Main	Goodyear	Three-Part	349K82-3	H34×9.25-18	19 400 lb	213 psi	225 MPH	14.5 in

Table 11.7.3 contains the landing gear strut and tire deflections. The touchdown rate utilized is known FAR 25 requirements. Shock absorption and tired efficiency values are taken from Roskam Part IV [47]. The landing gear load factor was selected to be 2.0 for landing and take off operations and for AETHER's FAR 25 certification.

Table 11.7.3 Landing Gear Strut and Tire Parameters for Main and Nose Gear

Parameter	Main Gear	Nose Gear
Touchdown Rate (ft/s)	12	12
Landing Weight (lbf)	74,600	74,600
Touchdown Kinetic Energy (ft-lbs)	334,000	334,000
Allowable Tire Deflection (ft)	0.47	0.33
Shock Absorption Efficiency	0.8	0.8
Tire Absorption Efficiency	0.47	0.47
Strut Stroke Landing (ft)	2.64	2.01
Landing Gear Load Factor	2	2

The slipper tank design was heavily influenced by the main landing gear and fuel storage. Due to the aft most center of gravity location lying slightly behind the wings, the landing gear was required to be integrated into the slipper tanks. Additionally, when the landing gear is fully extended, the landing tires lie outside of the fuselage, providing greater lateral stability. The main landing gear is designed to retract into the slipper tanks in a forward retraction mechanism. The retraction is shown in Figure 11.7.2. To begin, the drag brace first slides into a locking mechanism. After the strut has reached a suitable position, a pin then locks the brace into place. The gear is then fully retracted into the slipper tank. Due to the forward location of the nose gear, a spring actuator will be used to ensure double redundancy in the case of failure.

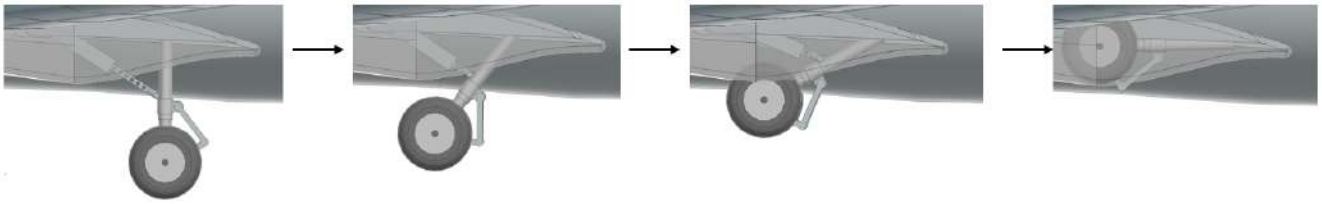

Figure 11.7.2 Landing Gear Retraction

12 Weight and Balance

12.1 CG Excursion Diagrams

Analysis of the center of gravity (CG) required all possible load cases to be investigated to ensure that the aircraft is flyable and cannot be damaged due to tip over. The trim system in the AETHER allows for the CG to be trimmed on the ground and in flight using the wing and empennage fuel tanks and gray water, clear water, and waste tanks. With the inclusion of this system, the CG had to be analyzed at the forward and aft trim locations of the tanks. Cargo, crew, and passengers were also analyzed at various locations to ensure that the CG remained within the allowable limits or was not required to be placarded otherwise.

Figure 12.1.1 depicts the CG excursion diagram for the 8,000 nmi range mission where the plots for both the forward and aft trim cases are shown. This case includes the extra pilots for the long range mission and all passengers and crew at maximum in their seats for takeoff and landing and the maximum baggage load as specified by the RFP requirements. Note that all missions analyzed included the maximum passenger and crew weight and the required baggage, the one shown in Figure 12.1.1 is the sizing mission scenario.

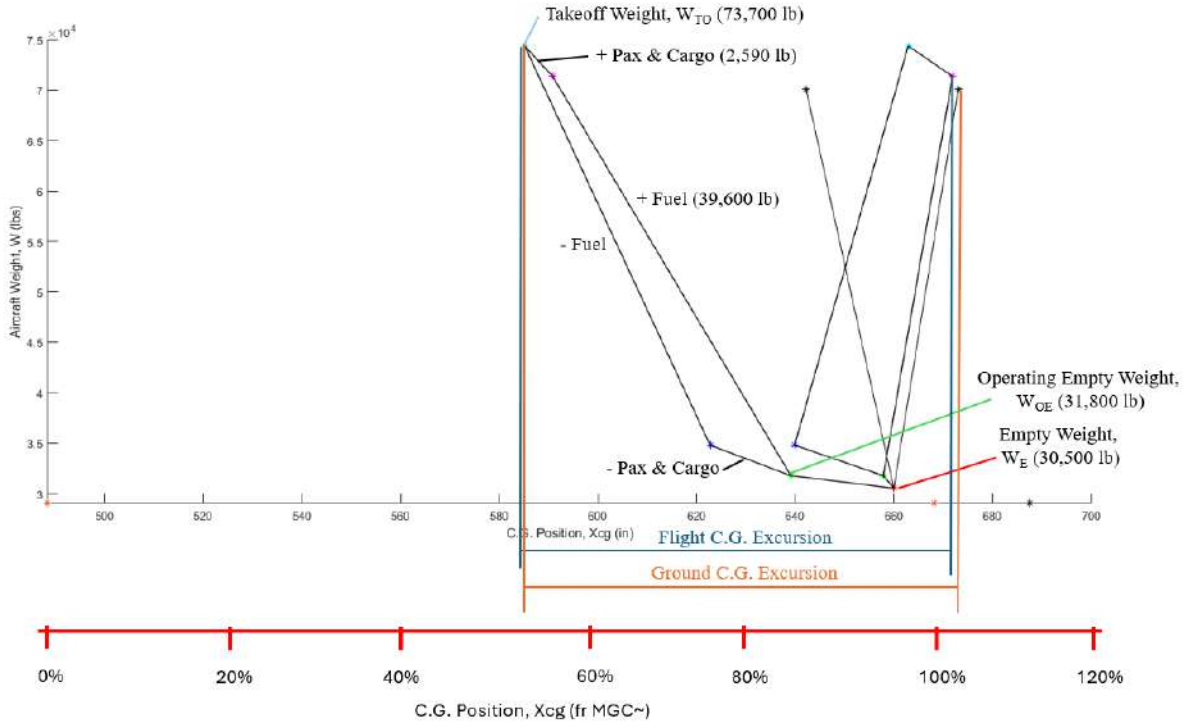

Figure 12.1.1 CG Excursion Diagram for Long Range Mission

12.2 Items to Take into account for CG Excursion

It should be mentioned that the ideal flight CG location is 630 inches from the nose - or 80 percent of the chord. Trim tanks allow for this to be achieved throughout the flight in most cases. With the acceptable flight range being 324 - 633 inches from the nose and the ground CG being no further aft than the landing gear - 688 inches from the nose - it was found that certain cases exceeded these parameters and thus required placarding.

For flight operations, it is required that the wine cargo be split in half between the forward and aft cold storage locations and that no more than 1970 lbs of combined cargo and passenger weight be beyond the forward aft lavatory door. For maintenance and ground handling, it was found that no more than 4,100 lbs may be in the baggage compartment with empty water trim and fuel tanks. In the conditions where the AETHER has full tanks in aft trim or has only full aft water tanks, the baggage compartment can only hold 2,800 lbs. If the empennage fuel tanks and the aft trim tanks need to be filled, it is required that the wing tanks are 80 percent full to prevent tip over.

13 Advanced CAD

The three-view of AETHER is shown in Figure 13.0.1. A situational rendering of AETHER is shown in Figure 13.0.2.

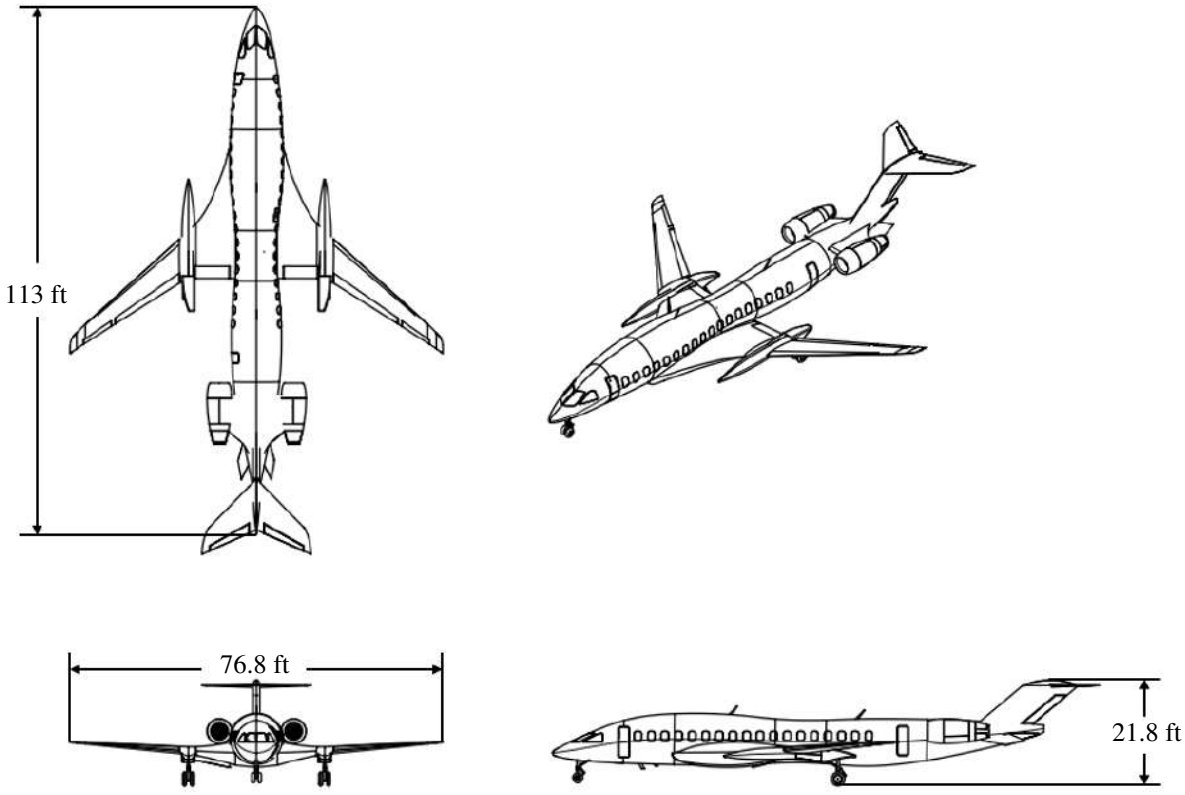

Figure 13.0.1 AETHER Three-View

Figure 13.0.2 Situational AETHER Rendering

13.1 Exploded View

Figure 13.1.1 depicts the aircraft in its individual segments. This includes the substructure, interior layout, engines, and outer mold line of the aircraft.

Figure 13.1.1 Exploded View

13.2 Substructure

Figure 13.2.1 shows the aircraft substructure, with the detailed substructure components outlined in the following subsections.

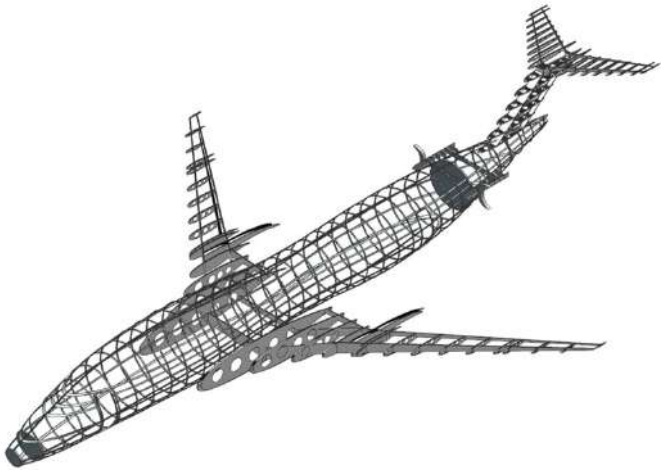

Figure 13.2.1 AETHER Substructure

13.2.1 Fuselage Substructure

The fuselage substructure consists of ring frames and longerons, shown in Figure 13.2.2. The initial ring frames were placed on the two connecting spars of the wings. This resulted in a ring frame spacing of 34 inches between each ring frame. The longerons spacing is slightly larger than those common in business jets due to the incorporation of a composite fuselage. This allows for higher strength in the fuselage, reducing the need for smaller spacing between longerons.

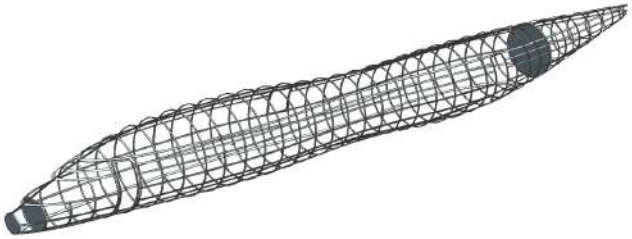

Figure 13.2.2 Fuselage Substructure

Table 13.2.1 Fuselage Substructure Characteristics

Frame Spacing	34 inches
Longeron Spacing	20 inches
Frame Depth	1 inch

13.2.2 Wing Substructure

Figure 13.2.3 shows the wing substructure with two spars at 25 % and 75% of the chord. The slipper tank is a fully monocoque structure, thus not requiring ribs, ring frames, and stringers. The characteristics of the wing substructure is shown in Table 13.2.2.

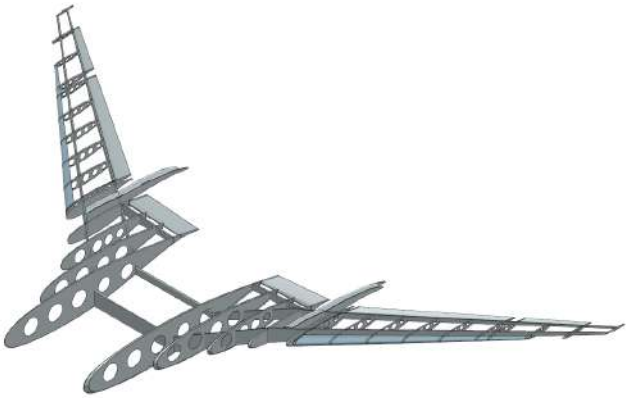

Figure 13.2.3 Wing Substructure

Table 13.2.2 Wing Substructure Characteristics

Rib Spacing	18–24 inches
Spar Thickness	0.125 inches
Forward Spar Location	25% chord
Aft Spar Location	75% chord

13.2.3 Horizontal Tail Substructure

The horizontal tail substructure features an elevator as the control surface and uses a two-spar design. The characteristics of the horizontal tail structure are presented in Table 13.2.3.

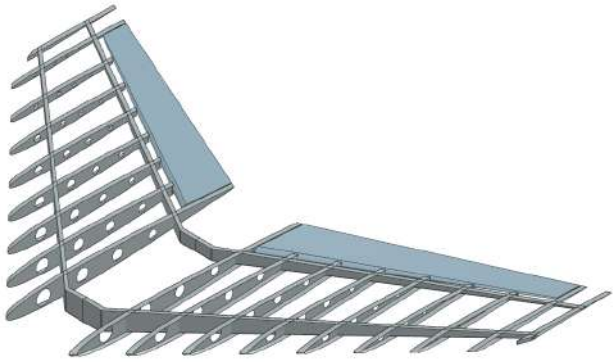

Figure 13.2.4 Horizontal Tail Substructure

Table 13.2.3 Horizontal Tail Substructure Characteristics

Rib Spacing	14.4 inches
Spar Thickness	0.125 inches
Forward Spar Location	25 % chord
Aft Spar Location	75 % chord

13.2.4 Vertical Tail Substructure

Similar to the horizontal tail, the vertical tail consits of a two-spar design with a rudder as the control surface. Table 13.2.3 shows the characteristics of the structure.

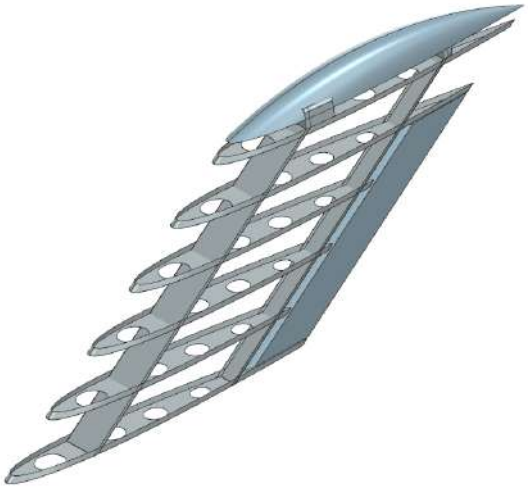

Figure 13.2.5 Vertical Tail Substructure

Table 13.2.4 Vertical Tail Substructure Characteristics

Rib Spacing	18 inches
Spar Thickness	0.125 inches
Forward Spar Location	25 % chord
Aft Spar Location	75 % chord

13.2.5 Engine Substructure

The engine substructure consists of two Y-struts per engine, holding the engine on its hard points which were highlighted in Figure 11.3.1. The engine mount is shown in Figure 13.2.6. The rear Y-strut holds the core engine via the bypass duct. The engine placement on the fuselage is according to AC 20-128A in order to avoid critical daman. Figure 13.2.7 shows the expected particle trajectory in the event of an uncontained engine failure. Red resembles the trajectory of very heavy parts like fan blades or large turbine disk fragments. Green resembles the trajectory of lighter turbine fragments that are unlikely to penetrate the fuselage. The fuel tanks are highlighted in orange. It can be seen, that the occupied cabin and the fuel tanks in the tail will be completely unaffected by uncontained engine failures.

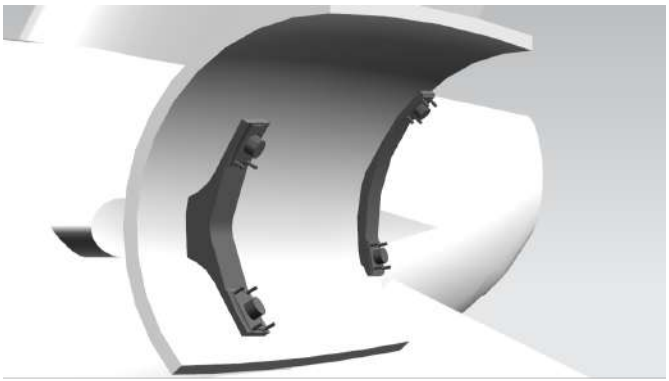

Figure 13.2.6 Engine Mount Substructure

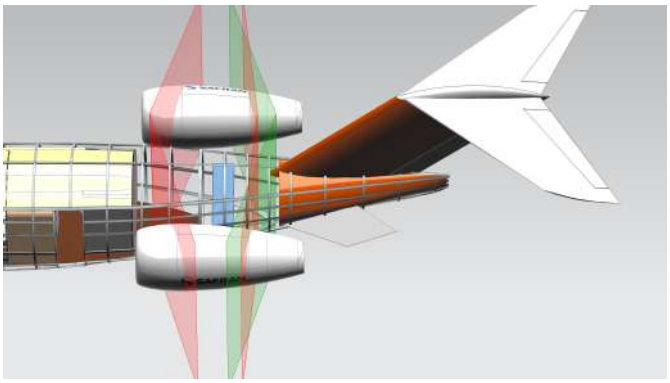

Figure 13.2.7 AC 20-128A Compliance

14 Manufacturing Analysis

Due to the complex shape of AETHER, a preliminary analysis into the required manufacturing processes is presented here.

14.1 Materials Breakout

Figure 14.1.1 illustrates that the skin is mainly carbon-PEEK composite, except for the engine nacelle. The engine nacelle material is Glass Laminate Aluminum Reinforced Epoxy, also known as GLARE.

Figure 14.1.1 Skin Materials

Figure 14.1.2 illustrates that the substructures are mainly carbon-PEEK composite, except for the forward bulkhead, structural components of the landing gear, and the structural supports of the engines.

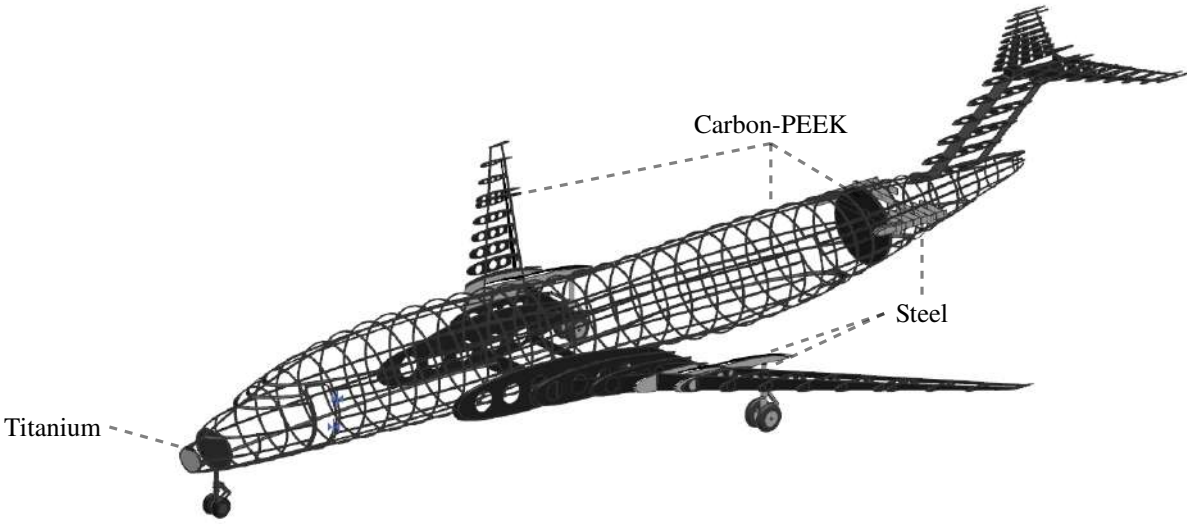

Figure 14.1.2 Substructure Materials

The materials for the airframe and/or exterior components are as listed in Table 14.1.1. Whereas, the materials for the internal components are as listed in Table 14.1.2.

Table 14.1.1 Airframe/Exterior Materials

Components	Material
Skin	Carbon-PEEK Composite
Ribs	Carbon-PEEK Composite
Spars	Carbon-PEEK Composite
Fuselage Frames	Carbon-PEEK Composite
Engine Nacelle	GLARE
Engine Structural Support	Steel
Torque Box	Steel
Landing Gear Strut	Steel
Landing Gear Wheel	Aluminum-Titanium Alloy
Landing Gear Tire	Rubber
Exterior Lights	Glass
Forward Bulkhead	Titanium
Aft Pressure Bulkhead	Carbon-PEEK Composite

Table 14.1.2 Interior Materials

Components	Material
Windows	Plexi Glass
Seat	Leather
Floor	Carpet
Interior Walls	Plastic

14.2 Required Tooling

Four plugs are used for the carbon-PEEK tape-laying process of the three sections of the fuselage skin. The plugs are mounted to their respective stands and the plug rotates about the attachment point, for example, as shown for Tooling 1 in Figure 14.2.1. Tooling 1 is for the nose section, Tooling 2 is for the forward section of the center fuselage, Tooling 3 is for the aft section of the center fuselage, and Tooling 4 is for the tail section.

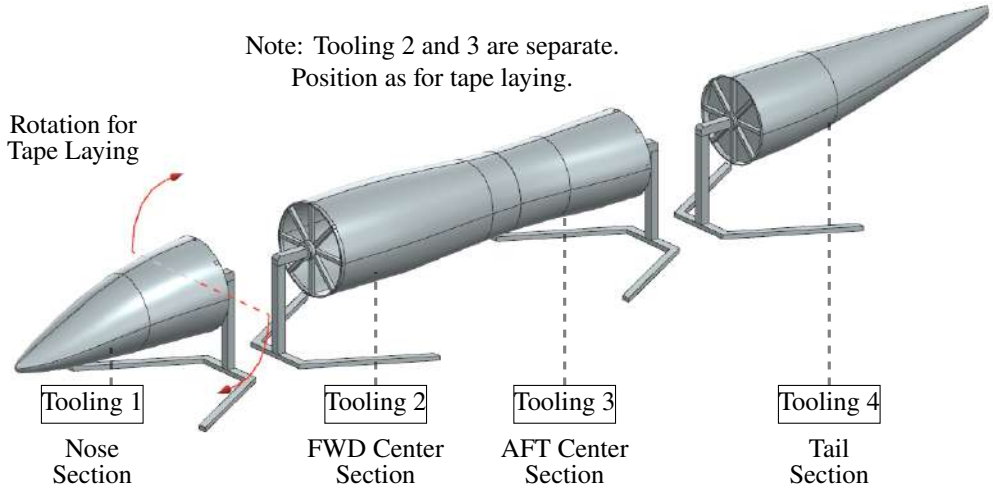

Figure 14.2.1 Fuselage Tooling

14.3 Manufacturing Process

For the manufacturing of the fuselage skin, the fuselage is divided into three sections for the Carbon-PEEK tape laying process. Once the tape laying is complete, the tooling would be removed as shown in Figure 14.3.1. It should be noted that only the removal of the center section of the fuselage tooling is shown since the process for the nose section and tail section are similar.

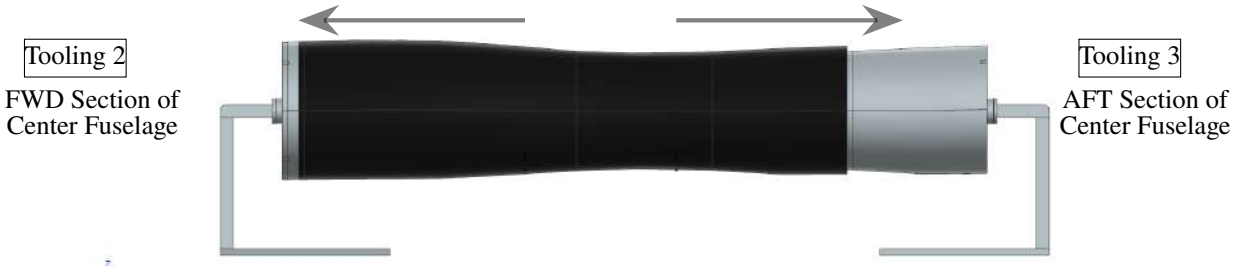

Figure 14.3.1 Removing Process for Center Section of Fuselage Tooling

The manufacturing of the ring frames will be outsourced. For the installation of the ring frames, step 1 would be to rotate the specific ring frame down so that the flat side faces up. Step 2 would be to reposition the ring frame inside the fuselage to the specific location for the ring frame being installed. Step 3 would be to rotate the ring frame into position. The steps for ring frame installation is as shown in Figure 14.3.2. The order that the ring frame will be installed is that the inner ring frame will be installed first, and then the remaining ring frames will be installed sequentially in the outboard direction. For example, the

ring frame for the forward section of the center fuselage will be installed as shown in Figure 14.3.2, red-highlighted frame, next, the remaining ring frames will be installed progressively toward the nose. Meanwhile, the aft section of the center fuselage will be installed starting from the ring frame located directly aft of the red-highlighted frame, with subsequent ring frames installed progressively toward the tail.

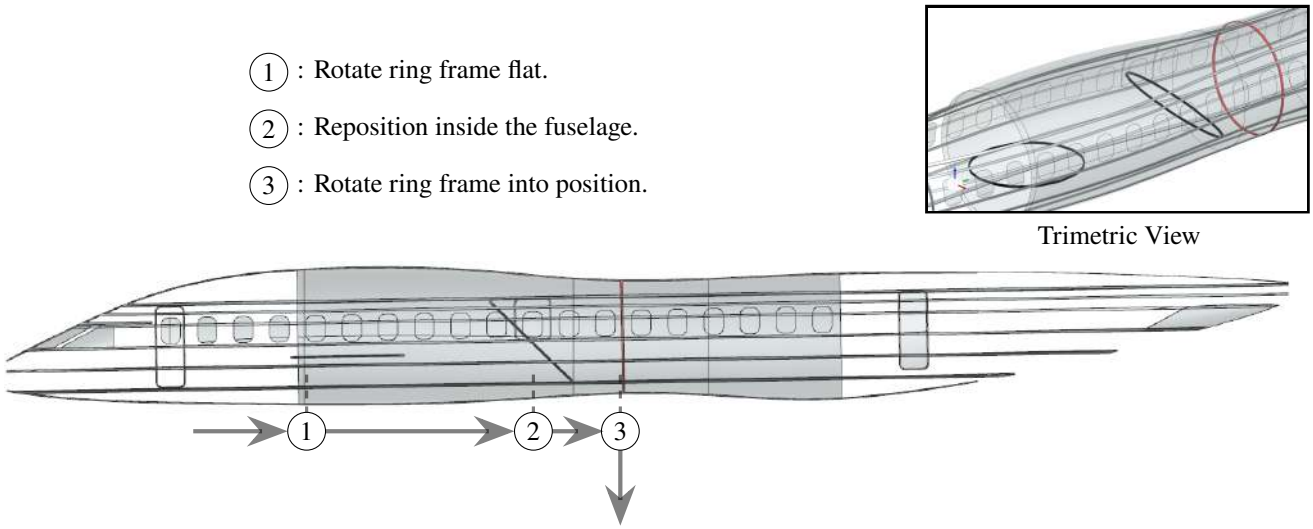

Figure 14.3.2 Ring Frame Installation

Once all the ring frames are installed, the nose section of the fuselage (section 1) and the tail section of the fuselage (section 3) will be installed, as shown in Figure 14.3.3.

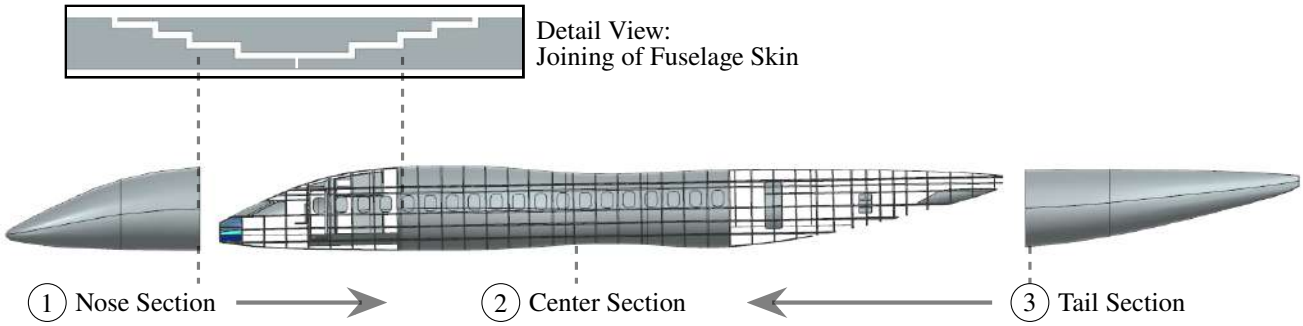

Figure 14.3.3 Fuselage Skin Joining

15 Aircraft Systems

15.1 Flight Control Systems

The flight control system for this aircraft is shown in Figure 15.1.1. The flight control system integrates both pilot input and autopilot commands into a highly redundant and fault-tolerant architecture. Three primary central processing units (CPUs) receive signals from the pilot's sidestick controllers as well as from autopilot systems, processing data from dedicated sensors and air data computer. These CPUs coordinate to command various flight control surfaces via multiple redundant channels, enhancing system reliability. The control surfaces include the ailerons, elevators, rudder, slats, and triple-slotted Fowler flaps, with separate signal pathways represented in different colors, indicating independent control lanes from each CPU. This

ensures that, in event of a failure in one CPU or channel, the aircraft maintains maneuverability and control. The integration of these elements provides responsive handling characteristics while maintaining safety and control integrity under various operational scenarios. The aircraft is equipped with three independent air data systems, each responsible for providing critical measurements to the flight control computers. Both the slipper tanks and nose section are instrumented with dedicated air data ports, each feeding into one of the three separate CPUs. This triple-redundant architecture ensures high reliability and fault tolerance, allowing continued operations and accurate flight data even in the event of sensor or processor failure.

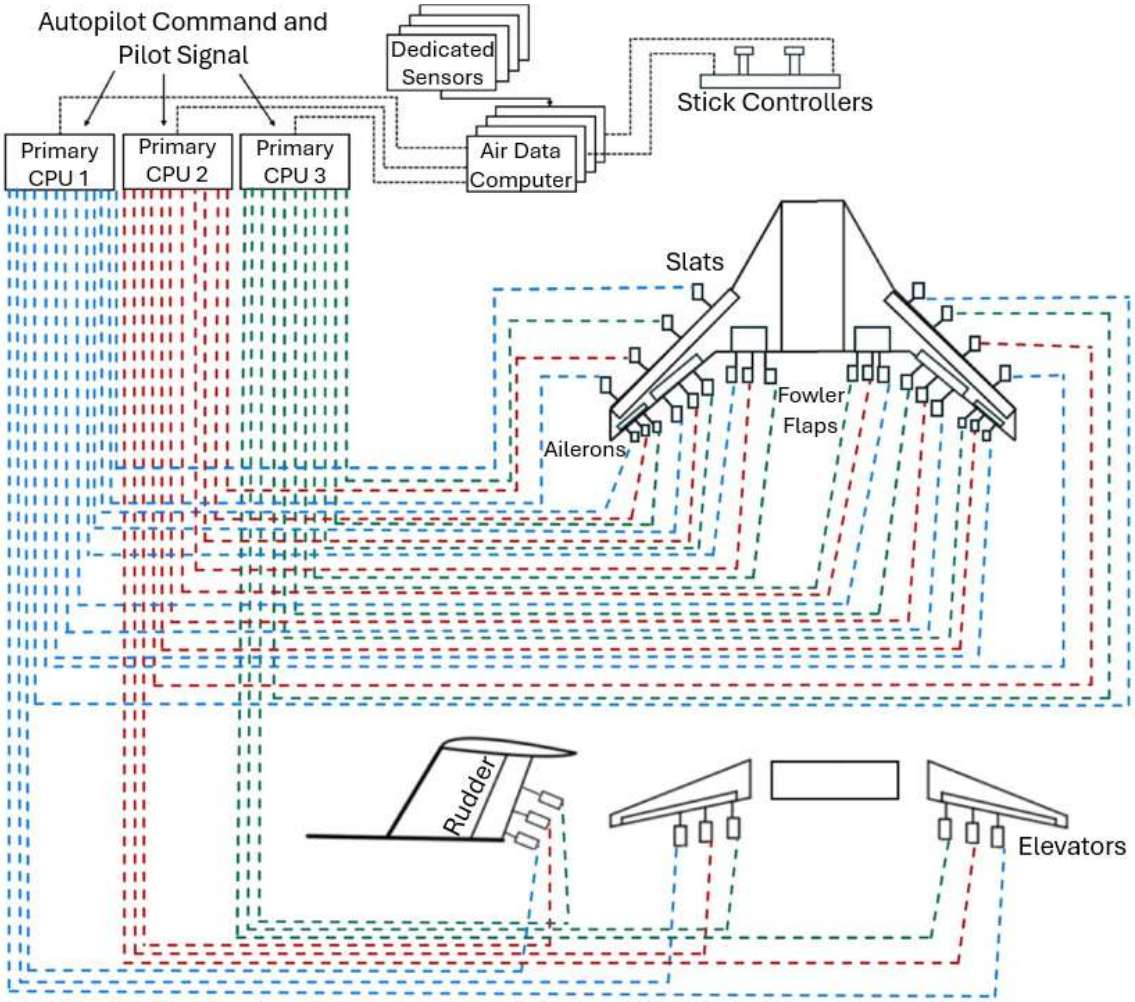

Figure 15.1.1 Flight Control Systems

15.2 Fuel Systems

The fuel system is dependent on the required fuel volume for the aircraft. Since AETHER is intended to cruise at a high Mach number for an extended range of 8,000 nautical miles, a large amount of fuel is required. The volume of the fuel required can be determined using the density of the fuel. The fuel properties used for calculations and the final fuel

Table 15.2.1 Fuel Properties [21]

Parameter	Value	Units
Fuel Weight	39600	lbf
Fuel Density	1.552	slug/ft^3
Required Fuel Volume	792	ft^3

volume are seen in Table 15.2.1.

To keep the entirety of the fuel outside of the fuselage, the fuel tanks were restricted to being only on the wing. However, due to the large amount of fuel required for the flight, two slipper tanks are used to provide adequate fuel.

The there will be 6 large fuel tanks in each wing, as shown in Figure 15.2.1. The fuel tanks end at 72% of the chord and begin at 3% of the chord. This is to account for the leading and trailing edge flaps as well as the de-icing system for the aircraft. To confirm the wing had the necessary fuel volume, a first order approach to approximating volume was used. Due to the complex geometry of the wing, Roskam's approximation of wing fuel volume was unable to be used. It should be noted that the empty section of the wing is to account for the flap track fairing and the slipper tank that will be placed in the section. The volume of each fuel tank inside of the wing is seen in Table 15.2.2.

In addition to the fuel tanks, two slipper tanks will also be used. This allows for the fuel volume not accounted for in the wing tanks to still remain outside of the fuselage. Each slipper tank contains approximately 63.5 cubic feet of fuel, resulting in an additional 127 cubic feet of fuel. The slipper tank and wing configuration is shown in Figure 15.2.1. The slipper tanks are able to dump fuel in case of emergency. The dump outlets are located at the bottom most point of the slipper tanks to ensure fuel is acting away from the fuselage. The fuel tank mechanism of choice is fuel bladders. The fuel bladders will be placed between the forward and aft spars at approximately 25% and 75%.The fuel tank mechanism of choice is fuel bladders. The fuel bladders will be placed between the forward and aft spars at approximately 25% and 75%.

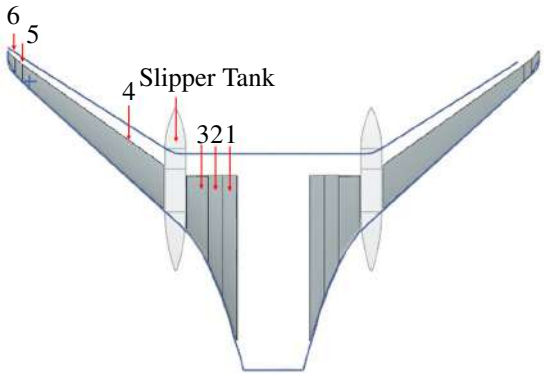

Figure 15.2.1 Fuel Tank Locations

Table 15.2.2 Volume of Fuel Sections

Section	Volume (in^3)	Volume (ft^3)
1	222 000	129
2	128 000	74
3	99 000	57
4	127 000	74
5	1260	0.73
6	664	0.38
One Wing	579 000	335
Two	1 160 000	670

Due to the aircraft's low wing configuration, a pump feed configuration is used to feed fuel throughout the aircraft. Three primary fuel pumps will be used. Boost pumps within the fuel tanks are used to ensure that the fuel reaches the engines. Additionally, there will be transfer pumps between the fuel tanks to allow the fuel to move throughout the tanks and maintain an even weight distribution. The slipper tank requires its own transfer pump to be able to feed into the wing's fuel system. Each engine will contain an engine driven fuel pump, allowing fuel to reach the correct pressure before entering the combustion chamber of the engine. The aircraft contains one refueling port on the right slipper tank to allow for ease of access and closeness

to the central fuel distribution lines. A side view of the fuel system is shown in Figure 15.2.2.

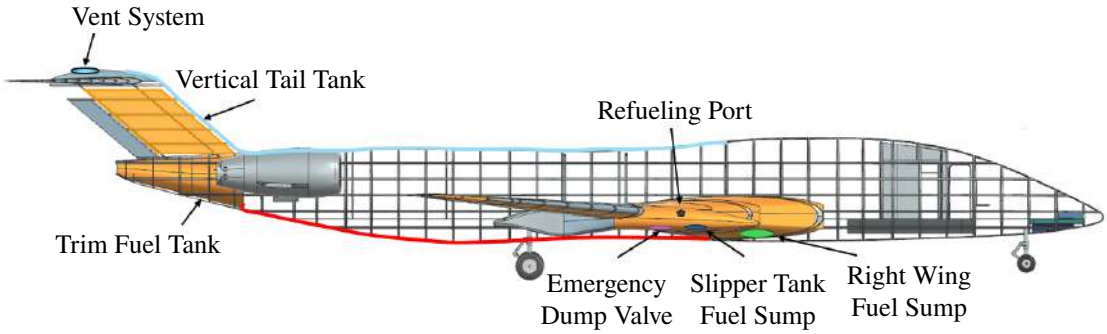

Figure 15.2.2 Side View Fuel System

Pressure refueling is used instead of gravity refueling. This allows quick entrance of fuel into the system and experiences automatic shut off when done refilling. A central cross feed will be used to fill the tanks symmetrically, as seen in Figure 15.2.3.

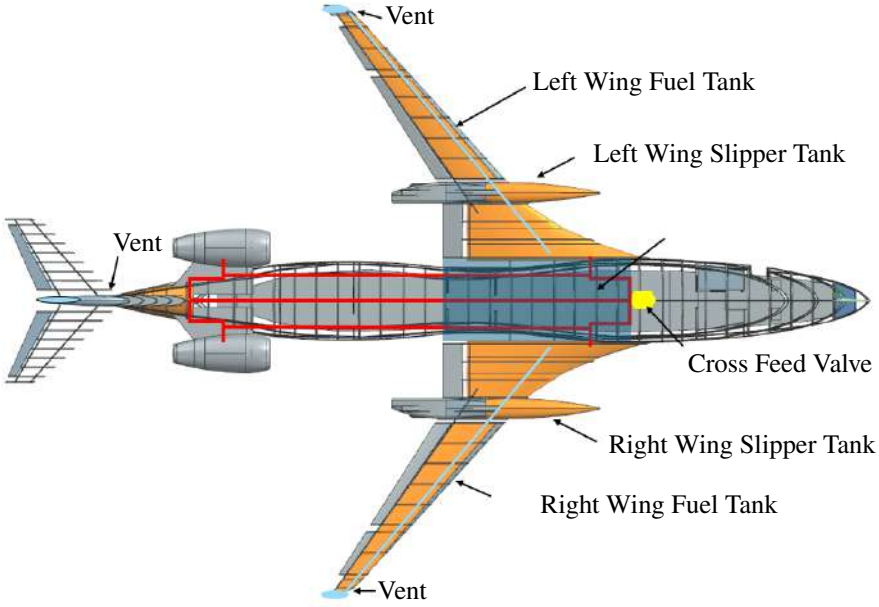

Figure 15.2.3 Side View Fuel System

15.3 Hydraulic Systems

The hydraulic system for the aircraft is shown in Figure 15.3.1. There are two separate hydraulic systems to provide redundancy in the event of a single hydraulic system failure. During normal operation, Hydraulic System 1 is the primary for the main landing gear actuators, the landing gear doors, the engine 1 thrust reverser, and the brakes. Hydraulic System 2 is secondary for these components and would normally be secured unless the system detects a Hydraulic System 1 failure or the system is manually switched over. In addition, during normal operation, System 2 is primary for the nose landing gear actuators, the nose landing gear steering, and the engine 2 thrust reverser. System 1 is the secondary and the system is normally closed for these components. In the event of a System 2 failure, the system will automatically switch to System 1.

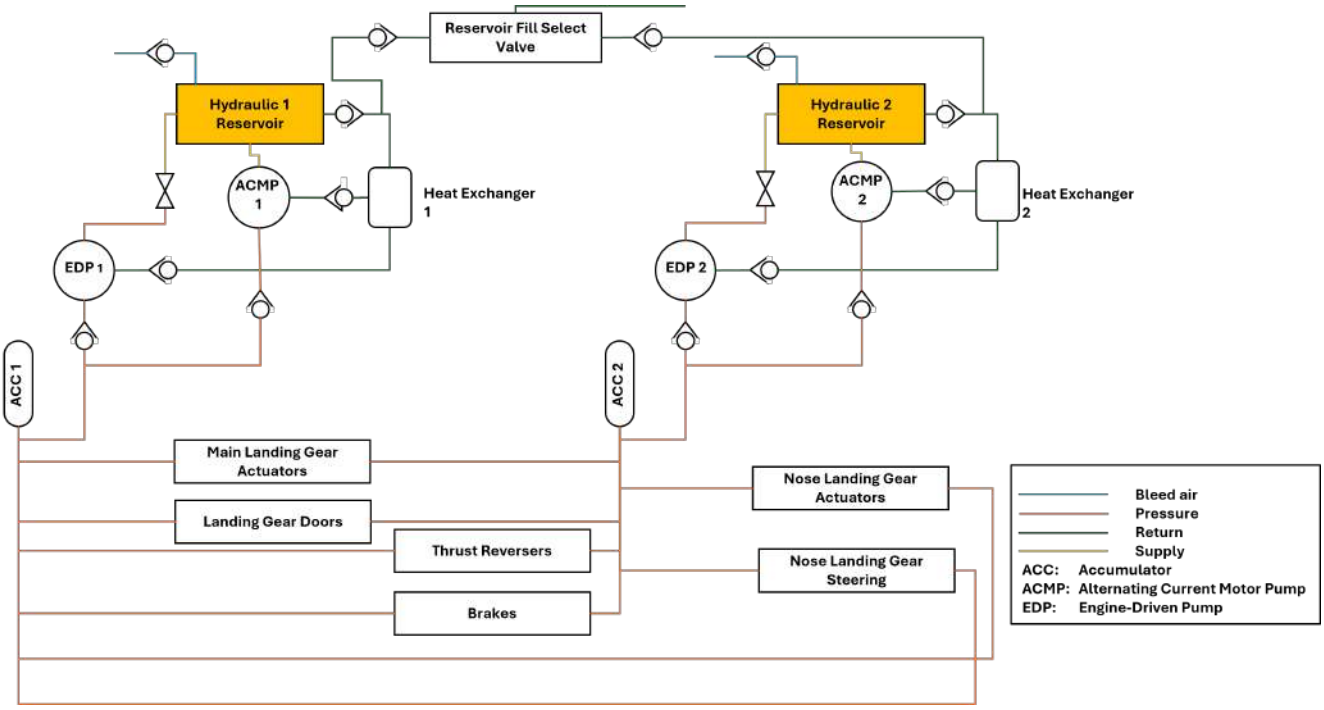

Figure 15.3.1 Hydraulic System

15.4 Electrical Systems

The electrical system for AETHER is shown in Figure 15.4.1.

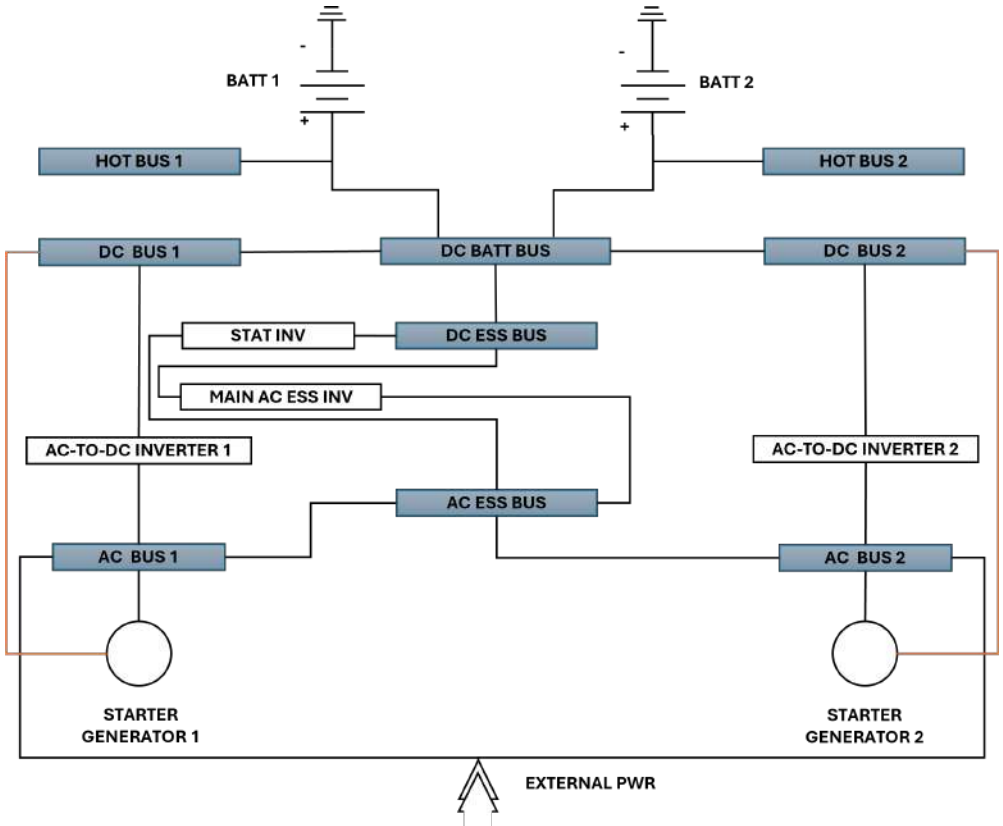

Figure 15.4.1 Electrical System

The direct current (DC) electrical system is shown in 15.4.2, which guides systems to their respective buses.

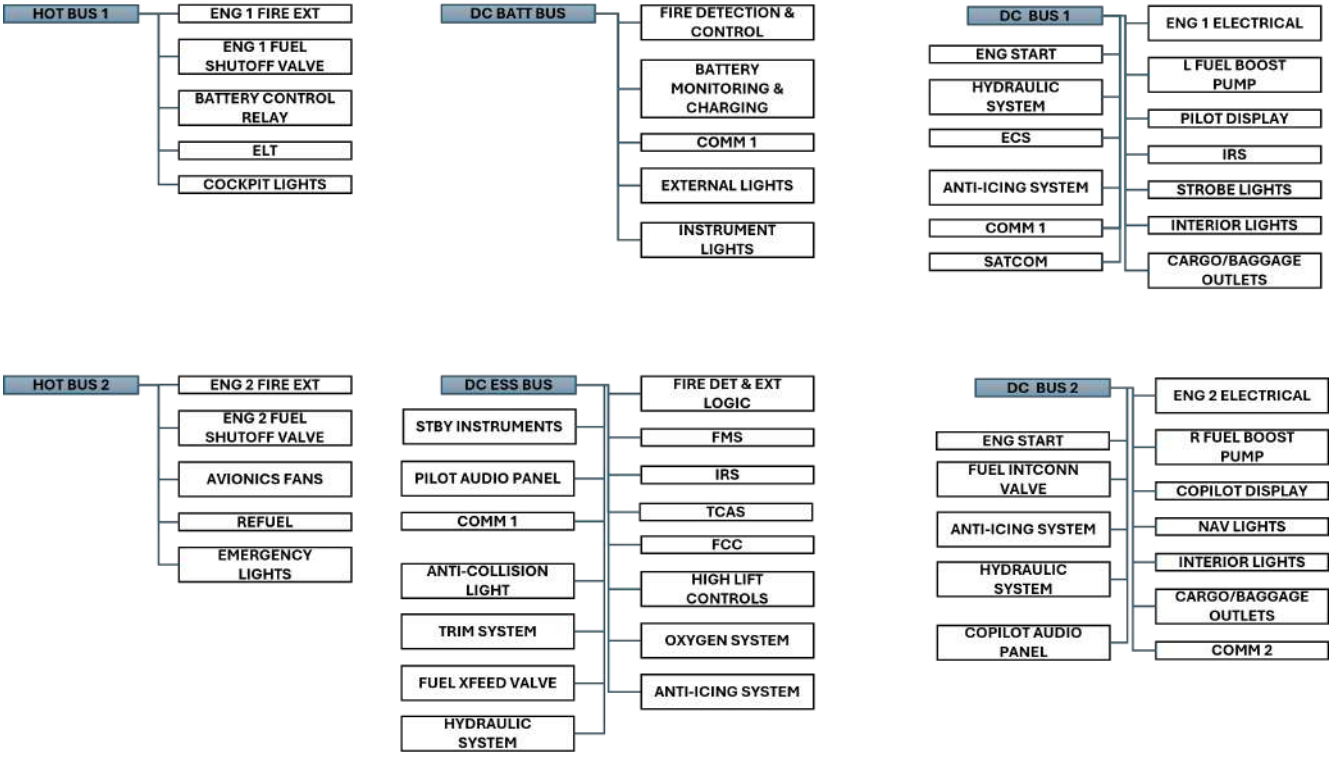

Figure 15.4.2 Direct Current Electrical System

The alternating current (AC) electrical system is shown in 15.4.3, which shows systems to their respective buses.

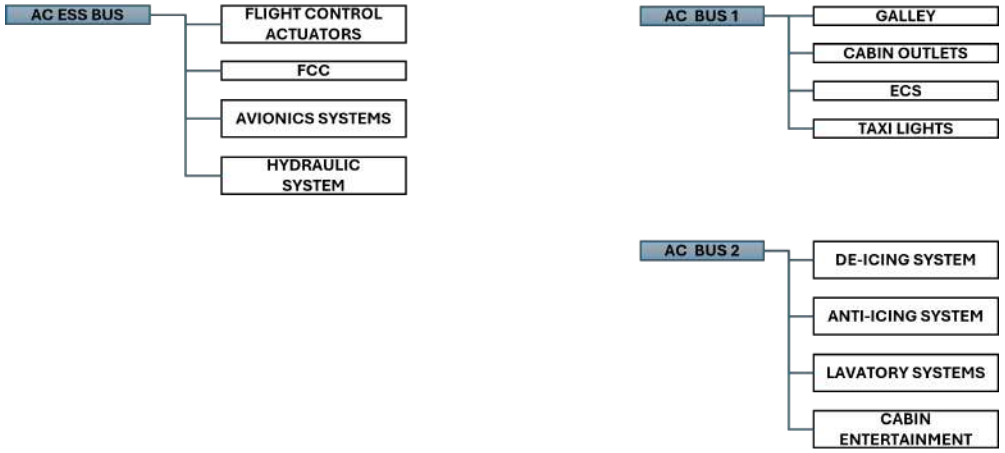

Figure 15.4.3 Alternating Current Electrical System

15.5 Escape Systems, Fire Detection, and Suppression System

The aircraft will have one Type 1 door located at the front left side for ingress and egress. There are two Type 2 doors: at the mid-left point of the fuselage and left side of the tail. The left Type 2 door is used for emergency egress and the back Type 2 is used for servicing and emergency egress. Figure 15.5.1 shows the aircraft escape system. In addition, the layout shows the location of the fire detection, suppression, and protection system.

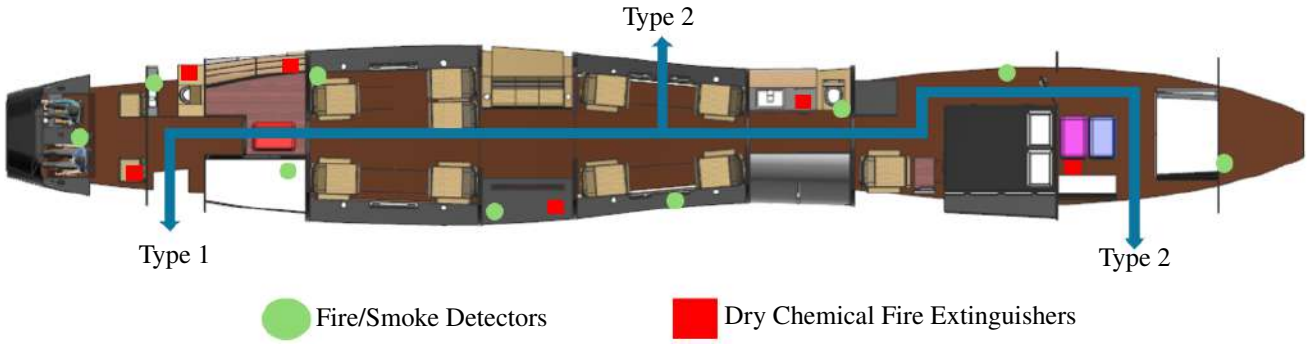

Figure 15.5.1 Escape System

15.6 Pressurization System

The pressurization system maintains a cabin pressure equivalent to 4,000 ft altitude like other market leaders during high-altitude flight. It is controlled by two automatic controllers that receive input from ambient and cabin pressure sensors. These controllers operate the outflow valve using dedicated motors to modulate internal cabin pressure relative to the external environment. Integral ambient sense ports and pressure relief valves serve as safety mechanisms to prevent excessive pressure differentials across the fuselage structure. Cabin controls in the cockpit interface with the system for manual override or mode selection, and a built-in test capability allows for routine system checks. The system ensures a breathable, controlled cabin environment, which is critical for both passenger comfort and physiological safety at cruising altitudes. The cabin pressurization system is shown in Figure 15.6.1.

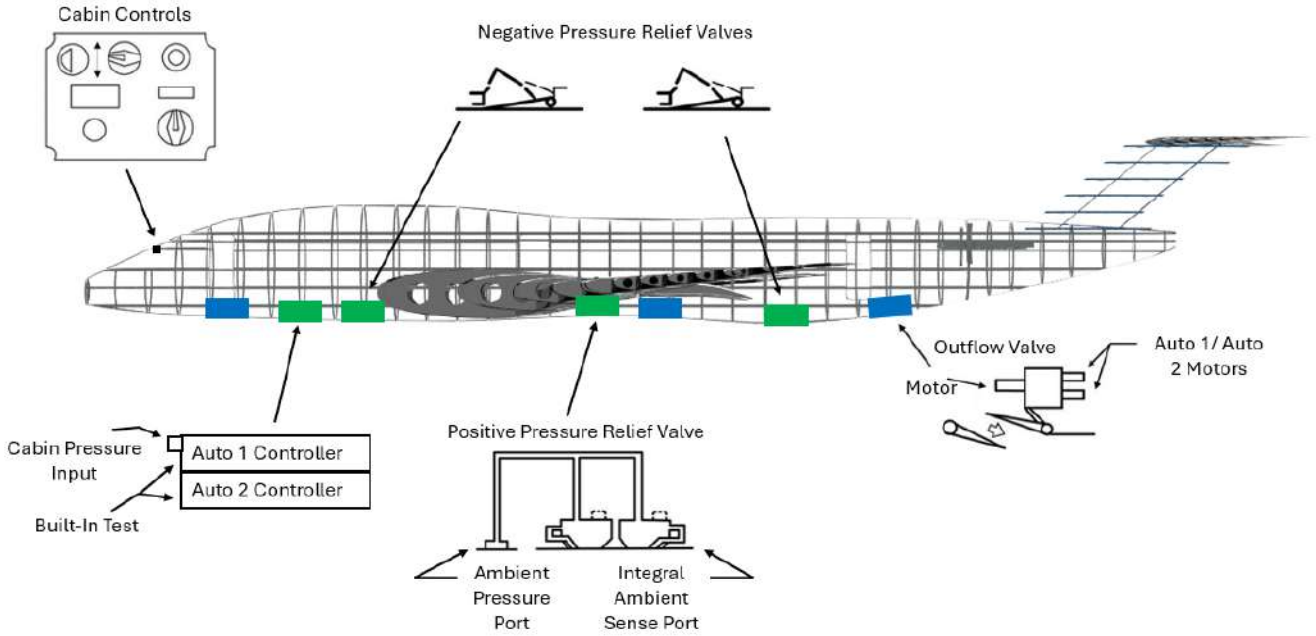

Figure 15.6.1 Pressurization System

15.7 Pneumatic System

The pneumatic system utilizes bleed air from the engine compressors, which is routed through ducting to preform multiple functions. One primary application is to maintain clear cockpit and cabin windows by directing warm pressurized air across the internal surfaces, preventing fogging and ice buildup. Cabin altitude is maintained at approximately $\frac{5}{8}$th of the external ambient pressure. The system incorporates PEEK (polyether ether ketone) tubing for its superior thermal and chemical resistance. This design supports a 62% lower cabin altitude density, improving physiological comfort and enabling better crew and passenger recover on long-duration flights.

15.8 Air Conditioning System

The air conditioning system is designed to enhance passenger comfort through a simplified and efficient airflow approach. It delivers fresh air to passengers, eliminating the need for a recirculation fan. Air enters the cabin from the overhead inlets at low velocity, ensuring a quiet and draft-free environment. The downward airflow promotes an even temperature distribution and natural convection, while the used air exits through a floor-level vent. In addition, each passenger has access to an individual air outlet, allowing personalized control of airflow direction and intensity. To further support hygiene and cabin comfort, dedicated air vents are installed in the aircraft lavatories near the toilets to continuously extract odors and maintain fresh air in these enclosed spaces. This configuration provides a quieter, cleaner, and more comfortable cabin environment, which makes it suitable for modern aircraft designs.

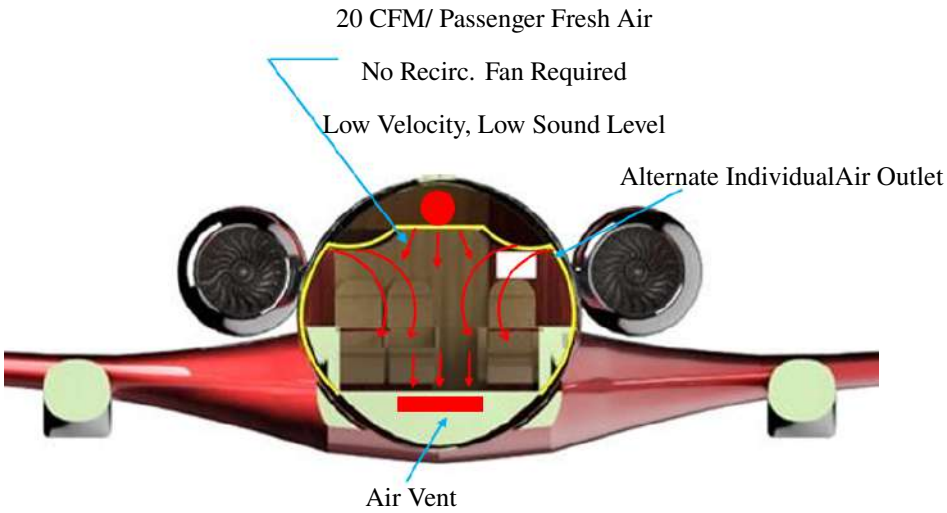

Figure 15.8.1 Air Conditioning System

15.9 Oxygen Systems

The cockpit oxygen system is supported by cylinder oxygen tanks, shown in Figure 15.9.1. These are easily accessible from the aircraft exterior for inspection and replacement. Control stations in the cockpit allow for the pilot and copilot to activate the system and regulate pressure.The oxygen system for the occupied cabin employs chemical generators to avoid the need for high pressure cylinders throughout the aircraft. This reduces the service and maintenance requirements on leaking valves or regulators.

15.10 Cabin Sterilization Systems

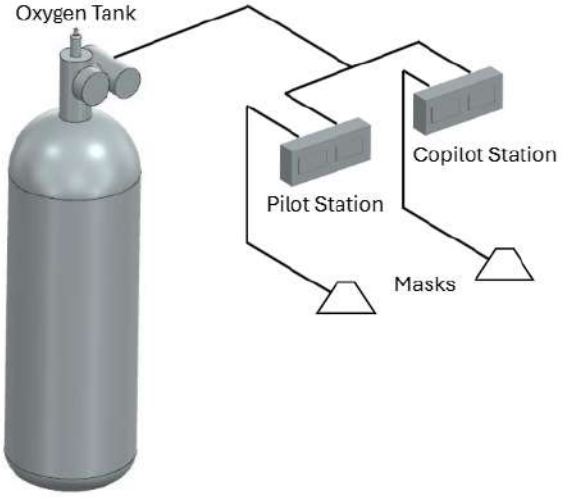

Figure 15.9.1 Cockpit Oxygen System

To address growing demands for health-conscious cabin environments, AETHER integrates a multi-model cabin sterilization system as part of its baseline design. AETHER's system will integrate multiple disinfection technologies, leveraging ultraviolet-C (UV-C) irradiation for continuous inactivation of airborne and surface pathogens, electrostatic spraying to uniformly apply disinfectant solutions across cabin surfaces, and ozone generation for oxidative sterilization of both air and materials [54] [55] [56]. Integrated ozone sterilization cycles offer deep sterilization of the cabin when unoccupied, while HEPA filtration maintains real-time particulate removal during flight. High contact cabin surfaces, such as the conference table and lavatories, are treated with durable antimicrobial coatings to suppress any growth of bacteria and viruses between disinfection cycles. This is compliant with both FAA and EASA health standards and minimizes the risk of pathogen transmission [57]. Additionally, it aligns with the expectations of VIP and executive transports, where cabin hygiene directly impacts passenger satisfaction.

15.11 Cockpit Instrumentation

The cockpit is designed to accommodate two pilots, with two jumper seats to accommodate two additional crew members. The instrumentation will include a Honeywell Anthem Flight Deck System, seen in Figure 11.1.1. The flight deck system has the ability to automate tasks, enhancing pilot's experience. It integrates flight management systems such as navigation, communication, and situational tools such as a weather radar system and a traffic collision avoidance system. It allows pilots to use artificial intelligence and data-driven insights to provide real-time updates on weather, air traffic, and flight conditions [58]. The Honeywell Anthem also includes the Honeywell SmartView Synthetic Vision System [59].

15.12 Anti-icing and Deicing Systems

To ensure safe operation in icing operations, the aircraft will use thermal systems that incorporate graphene-based heaters. These heaters are embedded in critical areas, such as the leading edge of the wings and the empennage. The system allows for rapid and efficient heating to be distributed across the length. It allows for several advantages such as a faster response time and improved integration on complex surfaces.

15.13 Window, Rain, Fog, and Frost Control Systems

To mitigate the effects of rain, the cockpit windows will be equipped with wipers. In addition, the windshield will have a hydrophobic coating. This feature allows the water to form into small droplets that can be more easily blown away or wiped off.

This improves pilot visibility in low-light conditions.

15.14 Lavatory, Galley, Water, and Waste Systems

The galley will be equipped with a mini refrigerator for wine and beverages, a microwave and oven for food preparation, and a dishwasher for cleaning dishes, shown in Figure 15.14.2. There will be two lavatories: one in the forward cabin and a handicap-accessible lavatory in the aft cabin, shown in Figure 15.14.1.

(a) Forward Lavatory

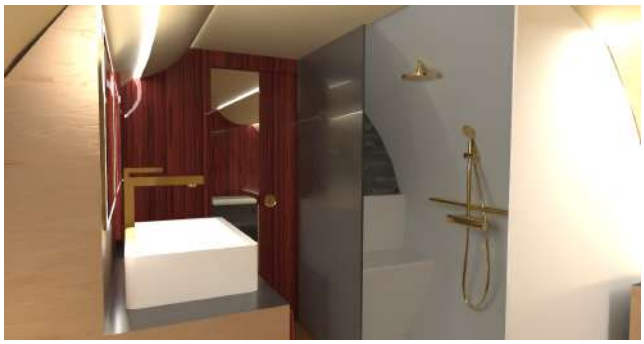

(b) Handicap Accessible Lavatory

Figure 15.14.1 Cabin Lavatories

Figure 15.14.2 AETHER Galley

The aircraft water and waste system, as shown in Figure 15.14.3, includes a water heater and sets of clean water tanks, gray water tanks, and waste tanks in the forward and aft sections of the aircraft. These tanks can be pumped forward or aft to trim the CG of the aircraft. Clean water tanks supply fresh water to the lavatory sinks, galley sink, and shower, and toilets for flushing. Gray water from sinks and the shower is directed into the gray water tanks, assisted by one-way and check valves that manage the flow direction and prevent backflow.

To save the use of freshwater, when sensors in the gray water tanks detect enough water, the gray water can be used to flush the toilets. It should be noted that the tanks have been sized to accommodate a hot 30 minute shower, 1 toilet flush per person, 10 seconds of hand washing per person, and an additional 5% in volume. Water saving faucets and shower head are specified to minimize water usage and minimize tank size.

Peristaltic pumps play a vital role in this system because they can move fluids through flexible tubing without exposing the fluid to external contamination. These pumps can be used to transfer fluids between their respective forward and aft tanks for trim, and pressurize water lines to supply the sinks, toilets, and shower efficiently.

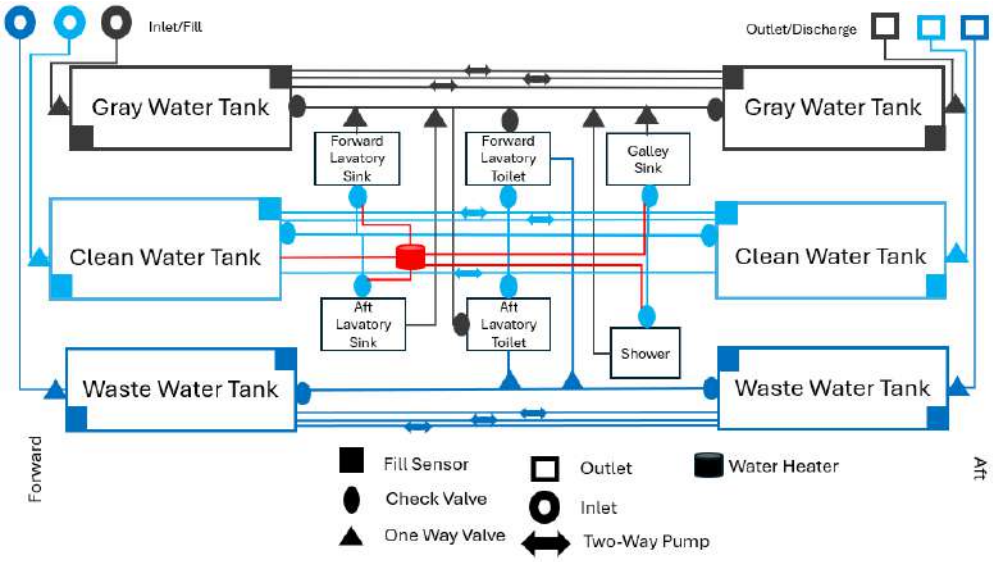

Figure 15.14.3 Water and Waste System

15.15 Safety and Survivability

The aircraft will feature systems and antennas designed to maximize safety and survival for crew and passengers. It will be equipped with an emergency locator transmitter (ELT) to send a distress signal in the event of an accident. In addition, there will be a Traffic Alert and Collision Avoidance System (TCAS). This system will be part of the flight controls, notifying air traffic control in the event of incoming traffic. In the right and left ceiling panels, the passenger masks are stored and will deploy in emergency situations. In addition, safety equipment for over water operations, such as a raft and life vests, are included in the cabin. The life raft water is located in the false ceiling in the conference room and life vests under all of the seat cushions.

15.16 Major Cargo Handling

The primary cargo consists of wine crates, which are stored in two main locations. Figure 15.16.1 illustrates the forward cargo handling area, while Figure 15.16.2 shows the aft cargo compartment. In the forward section, the wine is stored in a cold storage located beneath the forward cabin. These can be accessed using an under fuselage door. Additionally, some bottles of wine will be kept in the galley's refrigerator for easy access when requested by passengers. The aft storage also includes a refrigerated compartment, ensuring the wine remains properly preserved throughout the flight.

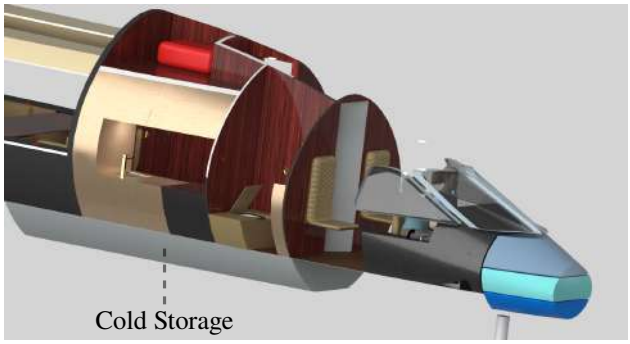

Figure 15.16.1 Forward Cold Storage

Figure 15.16.2 Aft Cold Storage

15.17 Cabin Baggage

There are several luggage storage compartments within the aircraft. Figure 15.17.1 illustrates the forward baggage compartments, while Figure 15.17.2 shows the aft baggage compartment. All luggage must be fastened with straps prior to takeoff to ensure safety. In addition to these compartments, passengers may utilize supplementary storage in the onboard closet, dresser, and the space underneath the bed for personal items.

Figure 15.17.1 Forward Baggage

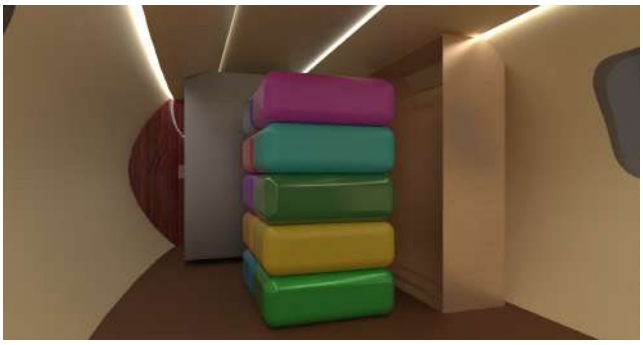

Figure 15.17.2 Aft Baggage

15.18 Ground Equipment and Servicing Vehicles Compatibility

When designing the ground operations, the safety and comfort of the ground crew and passengers were considered. Linemen from Hetrick Air Services at Lawrence Regional Airport were consulted for the ideal location of the fuel truck and fueling location, ground power unit (GPU), potable water cart, and lavatory cart. Figure 15.18.1 depicts a top view of the ground operations with the previously mentioned items, noting that the lavatory cart is not visible as it is located under the right engine. Figure 15.18.2 shows a right side view of AETHER ground operations rendered at the Lawrence Regional Airport (KLWC).

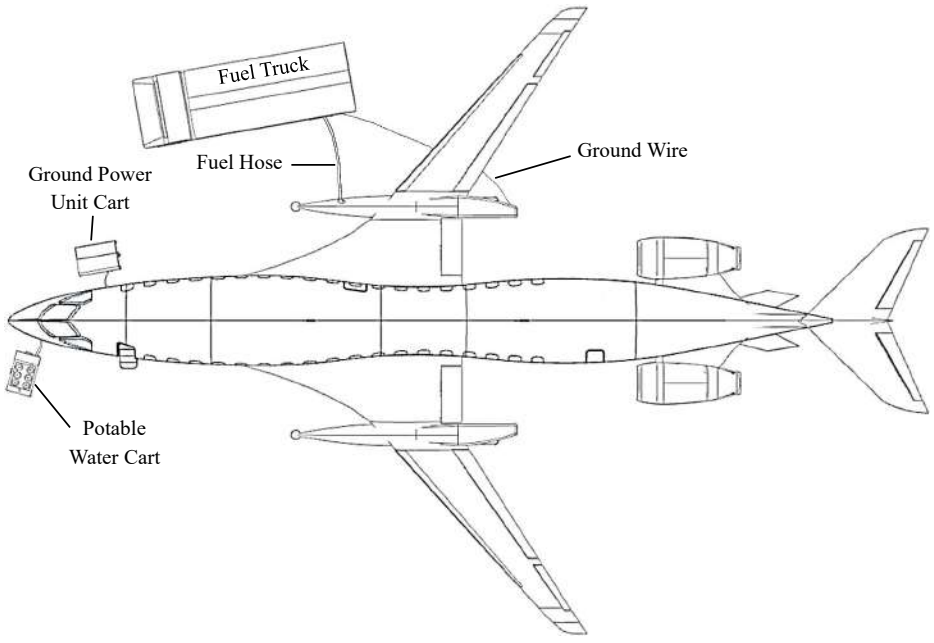

Figure 15.18.1 Top View of Ground Operations

Figure 15.18.2 Side View of Ground Operations at KLWC Airport

Before line personnel are allowed to perform services for the aircraft, the foam tank tip protectors must be put on the tips of the fuel tanks to prevent damage to the aircraft, ground equipment, and people. These covers are seen on the tips of the fuel tanks in Figures 15.18.1 and 15.18.2.

A single point refueling port is placed on the right slipper tank so that the fuel truck does not impede the boarding and unboarding of the aircraft. The grounding wire in the fuel truck is attached to the grounding point at the aft tip of the shock pod behind the slipper tank.

For crew safety, the GPU port is located at the nose of the aircraft. This was chosen with the consultation of lineman Erik Dallman, who shared that "typically [the GPU port is] located by the control panel underneath one of the engines, typically on the left side. Looks like on some of the bigger jets they are further up near the landing gear which I think would be safer and easier."

The water tank inlet ports and dump ports are located on opposite ends of the aircraft, with the inlets in the nose and drains in the tail. This is for sanitary purposes and passenger comfort. Keeping the inlets and drains separate helps prevent contamination of the inlets and keeps the passengers away from the pungent smell of waste water.

15.19 Entertainment System

AETHER is equipped with multiple USB ports and televisions to enhance customer satisfaction. Six televisions are distributed throughout the cabin, including two in the conference room for professional use. Additional televisions are located in the lounge areas and bedroom, providing entertainment options for passengers. Wi-Fi is available on board via a satellite connection, ensuring continuous internet access during flight.

16 Fault Tree Analysis

This fault tree analysis investigates potential failure modes and their root causes within an ultra long range business jet, with a focus on systems critical to safety, reliability, and mission success. The analysis systematically identifies and evaluates combinations of component failures that could lead to top-level undesired events, such as failure of tank and water systems, or degraded flight control.

16.1 Flight Control Surface Failures

A fault tree was developed to assess the risk of Loss of Flight Control (Figure 16.1.1), defined as the loss of pitch, roll, or yaw authority. Key contributors include actuator failures on elevators (three per side), rudders (three total), and ailerons (two per side), as well as failures in the triple-redundant flight control electronics. While redundancy mitigates single-point failures, loss of all actuators on one surface compromises axis control. Failure probabilities range from 1×10^{-5} to 6×10^{-4}, with CG trim issues also modeled as a related stability risk.

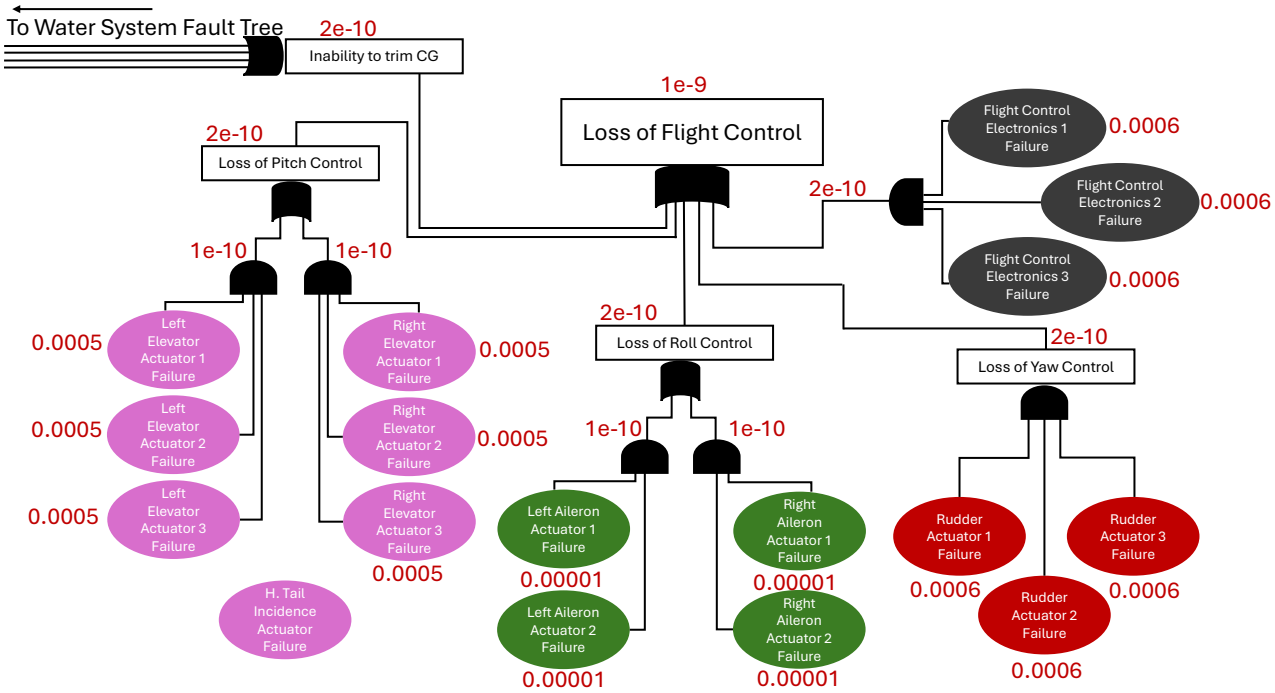

Figure 16.1.1 Flight Control Surfaces Fault Tree

16.2 Tank and Water System Pump Failures

The second fault tree (Figure 16.2.1) analyzes failures in the aircraft's fluid management systems, covering fuel trim, wastewater, gray water, and clean water pumps. Each system uses three redundant pumps to prevent single-point failures. Fuel trim pump failures pose significant risks to CG control and fuel balance, with failure rates around 4×10^{-4}. Water pumps, also essential for CG management, exhibit similar probabilities. The analysis highlights the need for robust redundancy and maintenance to ensure system reliability.

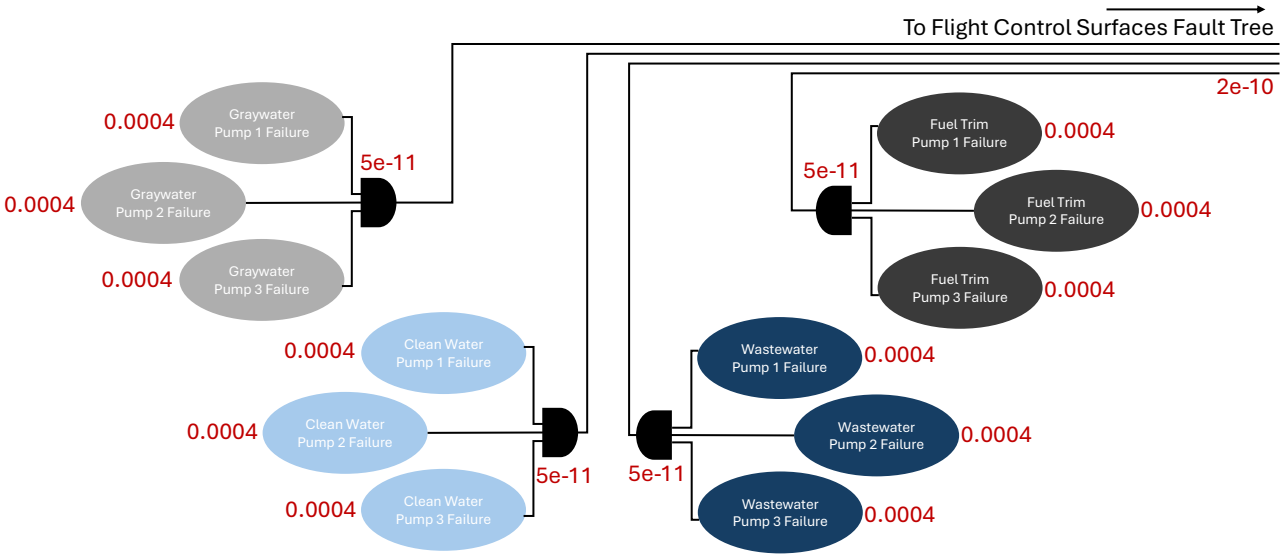

Figure 16.2.1 Water System Fault Tree

16.3 Major Loss of Life in a Survivable Crash

The final fault tree (Figure 16.3.1) examines potential causes of loss of life in an otherwise survivable crash. Key pathways include cabin fire from fuel leaks and extinguishing system failure, depressurization with pilot incapacitation or autopilot loss, and blocked emergency exits due to door failures ($\sim 7 \times 10^{-4}$). Additional risks stem from seatbelt or oxygen system failures. The analysis underscores the interplay between fire safety, life support, and evacuation systems, emphasizing the need to mitigate both likely and critical low-probability events.

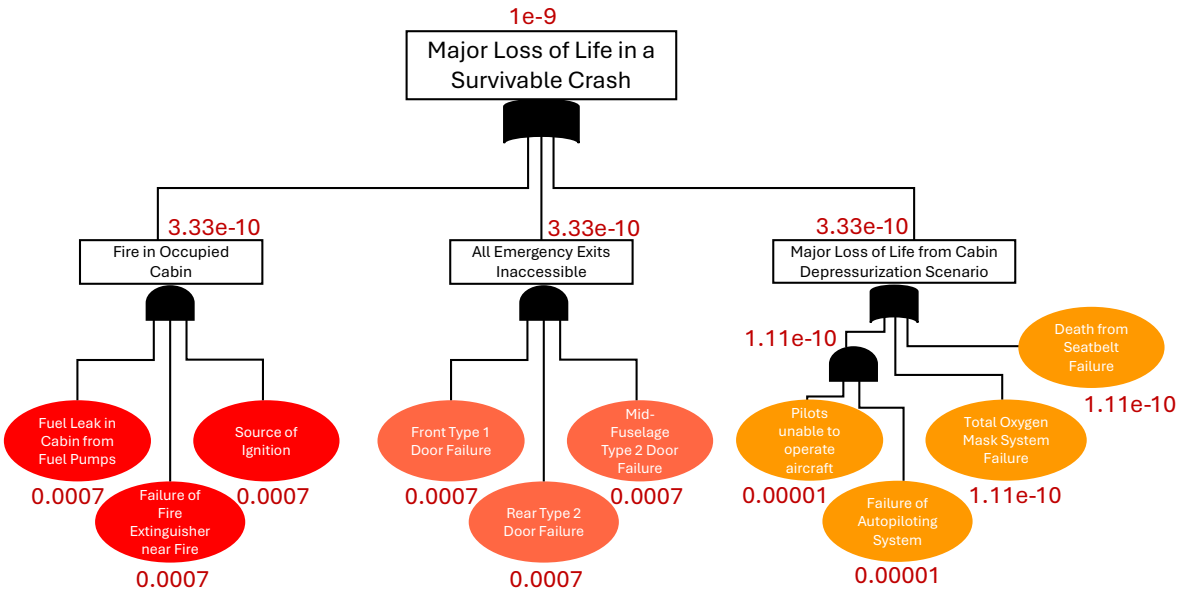

Figure 16.3.1 Loss of Life Fault Tree

17 Class II Stability and Control

The final stability and control analysis of AETHER was performed using the AAA dynamic modeling software. Table 17.0.1 gives the determined stability metrics for AETHER.

Table 17.0.1 AAA Stability Matrix Parameters

Stability Variable	AETHER
Load Factor per Angle of Attack, n/α (g's/rad)	8.023
Short Period Natural Frequency, ω_{nsp} (rad/s)	2.2195
Short Period Damping Coefficient, ζ_{sp}	0.275
Phugoid Natural Frequency, $\omega_{n_{ph}}$ (rad/s)	0.0429
Phugoid Damping Coefficient, ζ_{ph}	0.017
Feedback Gain due to Angle of Attack, k_α (deg/deg)	0
Dutch Roll Natural Frequency, $\omega_{n_{dr}}$ (rad/s)	0.441
Dutch Roll Damping Coefficient, ζ_{dr}	0.45
Sideslip Feedback Gain due to Rudder Deflection, k_β/δ_r (deg/deg)	2.7056
Roll Mode Time to Double Amplitude, t_R (s)	0.991
Spiral Mode Time to Double Amplitude, t_{2S} (s)	11.131

Tables 17.0.2 and 17.0.3 show the longitudinal and lateral stability derivatives of the aircraft, respectively, as generated by AAA. All derivatives were found to fall within the acceptable ranges to ensure stability as defined in Roskam's Flight Dynamics and Control, with the exception of C_{n_β} which was made stable with the use of a yawing feedback loop and sideslip feedback gain [60]. It should be noted that the aircraft was determined to be stable at a Mach number of 0.85 and a Mach number of 0.92.

Table 17.0.2 Longitudinal Stability Derivatives

Variable	AETHER
Lift Coefficient due to Forward Velocity, C_{L_u}	0.4900
Drag Coefficient due to Forward Velocity, C_{D_u}	0.1040
Pitching Moment Coefficient due to Forward Velocity, C_{m_u}	-0.2467
Lift Coefficient due to Angle of Attack, C_{L_α} (rad^{-1})	4.2302
Drag Coefficient due to Angle of Attack, C_{D_α} (rad^{-1})	0.6089
Pitching Moment Coefficient due to Angle of Attack, C_{m_α} (rad^{-1})	-0.8105

Variable	AETHER
Lift Coefficient due to Angle of Attack Rate, $C_{L_{\dot{\alpha}}}$ (rad^{-1})	1.0235
Drag Coefficient due to Angle of Attack Rate, $C_{D_{\dot{\alpha}}}$ (rad^{-1})	0
Pitching Moment Coefficient due to Angle of Attack Rate, $C_{m_{\dot{\alpha}}}$ (rad^{-1})	-3.6053
Lift Coefficient due to Pitch Rate, C_{L_q} (rad^{-1})	3.6466
Drag Coefficient due to Pitch Rate, C_{D_q} (rad^{-1})	0
Pitching Moment Coefficient due to Pitch Rate, C_{m_q} (rad^{-1})	-14.2440
Lift Coefficient due to Incidence Angle, C_{L_η} (rad^{-1})	0.4743
Drag Coefficient due to Incidence Angle, C_{D_η} (rad^{-1})	0.0057
Pitching Moment Coefficient due to Incidence Angle, C_{m_η} (rad^{-1})	-1.6706
Lift Coefficient due to Elevator Deflection, $C_{L_{\delta_e}}$ (rad^{-1})	0.0433
Drag Coefficient due to Elevator Deflection, $C_{D_{\delta_e}}$ (rad^{-1})	0.0006
Pitching Moment Coefficient due to Elevator Deflection, $C_{m_{\delta_e}}$ (rad^{-1})	-0.1525

Table 17.0.3 Lateral-Directional Stability Derivatives

Variable	AETHER
Side Force Coefficient due to Side Slip, C_{Y_β} (rad^{-1})	-0.4193
Rolling Moment Coefficient due to Side Slip, C_{l_β} (rad^{-1})	-0.1637
Yawing Moment Coefficient due to Side Slip, C_{n_β} (rad^{-1})	-0.0575 $\rightarrow$ 0.1
Side Force Coefficient due to Side Slip Rate, $C_{Y_{\dot{\beta}}}$ (rad^{-1})	-0.0795
Rolling Moment Coefficient due to Side Slip Rate, $C_{l_{\dot{\beta}}}$ (rad^{-1})	-0.0041
Yawing Moment Coefficient due to Side Slip Rate, $C_{n_{\dot{\beta}}}$ (rad^{-1})	-0.0478
Side Force Coefficient due to Roll Rate, C_{Y_p} (rad^{-1})	-0.0603
Rolling Moment Coefficient due to Roll Rate, C_{l_p} (rad^{-1})	-0.3723
Yawing Moment Coefficient due to Roll Rate, C_{n_p} (rad^{-1})	-0.1151
Side Force Coefficient due to Yaw Rate, C_{Y_r} (rad^{-1})	0.1968
Rolling Moment Coefficient due to Yaw Rate, C_{l_r} (rad^{-1})	0.2680
Yawing Moment Coefficient due to Yaw Rate, C_{n_r} (rad^{-1})	-0.1093
Side Force Coefficient due to Aileron Deflection, $C_{Y_{\delta_a}}$ (rad^{-1})	0
Rolling Moment Coefficient due to Aileron Deflection, $C_{l_{\delta_a}}$ (rad^{-1})	0.0251

Variable	AETHER
Yawing Moment Coefficient due to Aileron Deflection, $C_{n_{\delta_a}}$ (rad^{-1})	0
Side Force Coefficient due to Rudder Deflection, $C_{Y_{\delta_r}}$ (rad^{-1})	0.0480
Rolling Moment Coefficient due to Rudder Deflection, $C_{l_{\delta_r}}$ (rad^{-1})	0.0010
Yawing Moment Coefficient due to Rudder Deflection, $C_{n_{\delta_r}}$ (rad^{-1})	-0.0293

Figure 17.0.1 shows the trim diagram for AETHER at cruise. The current configuration is able to be trimmed given a horizontal tail incidence angle of 3 degrees and an X-location center of gravity at 53 ft.

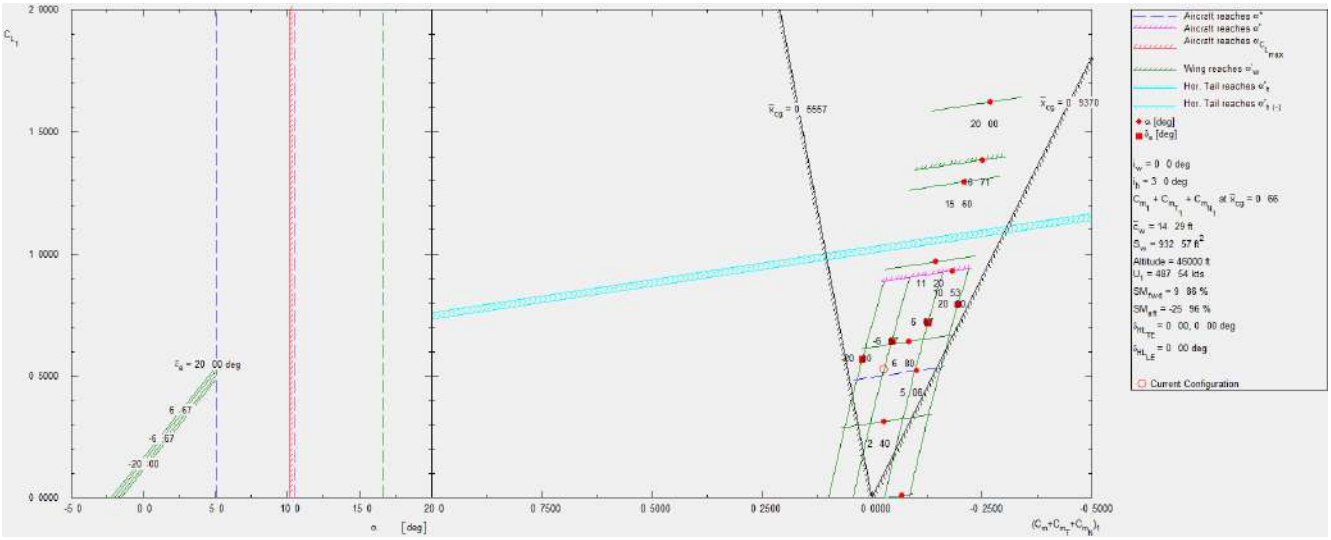

Figure 17.0.1 AETHER Trim Diagram During Cruise

Figure 17.0.2 shows the short period frequency requirement plot for level 1 handling qualities. AETHER appears to meet level 1 handling qualities with respect to short period frequency during cruise.

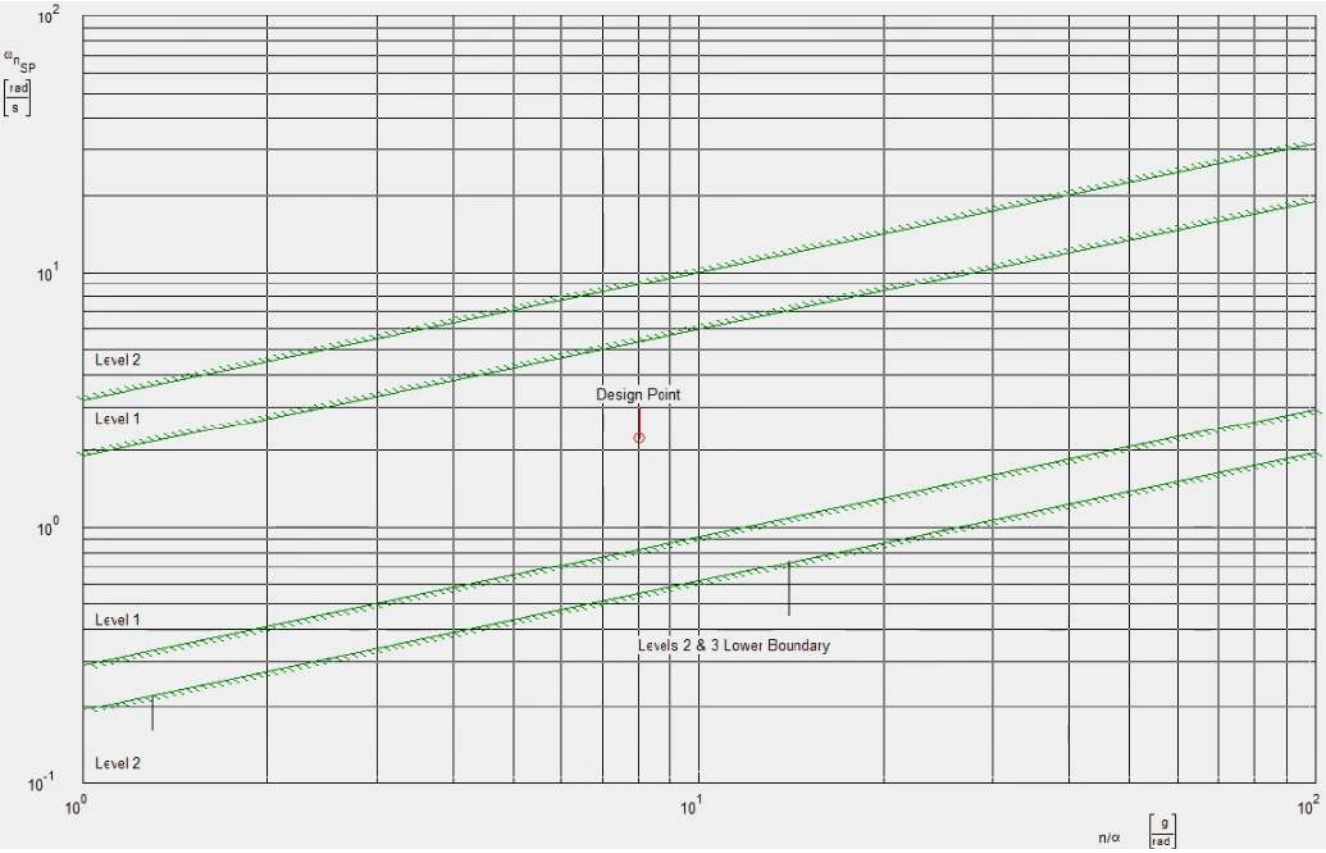

Figure 17.0.2 AAA Short Period Frequency Requirements during Cruise

Figure 17.0.3 shows the dutch roll frequency and damping ratio requirement plot generated by AAA. AETHER appears to achieve level 1 handling qualities in this flight mode at cruise conditions. The sideslip feedback gain due to rudder deflection was used to achieve level 1 handling qualities, as it acted as a defacto yawing moment coefficient due to sideslip angle to compensate for a slightly unstable c_{n_β}.

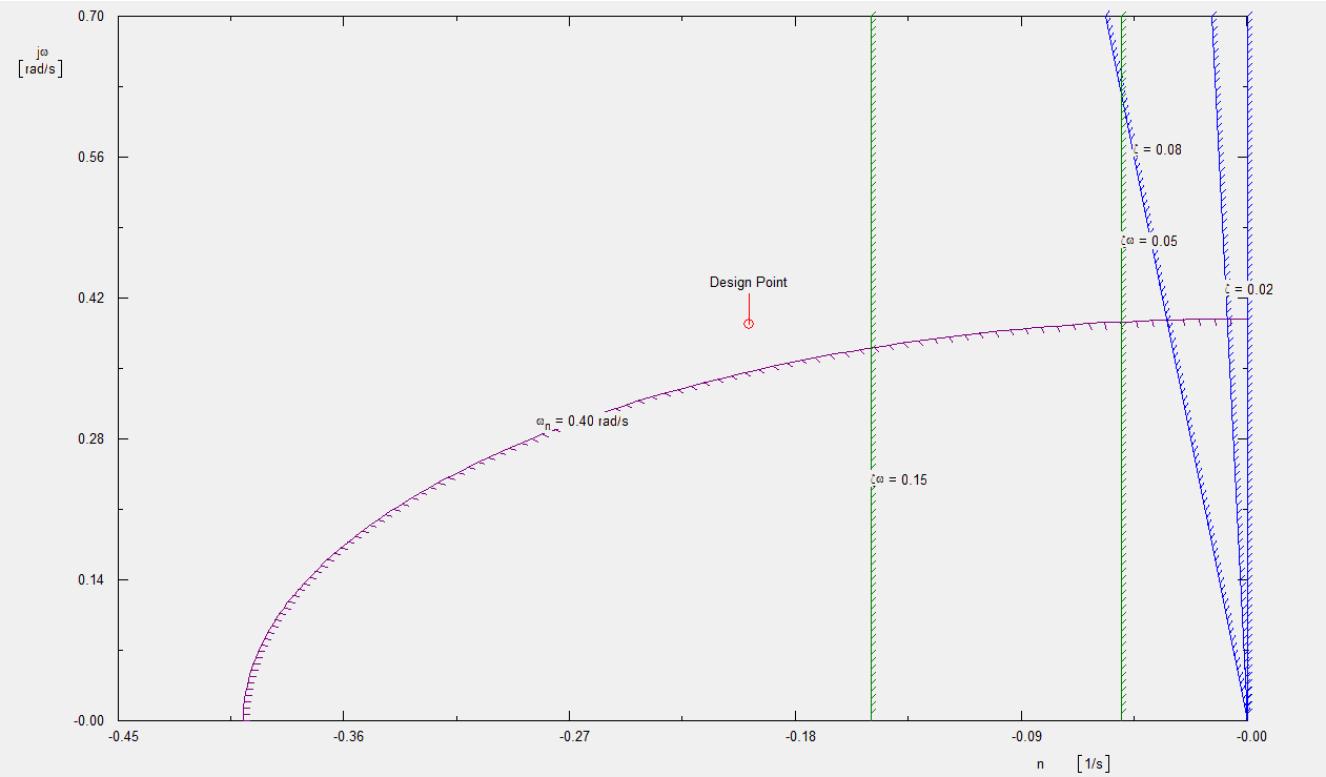

Figure 17.0.3 AAA Dutch Roll Frequency and Damping Ratio Requirements during Cruise

Although the preliminary analysis of AETHER suggests level 1 handling qualities in all flight modes and the ability to trim control surfaces, the AAA analysis software is limited in its robustness. It is recommended that further stability analysis be conducted, particularly with respect to trim requirements. A more accurate evaluation of moment coefficients would allow for a more accurate approximation of trim. Changes in the geometric characteristics of the wing, such as wing twist and incidence angle, are therefore recommended to promote a more even wing lifting distribution.

The ride quality comfort index was calculated for both an extreme gust (1 in a million chance of occurring), and a moderate gust (1 in 10,000 chance of occurring). The index was calculated with respect to the vertical acceleration of the aircraft, as it is the largest contributing factor to overall aircraft turbulence. The formal relationship between turbulence and vertical acceleration is given in Table 17.0.4.

Table 17.0.4 Vertical Acceleration Relation to Turbulence

Vertical Acceleration (g's)	Pilot Description of Turbulence
0.05	Negligible
0.10	Slight
0.10–0.15	Moderate
0.20–0.30	Moderately Heavy
0.30–0.60	Severe
0.60	Extreme

The final ride quality index is shown in Table 17.0.5. This shows that under severe turbulence the vertical acceleration is within a moderately heavy turbulence range. For more reasonable gusts, the ride quality is within a moderate turbulence range. This indicates that AETHER is able to provide customer satisfaction during turbulence, though there is room for improvement in future variants of the aircraft.

Table 17.0.5 Gust Response Comparison

Parameter	Severe Gust (23 ft/s)	Moderate Gust (14 ft/s)
Vertical Acceleration (g)	0.22	0.13
Lateral Acceleration (g)	-0.022	-0.013
Ride Quality Index	5.9	4.4
% Customers Satisfied	50	78

18 Performance

This section discusses the overall performance of the aircraft.

18.1 Takeoff

Table 18.1.1 gives the final performance metrics for AETHER. The performance metrics were calculated assuming ground conditions and landing gear down. Both the takeoff and landing field lengths are well within the 6000 foot limit, indicating AETHER has short takeoff and landing capabilities. However, per the Napa mission, the field length is limited to 5008 ft.

Table 18.1.1 AETHER Class II Performance Metrics

Performance Metric	AETHER
Takeoff Field Length, S_{TOL} (ft)	4590
Takeoff Ground Distance, S_{TOG} (ft)	1400
Takeoff Stall Speed, $V_{S_{TO}}$, (ft/s)	124

Figure 18.1.1 shows the takeoff ground distance and minimum takeoff field distance to overcome the minimum obstacle height of 35 feet specified by FAR 25.

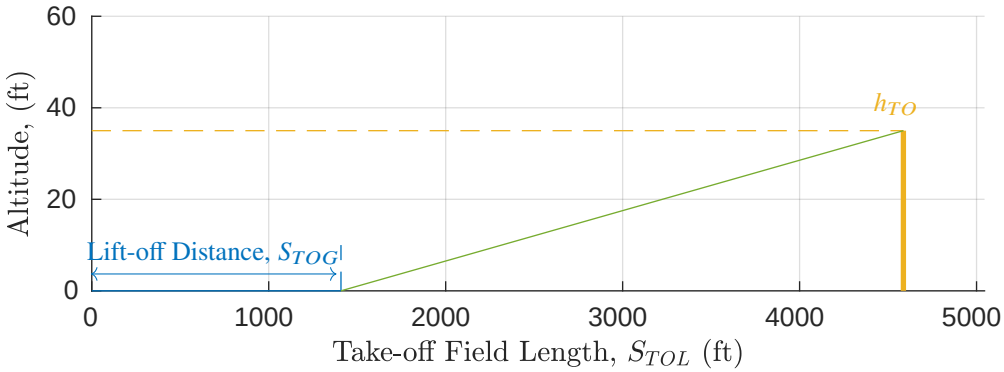

Figure 18.1.1 Takeoff Field Distance

18.2 Landing

The landing parameters are as listed in Table 18.2.1. The landing obstacle clearance required is 50 ft for applicable to all aircraft classifications, including FAR 25. In addition, the field distance is limited to 5008 ft for the Napa mission.

Table 18.2.1 AETHER Class II Landing Performance Metrics

h_L (ft)	V_{S_L} (ft/s)	V_{TD} (ft/s)	S_L (ft)	S_{LG} (ft)
50	100	123	3010	525

Figure 18.2.1 depicts the landing profile, including the touchdown and ground run phases.

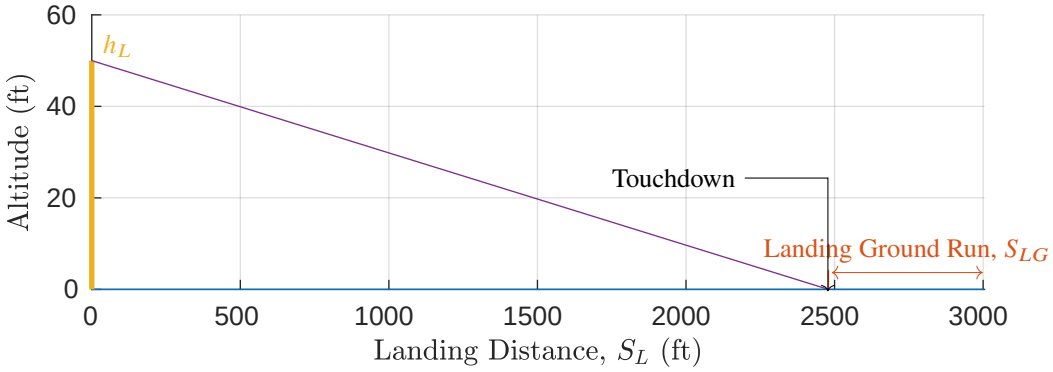

Figure 18.2.1 Landing

18.3 Drag Polar and Wetted Area

To increase the accuracy of the drag polar calculations the wetted area of each major aircraft component was found.

18.3.1 Fuselage Wetted Area

Equation 10 was used to find the wetted area of the fuselage by assuming a circular cross section. The fuselage wetted area was calculated to be 2160 ft^2.

$$S_{wet,fus} = \pi d_f l_f \left(0.50 + 0.135\frac{l_n}{l_f}\right)^{\frac{2}{3}} \left(1.015 + \frac{0.3}{\left(\frac{l_f}{d_f}\right)^{1.5}}\right) \tag{10}$$

Figure 18.3.1 displays the cross sections of the respective fuselage stations. The perimeter of each cross section was plotted to estimate the total wetted area of the fuselage. The wetted area as a product of fuselage length and perimeter is shown in Figure 18.3.2.

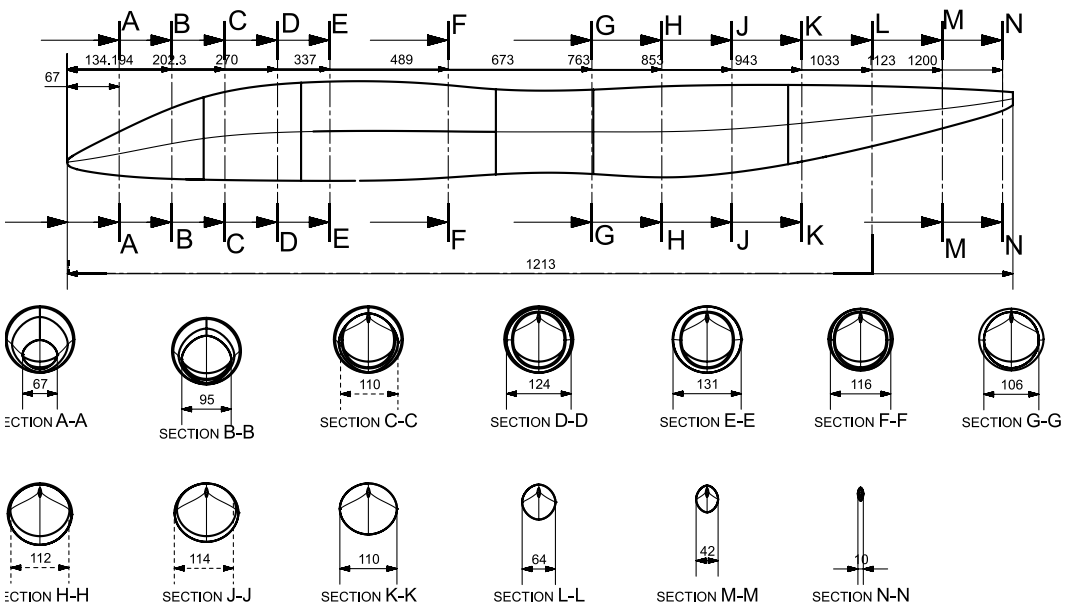

Figure 18.3.1 Fuselage Cross Sections

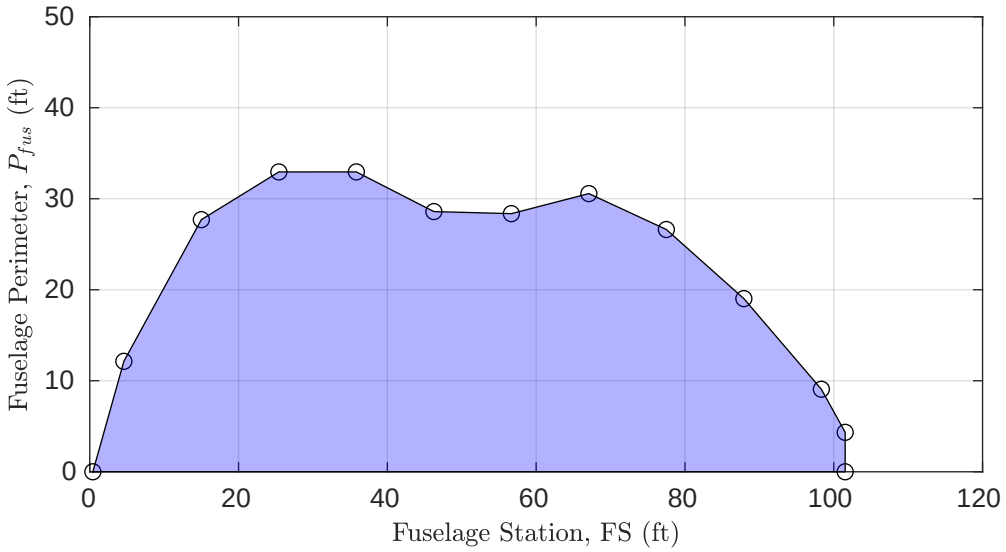

Figure 18.3.2 Perimeter Plot and Wetted Area

18.3.2 Engines Wetted Area

The engines had three components contributing to the overall wetted area, the fan cowling, gas generator, and plug. The final wetted area of the engines consisted of the sum of the wetted areas of these components and is given in Table 18.3.1.

Table 18.3.1 Engine Component Wetted Area

Component	Wetted Area, ft^2
Fan Cowling	91.8
Gas generator	232
Plug	37.4
Engine Total	361.2

18.3.3 Wing Wetted Area

Wing geometric characteristics found in Table 11.4.1 were used to find the wetted area of the wings. The wing wetted area was found to be 1670 ft^2.

18.3.4 Empennage Wetted Area

Like the wing, the geometric characteristics of the vertical and horizontal tails found in Tables 11.6.1 and 11.6.2, respectively, were used to find the wetted area of the empennage. The wetted area of the vertical tail was found to be 226 ft^2 and the wetted area of the horizontal tail was found to be 363 ft^2, making the total wetted area of the empennage 589 ft^2.

Table 18.3.2 Total Aircraft Wetted Area

Component	Wetted Area, ft^2
Fuselage	2.16×10^3
Wing	1.67×10^3
Nacelles	361.2
Horizontal Tail	363
Vertical Tail	226
Total	5150

18.3.5 Aircraft Wetted Area

The total aircraft wetted area was found to be 5150 ft^2, and is summarized in Table 18.3.2.

18.4 Stall

To produce the takeoff field strength and landing distance diagrams, the stall speed is calculated at each condition. Weight, thrust, and $C_{L_{max}}$ are altered for each condition. Maximum landing weight is determined to be 80% of the takeoff weight. The thrust inclination angle ϕ_T is 5 degrees. Equation 11 depicts the method of calculation for the stall speed at take off and landing, which are shown in Table 18.4.1.

$$V_S = \sqrt{\frac{W - T\sin(\alpha_{C_{Lmax}} + \phi_T)}{\rho C_{L_{max}} S}} \qquad (11)$$

Table 18.4.1 Stall Speeds

Flight Phase	Stall Speed (ft/s)
Takeoff	120
Landing	100

18.5 Climb

To determine the climb performance, the drag polars are placed on a Mach number vs. Thrust plot, shown in Figure 18.5.1. The drag polars represent the required thrust to avoid stalling. The dashed lines represent the available thrust, which is mapped from FJ44 data. The difference in these two lines gives the Specific Excess Power (SEP).

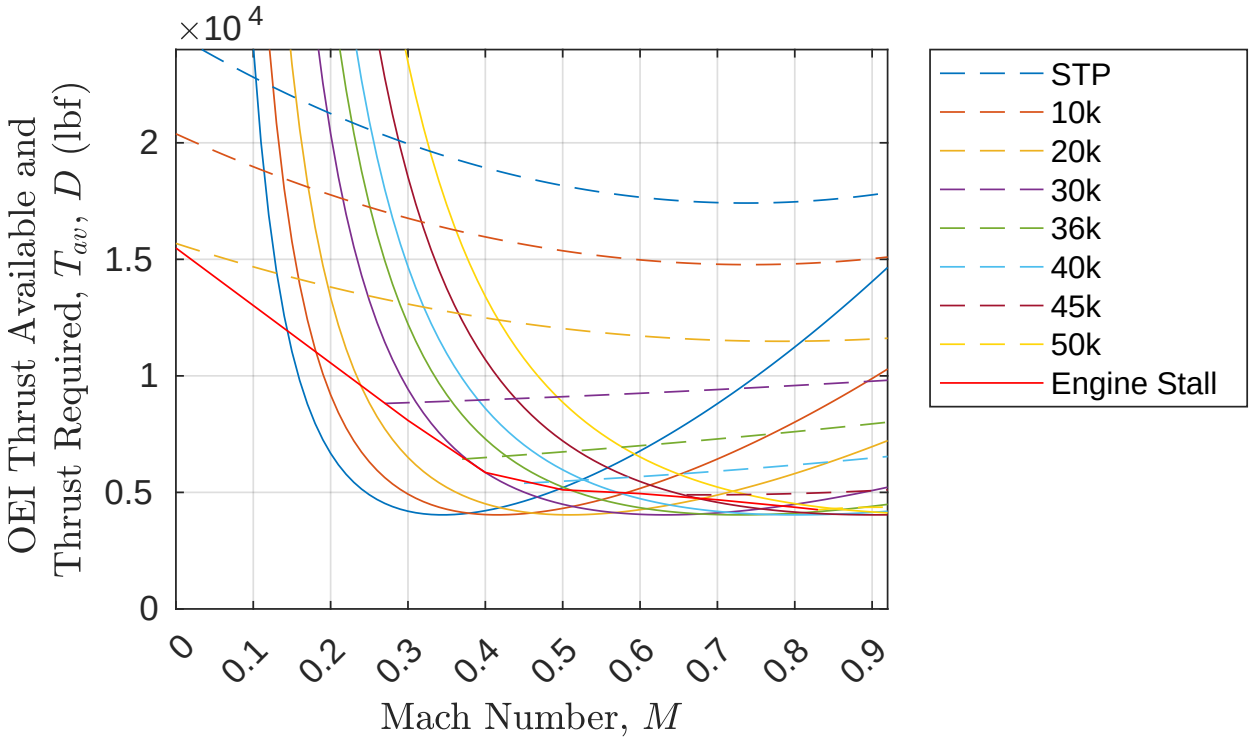

Figure 18.5.1 Thrust Available, Thrust Required vs Mach Number

The flight envelope in Figure 18.5.2 depicts the SEP curves with respect to Mach number and altitude.

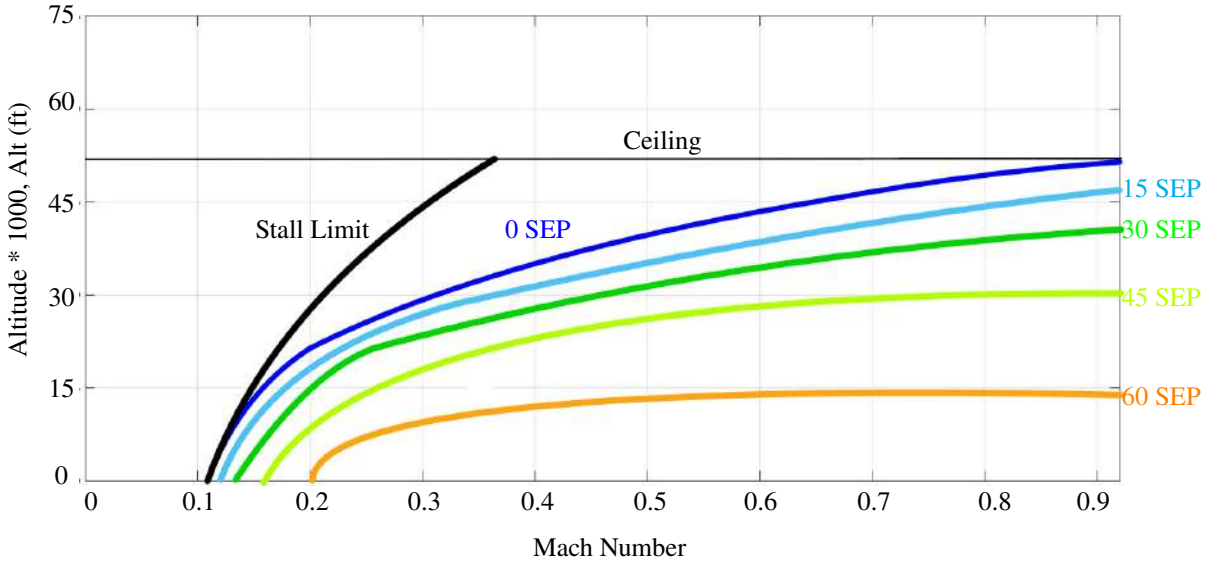

Figure 18.5.2 Flight Envelope from Specific Excess Power

19 Cost Analysis

The objectives of this section are:

1) Analyze business jet market predictions for the year 2030
2) Determine the most important technical aspects for the market in 2030
3) Develop competitive business strategy for the market
4) Determine reasonable prices and production rates based on the market analysis

19.1 Market Review

Multiple market reviews and studies have been conducted on the estimated market growth of business jets. The business jet industry is experiencing a significant transformation driven by fleet modernization. As of 2022, over one third of the business jets currently in service are over ten years old, giving reason to operators and charter providers to invest in new technology and modernization programs [37]. This wave of technological advancement has increased the value of business jets due to their advanced upgrades. As such, the growth rate of the business jet industry is expected to increase substantially.

The industry landscape is characterized by strong marked consolidation and manufacturer specialization. The top five business jet manufacturers Cessna, Gulfstream, Embraer, Bombardier, and Cirrus Aircraft collectively command 76% of the total active business jet globally [37]. The business jet market leaders for sales and success are as follows: Bombardier, Dassault, Embraer, Textron, Airbus Corporate Jets, Boeing Commerical Airplanes, Gulfstream, Sirius, Pilatus [36].

To create a comprehensive market review, aircraft from many of the major players were analyzed for the new price, current price today, number of vehicles currently in service, and number of historical vehicle sales. This data serves to create an overview of the current market pricing trends. Table 19.1.1 depicts this data for a multitude of benchmark aircraft.

Table 19.1.1 Current Pricing and Sales Trends for Competitive Aircraft [10, 22–33]

Aircraft	Price New (USD)	Current Price (USD)	Entry into Service	Vehicles Sold
Bombardier Global 8000	78 Million	N/A	2025	4
Embraer Lineage 1000E	53 Million	22.5 Million	2009	14
Dassault Falcon 10X	75 Million	N/A	2027	N/A
Bombardier Global 7500	81 Million	72 Million	2018	≈ 200
Airbus Corporate Jets ACJ319neo	105 Million	N/A	2019	N/A
Boeing Business Jets BBJ 737-700	71 Million	59 Million	1999	200
Gulfstream G800	72.5 Million	N/A	2025	N/A

19.2 Market Growth

The large business jet dominates the global business jet market and acts as a major driver for the advancement of the market [35][34]. There is an increase of High Net Worth Individuals (HNWI) who prefer comfort and long range capabilities,

characteristics most often seen in the large jet segment of the business jet market. HNWI individuals are defined as those who hold at least $1,000,000 in liquid assets. Large business jets account for approximately 82% of the total market value in 2024 [37]. The HNWI are capable of both purchasing and chartering large business jets, which further the growth of the market substantially. Additionally, ultra-high net worth individuals (UHNWI) are capable of purchasing large luxury business jets. UHNWI are more likely to spend on aircraft with a higher degree of luxury and further technological capabilities. The increase in the HNWI and UHNWI population has led to market growth in recent years. The historical growth period between 2015 and 2024 projects a substantial growth in the market over the next five to ten years.

Multiple market projections were examined to determine the approximate market growth from 2025 to the mid 2030s. Table 19.2.1 depicts the projected market growth over different time periods.

Table 19.2.1 Business Jet Market Analysis Reports [34–37]

Company	Current Year	Current Value	Expected Year	Expected Value
Mordor Intelligence	2025	25.69 Billion USD	2030	30.91 Billion USD
Growth Market Reports	2023	32.44 Billion USD	2032	47.38 Billion USD
Econ Market Research	2023	44.16 Billion USD	2032	67.34 Billion USD
Expert Market Research	2025	33.12 Billion USD	2034	61.81 Billion USD

From this data, the compound annual growth rate (CAGR) can be determined. Equation 12 depicts the process for calculating the CAGR.

$$CAGR = \left(\frac{\text{Expected Value}}{\text{Current Value}}\right)^{\frac{1}{\text{Expected Year} - \text{Current Year}}} - 1 \tag{12}$$

Table 19.2.2 CAGR for Various Market Forecasts

Time Period	CAGR
2025 - 2032	3.77 %
2023 - 2032	4.30 %
2023 - 2032	4.80 %
2024 - 2034	7.18 %

19.3 Choice of Attributes and Relative Value Index (RVI)

Due to the niche size of the ultra-long range (ULR) aircraft, three primary attributes were chosen.

1) Range : Key differentiator in the ULR segment - defines mission profile.

2) Cabin Volume: Directly affects comfort, space, and luxury appeal.

3) Cruise Speed: The ability of the aircraft to cover distances in a small amount of time is a high priority for HNWI.

These attributes are used to assign a relative value index (RVI) to the aircraft used in the market review. RVI aims to create a measure of the relative value of a product based on the analysis of the products attributes. Products of a higher value are expected to outperform products with a lower RVI if competitively priced. For ease of this analysis, only three aircraft are used: the Bombardier Global 8000, the BBJ 737-700, and the Embraer Lineage 1000E.

To begin calculating the RVI, a baseline is determined. A current market leader for the ULR market is the Global 7500.

This aircraft is able to travel long distances at a high mach number, with a maximum mach number of 0.90. This aircraft is assigned a value 1.0, the highest possible score for this analysis. The attributes of the selected aircraft are shown in Table 19.3.1.

Table 19.3.1 RVI Analysis Attributes

Aircraft	Maximum Speed ($Mach$)	Maximum Range (nmi)	Cabin Volume (ft^3)
Bombardier Global 7500 (base)	0.925	7700	2786
Bombardier Global 8000	0.94	7900	2236
BBJ 737-700	0.7	6500	5390
Embraer Lineage 1000E	0.82	4600	3914

Using the base model, each attribute is then normalized. It should be noted that the maximum score for each aircraft is 1.0. After each attribute is normalized, a weight is assigned to it. Due to the importance of high travel distance, this attribute is rated higher than others. Cabin volume remains high due to the importance of comfort. However, maximum speed remains the second highest rated due to recent trends in increases in Mach number. The weights for each attribute can be seen in Table 19.3.2. Finally, the RVI is calculated using Equation 13. The RVIs for each of the aforementioned aircraft are given in Table 19.3.3. As both the Global 7500 and Global 8000 aircraft are currently in the market and the BBJ 737-700 and Lineage 1000E entered into service over 15 years ago, an RVI of 0.95-100 is considered to be market competitive. Against the current top competitor, AETHER scores an RVI of **0.998** at a cruise Mach number of 0.92 and an RVI of **0.973** at cruise Mach number of 0.85, indicating that is highly competitive in ULR market.

Table 19.3.2 Associated Attribute Weight

Attribute	Relative Weight
Maximum Speed	0.325
Maximum Range	0.375
Cabin Volume	0.3

$$\text{RVI} = \sum w_i \cdot \text{Score}_i \tag{13}$$

Table 19.3.3 RVI for Selected Aircraft

Aircraft	RVI
Bombardier Global 7500 (base)	1.0
Bombardier Global 8000	0.94
BBJ 737-700	0.86
Embraer Lineage 1000E	0.81
AETHER (Mach 0.92)	0.998
AETHER (Mach 0.85)	0.973

19.4 Price and Production Quantity Determination

The price and production quantity is determined using both the RVI and the CGR. The initial price estimate for various units produced is shown in Figure 19.4.1. It should be noted that the profit margin of Figure 19.4.1 is based on the 10 % profit

of all aircraft produced distributed evenly. It can be seen that the Bombardier Global 7500, the aircraft bench marked for this market analysis, has a lower market price than the predicted price of AETHER. However, due to the high RVI score of AETHER and its larger cabin capacity, this is acceptable.

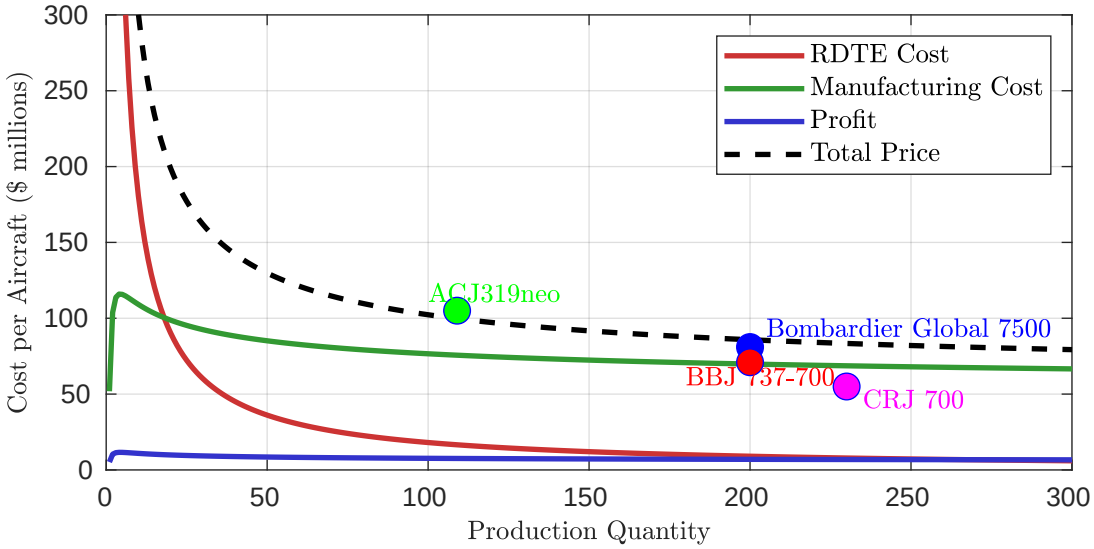

Figure 19.4.1 Price of Aircraft per Quantity Produced

The overall cost break down of manufacturing and acquiring an initial 200 unit run of AETHER is shown in Table 19.4.1. It should be noted that the direct operating cost of the aircraft is estimated from current operating costs of leading market jets [61]. Thus, the direct operating cost may be higher than presented here, but follows the overall trend of current business jets.

Table 19.4.1 Cost Breakdown

Cost Category	Amount (USD)
Development Cost	1,800,000,000
Fly Away Cost	52,000,000
Production Cost	12,000,000,000
Facilities and Labor Cost	1,900,000,000
Direct Operating Cost (per hour)	5,000

It should be noted that the current growth of the ultra long range business jet market is healthy. The average CAGR fore-casted for the decade of 2030 is approximately 5%. This indicates that the market will be able to handle a higher production rate of aircraft, and that the demand for such aircraft will be increased. The Bombardier Global 7500 was entered into service in 2018 and sold approximately 200 units over the course of seven years. This results in approximately two aircraft sold per month. Coupled with the average CAGR, sales per month in 2031 can be calculated using Equation 14. The predicted sales volume for aircraft in the class of the Global 7500 in the year 2031 is approximately three aircraft per month.

$$Sales_{predicted} = Sales_{current} \cdot (1 + CAGR)^{n} \tag{14}$$

With these factors in mind, the selected production point of AETHER is 200 units for the initial run. This sets the estimated aircraft price at **87 million USD**. With this price estimate, SkyBridge is predicted to break even on its research, development, testing, and evaluation costs within five years, which can be seen in Figure 19.4.2. Additionally, SkyBridge will retain an additional profit margin of 234 million dollars after the entire initial production run has been sold.

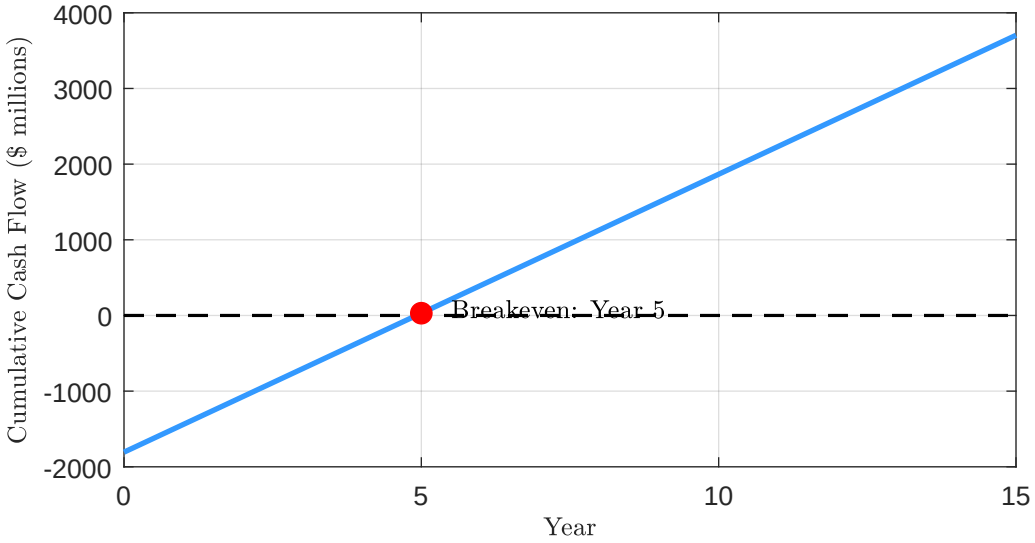

Figure 19.4.2 Cumulative Cash Flow

20 Life Cycle Analysis

The following chapter contains a Lifecycle Emissions Analysis (LCA) according to ISO 14040 for AETHER. The Analysis is based on previously conducted LCAs for the Airbus A320-200 [39], A330-200 [62] and Boeing 737-800 [63]. Results were obtained using Sphera GaBi and the latest EIO-LCA database [38]. Emissions during production, operation, and disposal are taken into account. However, it should be noted that there are often no dedicated aerospace databases and many values rely on assumptions.

The goal is to obtain a basic Lifecycle Emission Analysis for AETHER. Emissions considered are Unburned Hydrocarbons (HC), Carbon Monoxide (CO), Nitrous Oxides (NO_X) and Carbon Dioxide (CO_2).

20.1 Functional Units and Flow Chart

AETHER is an ultra long range business jet. Therefore, appropriate functional units are Passenger Kilometers Traveled (PKT), Vehicle Kilometers Traveled (VKT) and Aircraft Lifetime (AL). Fig 20.1.1 shows the LCA flowchart used for the LCA. Arrows resemble flows, while boxes show the most relevant processes. If they are highlighted by color, they are taken into account within this LCA. The main goal is to account for the main processes, however, the LCA can always be improved, which is why this more complex LCA flow chart is chosen.

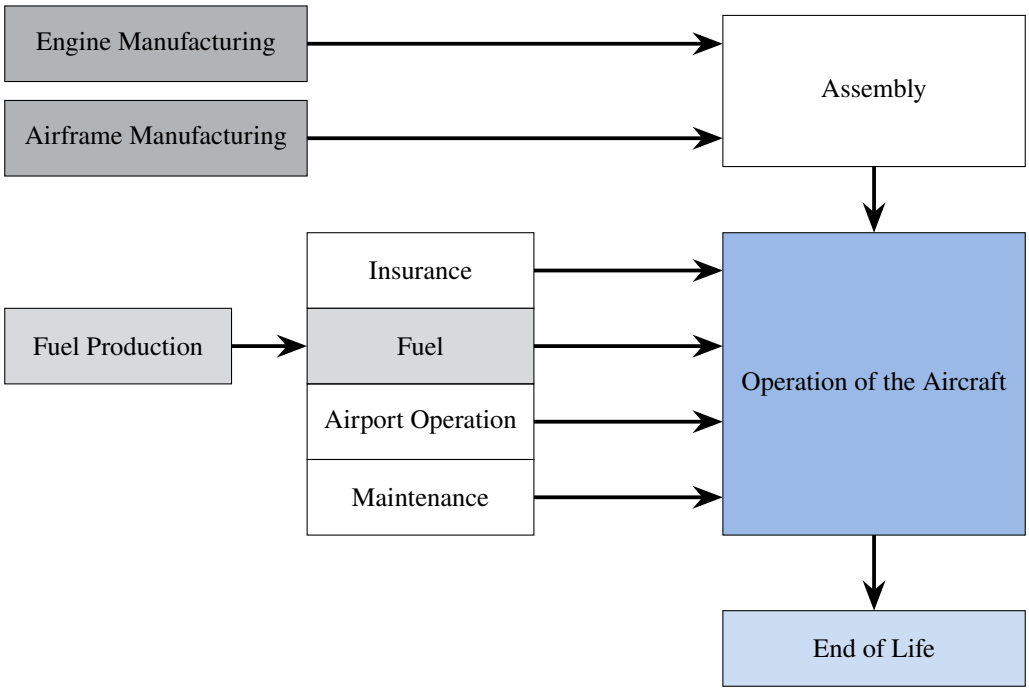

Figure 20.1.1 LCA Flowchart

20.2 Emissions due to Manufacturing

Emissions during manufacturing are obtained using the Economic Input-Output Lifecycle Assessment (EIO-LCA) method. It enables the user to obtain the environmental impact of a component by comparing its cost to similar components from the same market, requiring a substantial database. It is used to determine the environmental impact of the manufacturing processes, primarily the engine and airframe manufacturing.

20.2.1 Engine Manufacturing

The Safran Silvercrest engine is not yet in series production. As it has not yet been approved, it is difficult to estimate exactly how high the production costs will be, which in this case also include the certification costs. It is therefore assumed that one engine will cost 12 million US dollars, meaning that the total price for the engines will be 24 million US dollars.

Based on the latest EIO-LCA database from 2025 provided by the U.S. Environmental Protection Agency the price specific CO_2 emission index for aircraft engines is 0.105 kg/2018US$ [64]. In order to calculate the emissions, the inflation has to be considered: 1 2025US$ equals 0.79 2018US$. This results in 1.96×10^6 kg CO_2 emissions for engine manufacturing.

20.2.2 Airframe Manufacturing

The cost for Airframe Manufacturing was determined to be 63 million US dollars. According to the EIO-LCA database, the price specific CO_2 emission index for aircraft is 0.136 kg/2018US$ [64]. By accounting for inflation since 2018, this results in 6.77×10^6 kg CO_2 emissions for airframe Manufacturing.

20.3 Emissions during Operation

To determine the emissions of AETHER during operation, the main flight phases during an 8000 nmi flight need to be considered. For the Landing and Take-off (LTO) cycle according to ICAO standards data from the ICAO Aircraft Engine Emissions Databank [38] is used. By using the Emission Index (EI) provided in the databank and using the previously determined fuel fractions, one can obtain the emissions during the LTO cycle. It should be noted that since the Safran Silvercrest engine is not certified yet, data from the Pratt & Whitney PW815GA was used, since that engine is on a similar technology level. Table 20.3.1 shows the values used for the LTO cycle.

Table 20.3.1 LTO Cycle Emission Data from [38]

LTO Phase	EI HC (g/kg)	EI CO (g/kg)	EI NO_X (g/kg)	EI CO_2 (g/kg)
Take-Off	0.09	0.01	23.63	3150
Climb-Out	0.05	0	18.74	3150
Approach	0.03	2.23	11.24	3150
Idle	0.06	15.9	5.46	3150

Values from Verstraete [39] are used to determine the emissions during the cruise flight and loiter. The values are consistent with other sources and can be found in Table 20.3.2.

Table 20.3.2 Cruise and Loiter Emission Data from [39]

	EI HC (g/kg)	EI CO (g/kg)	EI NO_X (g/kg)	EI CO_2 (g/kg)
Cruise/Loiter	0.74	8.03	11.7	3150

Not only one mission profile can be used to determine the emissions during the service life of an aircraft. Business jets with a range of over 6000 nmi are rarely used exclusively for these routes. Rather, the average mission profile is a mixture of long-haul, short-haul and medium-haul routes. Some assumptions are made for the calculation of emissions during the operation of AETHER, which can be found in Table 20.3.3. Those assumptions rely on typical operational data for long-range business jets and were provided in a technical discussion by Rolls-Royce Germany.

Table 20.3.3 Average Operational Data for AETHER

Number of Passengers	8
Flight Hours p.a.	600 h
Long Range Missions (16 h) **p.a.**	12
Medium Range Missions (6 h) **p.a.**	43
Short Range Missions (2 h) **p.a.**	75
Estimated Lifetime	35 years

To determine the total emissions during an aircraft's lifetime, the emissions of the individual missions are calculated and then added together. A distinction is made between two scenarios: Scenario 1 comprises operation of AETHER with fossil kerosene only. Scenario 2 provides for operation in accordance with the blending quotas of Sustainable Aviation Fuel (SAF) applicable to airlines in the European Union as part of the ReFuelEU Aviation initiative. Operation with 100 % SAF throughout is considered unrealistic, as it will not be

possible to achieve full coverage in the foreseeable future by 2025. In addition, business jets, especially in the US, often operate from smaller airports that do not have an SAF infrastructure. At this point, however, it should be emphasized once again that operations with 100 % SAF are possible for AETHER.

In order to correctly record the reduction of emissions by SAF, the production of SAF and the associated CO_2 emissions must also be taken into account. To ensure comparability, a surcharge for production and transportation is also applied to fossil kerosene. At this point, it is assumed that this surcharge is 500 g/kg. The reduction of CO_2 emissions through SAF depends on the type of production, at this point we assume that including transportation and production an average reduction of 75 % can be achieved if 100 % SAF is used [65].

The data varies depending on the SAF type used. It can be assumed that all of the emissions under consideration remain constant, with the exception of CO_2 emissions. The main changes between Jet A1 and SAF emissions relate to Sulfur Dioxide (SO_2) and particulate matter, but these are not considered here [65].

Table 20.3.4 contains the emissions over the total service life of 35 years with entry into service in 2031. Emissions from maintenance, insurance and ground processes are neglected here, as also shown in the flow chart in Figure 20.1.1. Scenario 1 means 100 % fossil kerosene, scenario 2 applies the blending quotas for SAF according to ReFuelEU Aviation [66].

Table 20.3.4 Cruise and Loiter Emission Data from [39]

HC (kg)	CO (kg)	NO_X (kg)	CO_2 - Scenario 1 (kg)	CO_2 - Scenario 2 (kg)
3.48×10^5	2.52×10^5	3.87×10^5	1.20×10^8	6.2×10^7

20.4 End of Life Emissions

An end-of-life assessment is also required in order to be able to conclusively assess the climate impact of AETHER. The challenge here is that it is not yet possible to predict which recycling technologies will be available around 2060, when the first aircraft will reach the end of their service life. It can be assumed that almost all materials used in AETHER can then be recycled. This is already the case for all metallic materials such as aluminum, steel and titanium alloys. The biggest challenge will be the recycling of carbon fiber reinforced polymer composites (CFRP) and glass laminate aluminum reinforced epoxy (GLARE) materials. This is not yet possible on an industrial scale, but methods that have already been developed will be scalable to an industrial scale in the foreseeable future. It is already possible to recycle and reuse carbon fiber composites. [67, 68]

The most promising technology for recycling carbon fiber composites is pyrolysis. It has already been tested for CFRP from the aviation industry and enables a significant reduction in energy consumption during production and therefore also emissions by up to 80 percent [67]. Such emissions are not taken into account for this LCA, since the materials will be used in a new product.

Based on the assumption that all key materials can be recycled, it is assumed in this LCA that the end of life of AETHER does not result in any significant emissions. Unlike today, it is not expected that the CFRP or GLARE used will be incinerated or landfilled. All other materials that cannot be recycled are of an order of magnitude that cannot be determined without access to detailed and costly databases.

20.5 Life-Cycle Impact Assessment

In order to classify the emissions of AETHER, they are converted into the previously defined functional units. Those were Aircraft Lifetime (AL) or total emissions, Passenger Kilometers Traveled (PKT) and Vehicle Kilometer Traveled (VKT). The results can be found in Table 20.5.1.

Table 20.5.1 Total Emissions of AETHER

	AL (kg)	VKT (kg/km)	PKT (kg/km)
HC	3.48×10^{5}	1.79×10^{-2}	2.24×10^{-3}
CO	2.52×10^{5}	1.30×10^{-2}	1.62×10^{-3}
NO_X	3.87×10^{5}	1.99×10^{-2}	2.49×10^{-3}
CO_2 - Scenario 1	1.29×10^{8}	6.64	8.30×10^{-1}
CO_2 - Scenario 2	7.08×10^{7}	3.64	4.55×10^{-1}

If you compare the emissions with the results from Verstraete [39], you can see that the emission values are in the same order of magnitude as the Airbus A320 examined there. However, a direct comparison is not appropriate due to the different operational profile. Nevertheless, the trend is that AETHER will be significantly more environmentally friendly than previous long-haul jets in terms of NO_X and CO emissions.

In terms of CO_2 emissions one can see, that emissions in scenario 2 are way lower than in scenario 1, resembling the impact of SAF blending quotas. The SkyBridge team recommends operation according to these quotas for AETHER.

21 AETHER Variant 200

The design philosophy of the SkyBridge Team is to push limits and perfect comfort. A mechanism to push the boundaries of technology and achieve superior comfort is to utilize a gust mitigation system. This system can mitigate turbulence unlike other aircraft and provide superior ride quality. With the technology the team is looking to use, it is expected that this would be certified after the entry into service date of the first variant of the AETHER. This system will instead be integrated onto the -200 variant of the AETHER.

21.1 Boundary Layer Over a Flat Plate

A dynamically aerocompliant (DAC) actuator responds elastically to gusts. When the aircraft encounters a positive gust, the increased aerodynamic load on the flap will cause a trailing edge up hingemonment and subsequently decrease the lift of the airfoil. The airfoil then responds to the gust and alleviation is achieved [14]. This is possible because the change in angle of attack and change in camber become physically related, as seen in Figure 21.1.1.

The advantages of DAC flap mechanisms include, increased static margin and decreased turbulence.

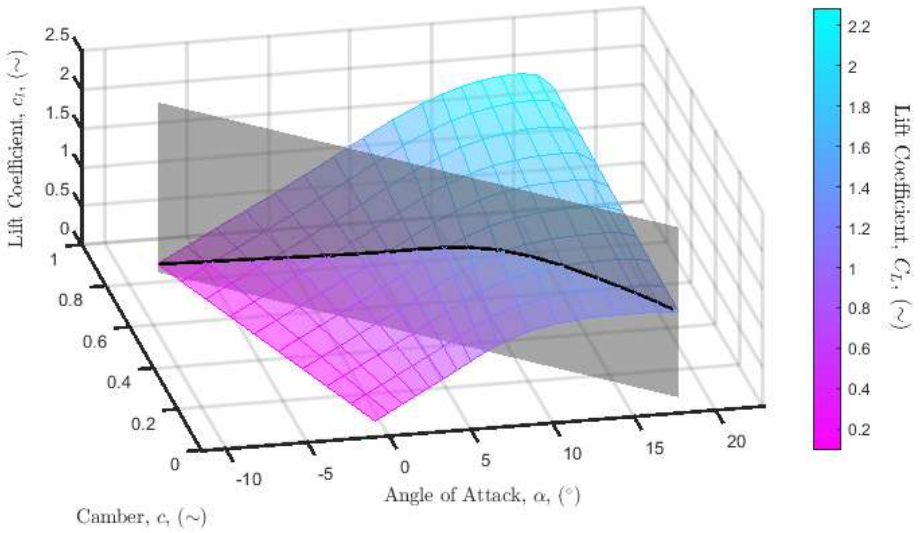

Figure 21.1.1 3D View Projection: Relating c and α Allows the 3D Lift Surface to be Traversed Diagonally [14]

The dynamic aerocompliant mechanism, shown in Figure 21.1.2, will be implemented with the use of aerospace certified pneumatic bellows. A close up view of the hinge mechanism for the flap is shown in Figure 21.1.3. This shows the bellow that will expand and contract to allow the flap to be actively controlled or remain neutrally buoyant, then Figure 21.1.4

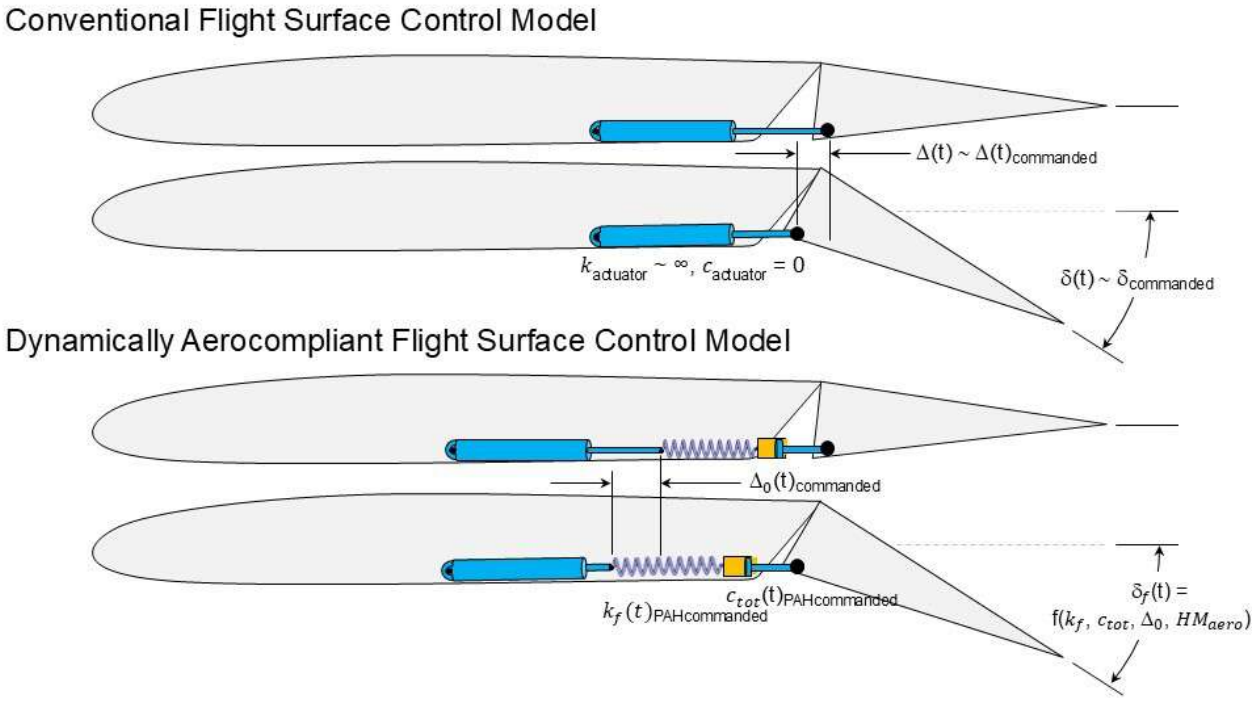

Figure 21.1.2 The Deflection of a Dynamically Aerocompliant Flap is a Dynamical Function of Aerodynamic Hinge Moments, and the Commanded Values of Stiffness, Damping, and Deflection [14]

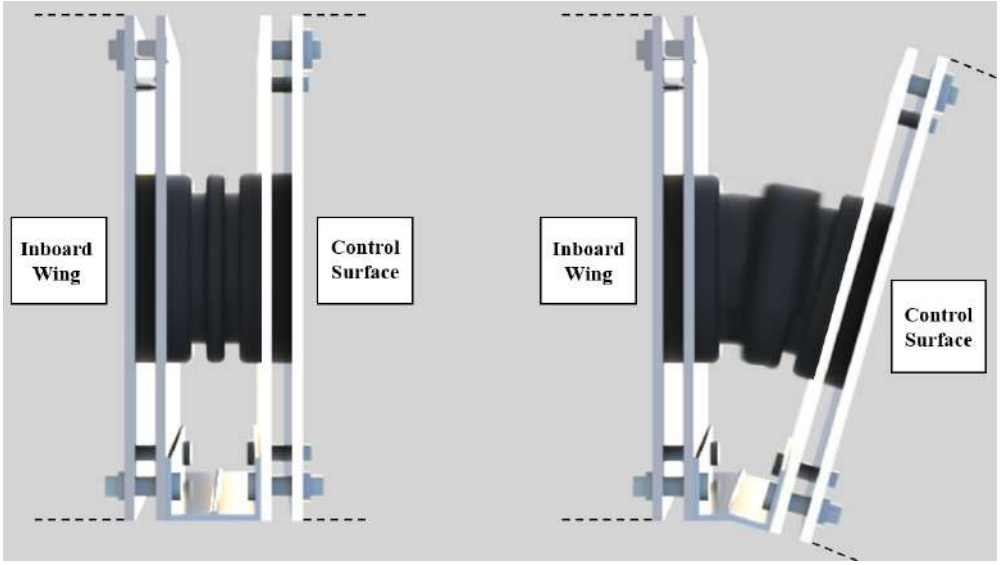

Figure 21.1.3 Dynamic Aerocompliant Control Mechanism [15]

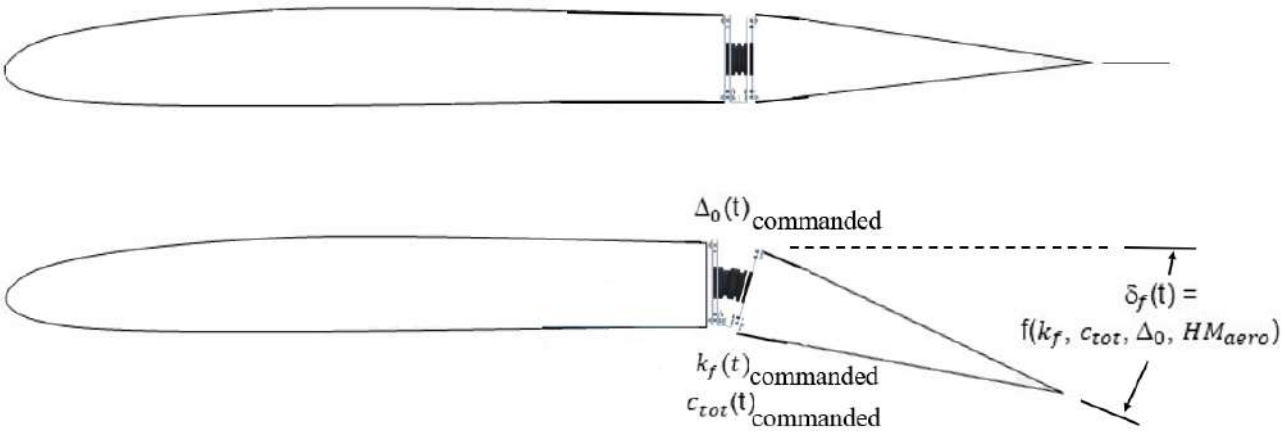

Figure 21.1.4 Integration of a Dynamic Aerocompliant Control Mechanism [15]

The stability and control derivatives of the aircraft were fed into a 6 Degree of Freedom (DOF) simulation of the aircraft. The flap stiffness, damping ratio, and steady state commanded deflections were determined by genetic optimization. The 6-DOF simulation of AETHER, in conjunction with the DAC flap dynamic model from [14], provided a basis for comparison of vehicle dynamics. The Power Spectral Density (PSD) versus frequency for an angle of attack step input, shown in Figure 21.1.5, show s a reduction of 15 decibels in the vertical acceleration amplitude for frequencies greater than 1Hz with respect to the response of a rigid-wing aircraft.

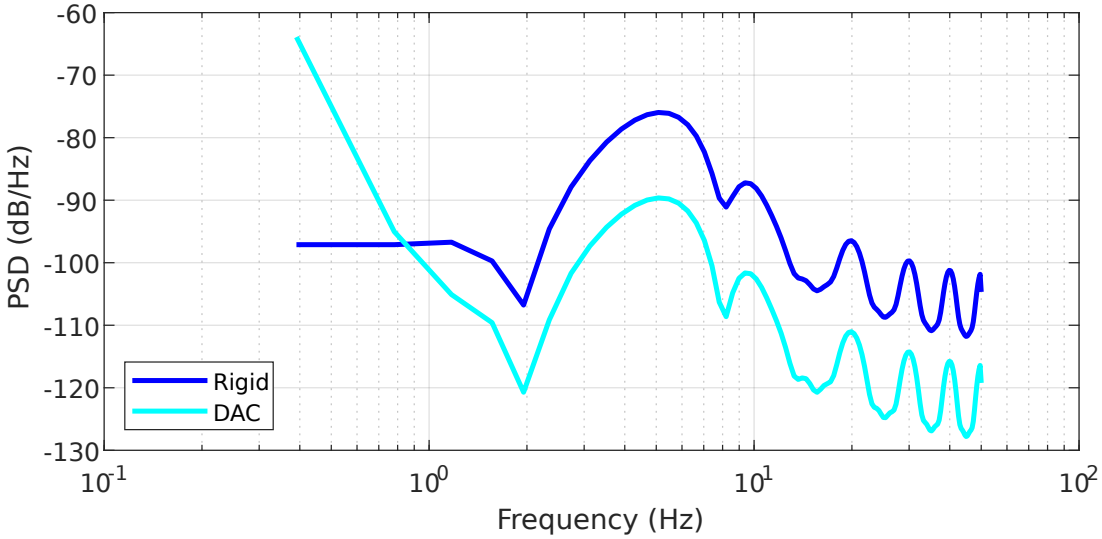

Figure 21.1.5 Aircraft Using DAC Shows Decreased Vertical Acceleration Response Angle of Attack Step Input at High Frequencies

Accelerations faster than 2Hz are significantly reduced by using dynamic aero-compliance the lower frequencies. Accelerations in the 5Hz and slower range can be alleviated by an elevator control loop. Human sensitivity to gust peaks above 5Hz. The damping provided by the flap is an improvement over the rigid actuator aircraft at frequencies 1Hz and faster. Over a 6 hour flight the accumulated fatigue due to the vibration is significant [69] and a reduction in the experienced acceleration is important. The maximum acceleration of AETHER to an elevator singlet input is reduced by 60% using DAC as seen in Figure 21.1.6.

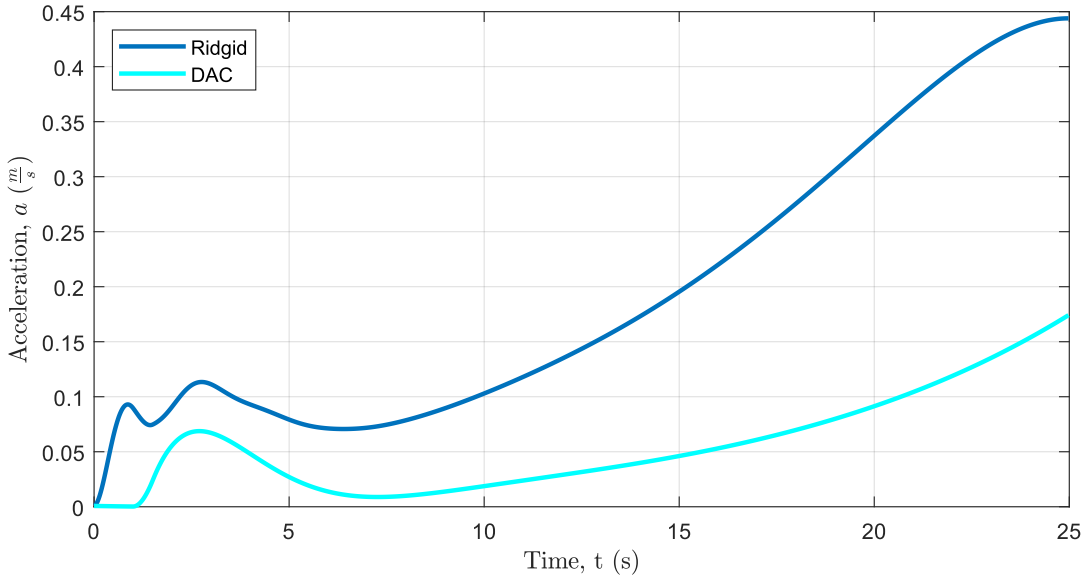

Figure 21.1.6 DAC Results in Decreased Acceleration Response to Elevator Singlet Input

Ride quality, evaluated in cruise with severe Dryden turbulence [70], showed a 10% improvement in vibration dose value (VDV), defined by ISO 2631 [71], with un-optimized DAC actuators in comparison to rigid actuators; These results are depicted

in Figures 21.1.7 and 21.1.8. The authors did not have time to optimize the the DAC actuators for the Dryden gust field but believe that further optimization will result in comparable performance to the angle of attack step input.

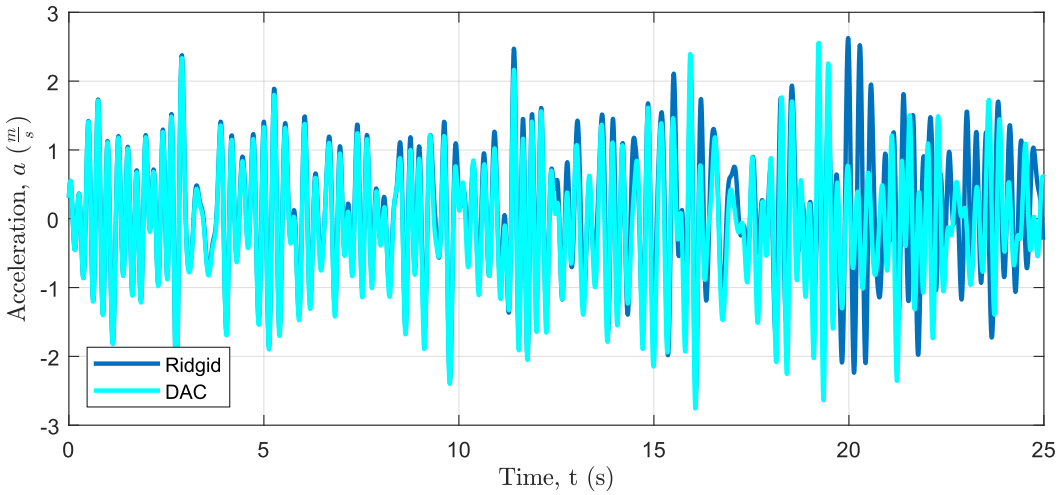

Figure 21.1.7 Un-optimized DAC Actuators Provide Reduced Acceleration In Severe Dryden Turbulence Compared To Conventional Actuators

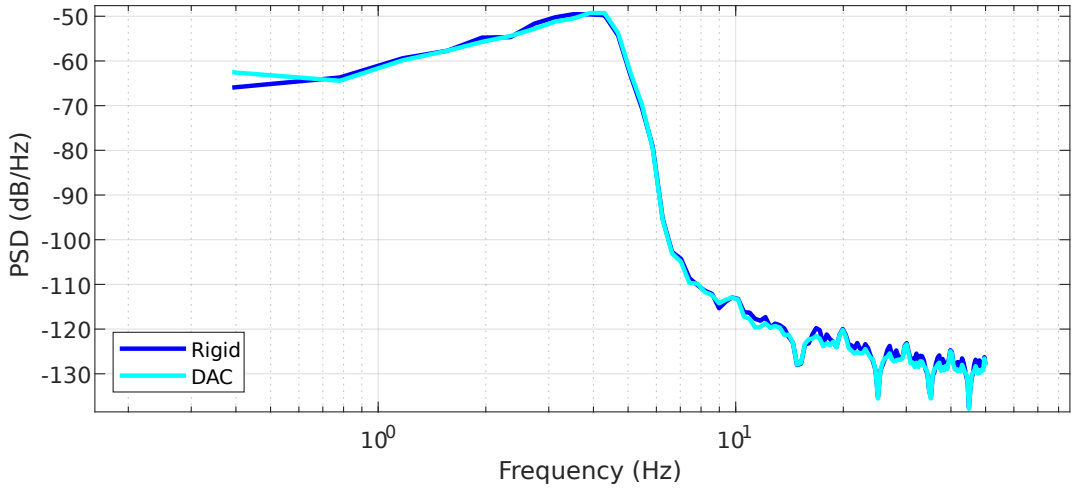

Figure 21.1.8 Un-optimized DAC Actuators Demonstrate Some High Frequency Gust Alleviation

The implementation of the DAC actuators to AETHER significantly increases customer satisfaction in rid quality, as shown in Figure 21.1.9. This demonstrates that both AETHER-100 and AETHER-200 variants exceed the comfort of other leading business jets, further proving the validity of the design.

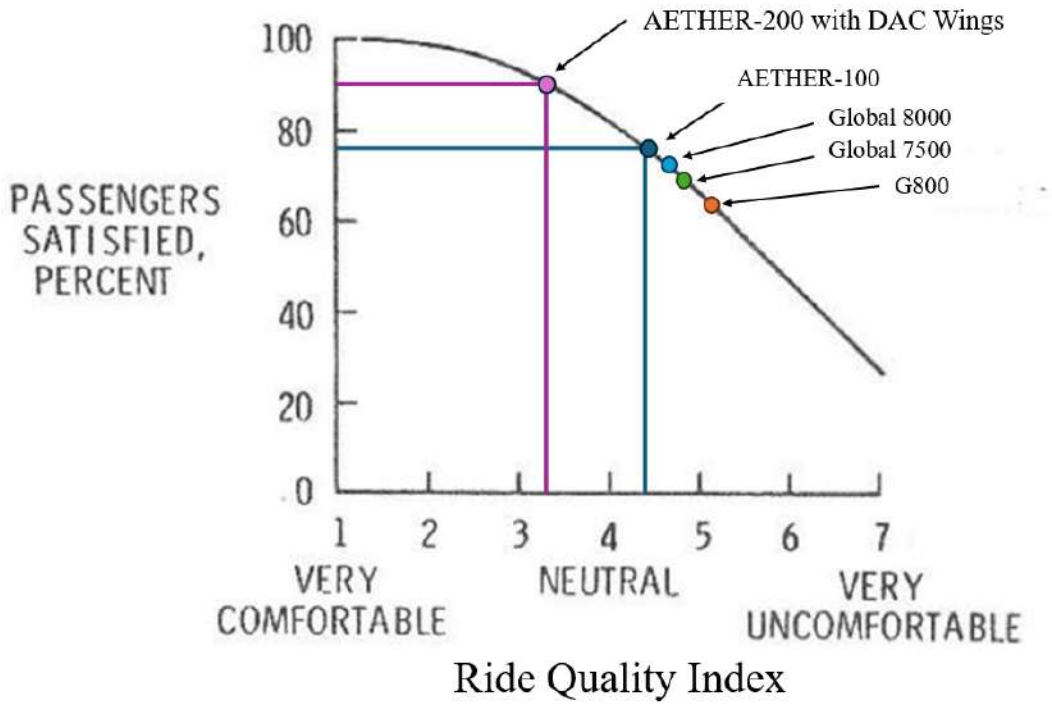

Figure 21.1.9 Ride Quality Index of Various Aircraft

References

[1] "Graduate Team Aircraft Design 2025: Ultra-Premium Long-Range Business Jet," AIAA, 2025. URL https://www.aiaa.org/docs/default-source/uploadedfiles/membership-and-communities/university-students/design-competitions/graduate-team-aircraft-design-2025_ultra-premium-long-range-business-jet.pdf?sfvrsn=84208d0f_2.

[2] Nale, D. D., and Wolz, R. R., "Continuous Renewal of the Gulfstream Product Line (or Past, Present, and Future Gulfstream Products)," *AIAA/ICAS International Air and Space Symposium and Exposition: The Next 100 Years*, Dayton, OH, 2003.

[3] "Gulfstream G800," Gulfstream Aerospace Corporation, 2025. URL https://www.gulfstream.com/en/aircraft/gulfstream-g800/.

[4] "Bombardier Global 8000," Bombardier, 2025. URL https://bombardier.com/en/aircraft/global-8000.

[5] "Dassault Falcon 10X," Dassault, 2025. URL https://www.dassaultfalcon.com/businessjets/falcon-10x/.

[6] "Boeing Businessjet," Boeing, 2025. URL https://businessjets.boeing.com/select/.

[7] "Airbus Corporate Jet TwoTwenty," Airbus, 2025. URL https://www.acj.airbus.com/en/exclusive-aircraft/acj-twotwenty.

[8] "Embraer Lineage," Global Jet Centre, 2025. URL https://globaljetcentre.com/aircraft/embraer-lineage-1000/.

[9] "Bombardier Global 7500," Bombardier, 2025. URL https://bombardier.com/en/aircraft/global-7500.

[10] "AIRBUS ACJ319NEO Specifications, Cabin Dimensions, Performance," , 2024. URL https://www.acj.airbus.com.

[11] "Embraer Lineage," Embraer, 2025. URL https://executive.embraer.com/global/en/lineage-1000e.

[12] "Boeing Businessjet Max," Boeing, 2025. URL https://businessjets.boeing.com/737-max/.

[13] "Silvercrest engine," Safran, 2019. URL https://www.safran-group.com/pressroom/silvercrest-2019-07-17.

[14] Poznański, J., Reida, R., Braaten, N., and Barrett-Gonzalez, R., "Decoupling Lift from q and alpha: Sailplane Design Optimization with Dynamically Aerocompliant Wings," *2025 AIAA SciTech Forum*, American Institute of Aeronautics and Astronautics, Orlando, FL, USA, 2025. https://doi.org/10.2514/6.2025-1618, URL https://kuscholarworks.ku.edu/handle/1808/35951.

[15] Braaten, N., "Dynamic Aerocompliant Control Mechanism," , 2025. Provided: May 16, 2025.

[16] AirNav, "Teterboro Airport," , 2025. URL https://www.airnav.com/airport/kteb.

[17] Wikipedia, "Le Bourget Airport," , 2025. URL https://de.wikipedia.org/wiki/Flughafen_Le_Bourget.

[18] OpenNav, "London City Airport," , 2025. URL https://opennav.com/airport/EGLC.

[19] Engadin Airport, "Samedan/St. Moritz Aiport," , 2025. URL https://www.engadin-airport.ch/.

[20] "Data Section - Tires," Goodyear Aviation, 2022. URL https://www.goodyearaviation.com/resources/pdf/Data-Section-2022.pdf, retrieved: March 11, 2025.

[21] Albright, J., "Fuel Density," , 2021. URL https://www.code7700.com/fuel_density.htm, accessed: April 5, 2025.

[22] "Bombardier Global 8000 Specs | Compare Private Planes," , 2024. URL https://www.compareprivateplanes.com.

[23] "NetJets Inks Order For 4 Bombardier Global 8000 Business Jets Worth $312 Million," , 2024. URL https://www.netjets.com.

[24] "Embraer Lineage 1000 Overview (2008 - 2013) | Jetcraft," , 2024. URL https://www.jetcraft.com.

[25] "Embraer Lineage 1000 Ownership Costs with Budget Calculator," , 2024. URL https://www.jetcraft.com.

[26] "Dassault Falcon Revenues Jump 39% in First Half of 2024," , 2024. URL https://www.corporatejetinvestor.com.

[27] "Dassault Falcon 10X Deliveries Slated To Begin In 2027," , 2024. URL https://www.aviationweek.com.

[28] "Dassault Falcon 10X Price, Range and Passenger Capacity 2022," , 2022. URL https://www.aircraftbuyer.com.

[29] "Global 7500 for Sale - Used Global 7500 Price," , 2024. URL https://www.jetcollection.com.

[30] Bombardier, "Bombardier's Global 7500 Business Jet Soars to New Heights, Continues Record-Setting Pace with 75 Speed Records," , 2024. URL https://www.bombardier.com.

[31] "BBJ 737 for Sale - Used BBJ 737 Price," , 2024. URL https://www.jetcollection.com.

[32] "Gulfstream G800 Price - Gulfstream G800 Cost," , 2024. URL https://www.jetcollection.com.

[33] "The Latest Updates To The Gulfstream G800," , 2024. URL https://www.jetcollection.com.

[34] "Business Jet Market Report," , 2025. URL https://www.econmarketresearch.com/industry-report/business-jet-market/.

[35] "Business Jet Market - Global Industry Analysis," , 2025. URL https://growthmarketreports.com/report/business-jet-market-global-industry-analysis.

[36] "Business Jets Market Report," , 2025. URL https://www.expertmarketresearch.com/reports/business-jets-market.

[37] "Business Jet Market Report," , 2025. URL https://www.mordorintelligence.com/industry-reports/business-jet-market.

[38] "ICAO Aircraft Engine Emissions Databank," Tech. rep., EASA, 2024.

[39] Verstraete, J., "Creating a Life-Cycle Assessment of an Aircraft," Master's thesis, Hamburg University of Applied Sciences, 2012.

[40] Honeywell, "2024 Global Business Aviation Outlook," Tech. rep., Honeywell Aerospace, 2024.

[41] "Airbus Corporate Jet Neo," Airbus, 2025. URL https://www.acj.airbus.com/en/exclusive-aircraft/acjneo.

[42] "Aspen-Pitkin County Airport/Sardy Field," , 2025. URL https://www.airnav.com/airport/kase.

[43] Aspen Airport, 2025. URL https://www.aspenairport.com/.

[44] Airnav, "Napa County Airport," , 2025. URL https://www.airnav.com/airport/KAPC.

[45] Airnav, "Van Nuys Airport," , 2025. URL https://www.airnav.com/airport/KVNY.

[46] AC-U-KWIK, "Mexico City/Lic Benito Juarez International," , 2025. URL https://acukwik.com/Airport-Info/MMMX.

[47] Roskam, J., *Airplane Design Part I-VIII*, DARcorporation, 1140 Wakarusa Drive, Suite 500, Lawrence, KS, 2018.

[48] Roskam, J., "Full Configuration Transonic Airplane Lift and Drag Data from Wind Tunnel Testing," , 1987. AE 521 Aircraft Design I, Lawrence, Kansas.

[49] Raymer, D. P., *Aircraft Design: A Conceptual Approach*, AIAA, 1989.

[50] Federal Aviation Administration, D. o. T., "14 CFR Part 25," , 2025. URL https://www.ecfr.gov/current/title-14/chapter-I/subchapter-C/part-25?toc=1.

[51] Boeing, "Side and Top View of Area Ruled Boeing 747," , . Retrieved: March 6, 2025.

[52] Barrett, R., "Discussion of Empennage Airfoils," , . Discussed: March 8, 2025.

[53] Federal Aviation Administration, "Advisory Circular 150/5335-5D: Standardized Method of Reporting Airport Pavement Strength – PCN," , 2025. URL https://www.faa.gov/documentLibrary/media/Advisory_Circular/150-5335-5D-Pavement-Strength-202501.pdf.

[54] Peters, L., "Embraer Looks To UVC Lights For Aircraft Disinfection," , Aug. 2020. URL https://simpleflying.com/embraer-uvc-aircraft-disinfection/, accessed: 2025-05-15.

[55] Lehmann, L., and Schulz, A., "Cabin Disinfection: Evaluating Different Technologies," *FAST Magazine*, 2021. URL https://aircraft.airbus.com/en/newsroom/news/2021-08-cabin-disinfection, accessed: 2025-05-15.

[56] International Air Transport Association, "Aircraft Cleaning and Disinfection During and Post Pandemic," Tech. Rep. Edition 2, International Air Transport Association, January 2021. URL https://www.iata.org/contentassets/094560b4bd9844fda520e9058a0fbe2e/aircraft-cleaning-guidance-covid.pdf, accessed: 2025-05-15.

[57] German Aerospace Center, "Comprehensive Analysis of Pathogen Transmission and Mitigation Strategies in Aircraft Cabins: Airflow, Surfaces, and Disinfection," Tech. Rep. HEALTH D1.1, European Union Aviation Safety Agency, January 2025. URL https://www.easa.europa.eu/en/downloads/141768/en, accessed: 2025-05-15.

[58] Honeywell, "Honeywell Anthem," , 2025. URL https://aerospace.honeywell.com/us/en/products-and-services/products/cabin-and-cockpit/avionics/integrated-flight-decks/honeywell-anthem, accessed: 2025-04-03.

[59] Pullen, J., "Honeywell Operates First Flight with Anthem Integrated Flight Deck," *Aviation Today*, 2023. URL https://www.aviationtoday.com/2023/05/16/honeywell-operates-first-flight-with-anthem-integrated-flight-deck/.

[60] Roskam, J., *Airplane Flight Dynamics and Automatic Flight Controls Part I*, DARcorporation, 1140 Wakarusa Drive, Suite 500, Lawrence, KS, 2001.

[61] Marsh, A. K., "Hourly operating costs of 45 jets compared," *AOPA*, 2015. URL https://www.aopa.org/news-and-media/all-news/2015/november/16/hourly-operating-costs-of-45-jets-compared, accessed: 2025-05-16.

[62] Lopes, J., "Life Cycle Assessment of the Airbus A330-200 Aircraft," Master's thesis, Universidade Técnica de Lisboa, 2010.

[63] Chester, M., "Life-cycle Environmental Inventory of Passenger Transportation in the United States," Ph.D. thesis, UC Berkeley, 2008.

[64] "Supply Chain GHG Emission Factors for US Commodities and Industries," Tech. rep., U.S. Environmental Protection Agency, 2025.

[65] Song, Z., Li, Z., and Liu, Z., "Comparison of Emission Properties of Sustainable Aviation Fuels and Conventional Aviation Fuels: A Review," *Applied Sciences*, Vol. 14, No. 13, 2024. https://doi.org/10.3390/app14135484, URL https://www.mdpi.com/2076-3417/14/13/5484.

[66] "ReFuelEU Aviation," Tech. rep., EASA, 2025.

[67] Ateeq, M., "A state of art review on recycling and remanufacturing of the carbon fiber from carbon fiber polymer composite," *Composites Part C: Open Access*, 2023.

[68] Scelsci, L., Bonner, M., Hodzic, A., Soutis, C., Wilson, C., Scaife, R., and Ridgway, K., "Potential emissions savings of lightweight composite aircraft components evaluated through life cycle assessment," *eXPRESS Polymer Letters Vol.5*, 2010.

[69] Hanson, C., Andrade, S., and Pahle, J., "Experimental Measurements of Passenger Ride Quality During Aircraft Wake Surfing," *2018 AIAA/CEAS Aeroacoustics Conference*, American Institute of Aeronautics and Astronautics, Atlanta, GA, USA, 2018. https://doi.org/10.2514/6.2018-3561, URL https://ntrs.nasa.gov/api/citations/20180004506/downloads/20180004506.pdf.

[70] U.S., D. o. D., "MIL-F-8785: Flying Qualities of Piloted Aircraft," Standard MIL-F-8785, Department of Defense, Washington, D.C., USA, 1980. URL https://www.dtic.mil/DTICOnline/downloads/ADA087966.pdf.

[71] for Standardization, I. O., "ISO 2631: Mechanical Vibration and Shock - Evaluation of Human Exposure to Whole-Body Vibration," Standard ISO 2631-1:1997, International Organization for Standardization, Geneva, Switzerland, 1997. URL https://www.iso.org/standard/7612.html.